PROCESS DEVELOPMENT AND CHARACTERIZATION OF AN OXIDE DISPERSION STABILIZED NICKEL BASE SUPERALLOY

by

CHARLES HUBERT SMITH

B.S., Georgia Institute of Technology
(1976)

M.S., Georgia Institute of Technology
(1977)

Submitted in Partial Fulfillment

of the Requirements for the

Degree of

DOCTOR OF PHILOSOPHY

at the

Massachusetts Institute of Technology

June, 1982

Signature of Author . . . . . .
Department of Materials Science and Engineering, August 6, 1982.

Certified by . . . . . .
Thesis Supervisor

Accepted by . . . . . .
Chairman, Departmental Committee on Graduate Students

PROCESS DEVELOPMENT AND CHARACTERIZATION OF AN OXIDE DISPERSION STABILIZED NICKEL BASE SUPERALLOY

by

CHARLES HUBERT SMITH

Submitted to the Department of Materials Science and Engineering on August 6, 1982 in partial fulfillment of the requirements for the degree of Doctor of Philosophy.

ABSTRACT

A possible cost-effective method for processing Ni-base alloys by relatively simple steps was successfully developed.

The process, very simple and fast, was effected through: melting or remelting of fully alloyed master alloys then atomization to produce high yields of fully alloyed fine powders; conversion of the fine powders to flakes by attrition then ball milling to incorporate the very fine refractory oxide particles. Excellent dispersion of the oxides, viz. Al_2O_3, Y_2O_3 and Y-Al-O_3 was obtained, resulting in a particle diameter of 210 to 790°A and an interparticle spacing that was less than 0.2μ.

Two types of alloys were processed; an experimental solid solution alloy with a high chromium content (20 w/o) and a high volume fraction γ' superalloy (IN 100). Significant contamination by Cr_2O_3, TiO or Al_2O_3 never occured. It was established that the oxide dispersion stabilized (ODS) superalloy had 59.1 v/o γ' after processing.

The as-extruded bar had submicron size equiaxed grains, with a substructure that was highly worked and strained, containing a high dislocation density. This fine grain structure contributed to extremely high room temperature strength, with stress rupture strength that increased with increasing oxide content and with combination precipitation strengthening and oxide stabilizing.

Using a solid state crystal growing process named ZAP (Zone Aligned Polycrystals), large columnar grains with (100) fiber texture and a high grain aspect ratio (GAR) were produced. Stress rupture testing of ZAP product indicated that this material is approximately twice as strong as the same material given a conventional recrystallization heat treatment and about four times stronger than the as-extruded material. The ODS superalloy gave a 1093°C/100 hour rupture stress of 22 ksi (152 MPa). Stress rupture ductilities of ZAP products varied between 2 and 9%.

Thesis Supervisor: Nicholas J. Grant

Title: ABEX Professor of Advanced Materials

TABLE OF CONTENTS

LIST OF FIGURES

LIST OF TABLES

ACKNOWLEDGEMENTS

The author wishes to direct his profound gratitude to his thesis supervisor, Professor N. J. Grant, for his technical and personal guidance and his constant encouragement throughout the course of this project. His appreciation is also extended to Professors K. C. Russell, R. M. Pelloux and M. C. Flemings who served on the Thesis Reviewing Committee.

His thanks is meted out to the clearly unselfish members of Professor Grant's group: C. Ashdown, F. Dabkowski, E. Ting, A. Lee, B. McCormick, S. Kang, V. Franetovic, Y. Hara, K. Yu and Dr. P. Domalavage. Their unfailing help and crystallizing ideas and discussions contributed generously to this work and to my thinking in various ways. Their comraderie made my sojourn at M.I.T. fulfilling and enjoyable. Thanks also to Lisa Kaminski who typed the manuscript.

Finally, the author's greatest appreciation goes to his parents and brothers and sisters, without whose support this work would never have been accomplished.

This project was supported by the Department of Energy (DOE), by the Defense Advanced Research Projects Agency (DARPA) and by HOWMET. The author wishes to thank them for their sponsorship.

CHAPTER I

Introduction

It has long been appreciated by aircraft engine manufacturers that increasing the turbine inlet temperature offers attractive advantages in aircraft turbine performance and economy. A significant amount of improvement in the turbine inlet temperature has been made possible by advances in material capability. One of the most demanding parts in the gas turbine is the first stage turbine blade, which is subjected to severe combinations of stress, thermal shock, low cycle fatigues, time and temperature in a hostile environment. Present day turbine blade alloys are nickel-rich solid solution matrices hardened primarily by coherently ordered γ' precipitates (1). Dissolution and coarsening of γ' impose an upper limit on the alloy operating temperature of the current turbine blades, despite advances in process technologies such as directional solidification columnar and single crystal structures (2).

Oxide dispersed (OD) (also oxide dispersion stabilized, ODS) alloys have attracted great attention as advanced high temperature materials, because they can retain useful strength levels up to a relatively high fraction of their melting temperatures (3). The high temperature strength of OD alloys is due to the presence

of fine, uniformly dispersed, stable oxide particles. These oxide particles lead to direct strengthening by acting as barriers to dislocation motion (4,5,6). Further, indirect strengthening arises because the oxide particles can stabilize the final grain size and shape following thermomechanical processing and heat treatment (5,6,7). Typically, the oxide particles act in conjunction with a highly preferred orientation and an elongated grain structure (high grain aspect ratio: GAR).

In the past, oxide dispersion stabilization was applied successfully primarily with pure metals such as tungsten (8), aluminum (9), copper (10), nickel (11, 12), iron (13, 14), and many others. These early developments have generated interest in applying ODS principles to more complex alloy systems where solid solutions, coherent phase precipitation, and sub-structure strengthening may all interact.

The ability to combine the benefits of oxide dispersion stabilization for high temperatures, and γ' strengthening for intermediate temperatures, was most recently demonstrated using a mechanical alloying process (15). Since the reported successes in 1970 (and later) by the International Nickel Company, the mechanical alloying technique for preparing OD super-alloys has been applied by numerous investigators (16-20).

The process is a high energy, dry milling process in which a mixture of metal powders and master alloy powders or particulates and very fine oxide particles is subjected to continuous kneading, agglomerating, fracturing, and rewelding in an energetic grinding ball charge in an inert atmosphere.

Although these alloys have exhibited the best mechanical properties and alloy stability at high temperatures to date, the high cost of processing restricts their use considerably.

The intent of this research program was to cost effectively develop, process, and fully characterize oxide dispersion stabilized Ni-base alloys. Full characterization involved determining such parameters as the oxide particle size, shape, and distribution, the oxide (and γ') volume fraction and their respective interparticle spacings; the grain size, grain shape and grain texture; the intragranular structure (i.e., the dislocation density and distribution).

CHAPTER II

History

Oxide dispersion stabilized alloys were believed to owe their stability and strength to the incorporation of ultrafine particles of a stable oxide; for example, due to fine ThO_2 particles in tungsten (8). Irmann's (9) and Von Zeerleder's (78) discovery that aluminum could be strengthened by its own oxide furthered still greater interest in OD alloys. The elevated temperature strength of SAP alloys was far superior to that of conventional precipitation strengthened aluminum. Studies by Grant et al (79,80) and Lenel et al (22) showed that the strength of these alloys increased with higher volume fraction of the fine oxide and with decreasing interparticle spacing for alloys with uniformly dispersed oxides. Bloch's (23) review summarized the earlier work associated with the development of SAP materials.

Methods of Producing Oxide Dispersed (OD) Alloys

The majority of the OD alloy fabrication techniques utilize fine powder materials in order to achieve a uniform dispersion of fine oxide particles in the metal matrix. Many of the more recent techniques combined oxide dispersions with solid solution strengthening in alloy systems free of highly reactive elements (oxide formers). A brief review of the nature and limitations of each of these techniques will be attempted here.

The SAP method employs metal powders which spontaneously form a thin adherent oxide film. During the process of extensive deformation during consolidation, the oxide film is fragmented and finely dispersed. This technique has also been applied to magnesium (24), tin (25), and zinc (26). This method is confined only to simple two-phase systems.

Mechanical blending involves the direct mixing of ultrafine metal powders with a much finer refractory oxide powder. Although the oxide particle spacing is largely restricted by the size of the initial metal powders, this method has been successfully used to produce a wide variety of dispersion strengthened materials such as Cu (27), Ni (28-30), and Fe (31-33). Powder sizes of less than 5μ are required to obtain satisfactory interparticle spacings. Powders this fine containing γ' formers such as aluminum and titanium are very reactive because of their high specific surface area, and excessive oxidation of aluminum and titanium can ensue.

Thermal decomposition of inorganic salts (metal and oxide forming salt, oxide plus metal forming salt, or salt solutions of metals and oxides) which are then decomposed to form a mixture of metal powders coated with fine oxide particles has been used to manufacture copper (34), nickel (35,35), and iron (31,37) OD alloys.

Limitations in processing here are similar to those for mechanical blending. Furthermore, the oxidizing potential of the reaction products of the salt decomposition step can create contaminating problems.

Direct reduction of the matrix element(s) in an intimate mixture of metal oxides obtained by precipitation from complex salts has been used to produce iron-alumina alloys (13), and is currently used to produce commercial Ni-thoria alloys (38). If chromium, aluminum, titanium, and other refractory oxide formers are present in the alloy matrix, reduction (hydrogen, for example) is not possible because of the stability of oxides up to the melting temperature of the alloys.

Internal oxidation, wherein oxygen is allowed to diffuse into a noble metal or alloy matrix containing a small quantity of a highly reactive oxide forming element is an effective method of achieving fine oxide dispersions. The dissolved oxygen selectively oxidizes the reactive element(s), and forms a fine oxide dispersion throughout the alloy. The source of oxygen may be from the chemical equilibrium between water vapor and hydrogen, between another metal and its oxide, or from the reduction of the matrix elements natural surface oxide (39). Since experimental research (12) verified that the size of the dispersoid increases with depth of penetration, and the rate of oxide penetration follows

a parabolic rate law (8,12,40), it is important to use the finest powders possible for internal oxidation and to optimize all other variables. For an alloy containing reactive γ' forming elements such as aluminum and titanium in nickel alloys, the oxygen potential could not be raised above the extremely low values required to oxidize the Al and Ti, as well as the Cr. Internal oxidation techniques have been widely applied to many simple OD alloys of which only a partial listing includes Fe-BeO (41,42), Ni-Co-Mo-BeO (5,43), Fe-Al_2O_3 (32), Cu-Al_2O_3 (10,39,44), Ni-Al_2O_3, TiO_2, Cr_2O_3, SiO_2 (12), Cu-SiO_2 (12) and Cu-BeO (45).

The mechanical alloying process exploits high energy attrition or ball milling to intimately combine a mixture of ductile metal powders with inert fine oxide particles in an inert atmosphere. Because this process is a "cold welding, cold alloying" process, the preparations of the master alloy blends and the subsequent attrition times are very long and expensive. Even though mechanical alloying is the only fabrication technique to date capable of combining oxide dispersion with the corrosion resistance and intermediate temperature strength of complex, highly alloyed materials, such as those with large amounts of γ' precipitates; and even though excellent mechanical properties and alloy stability at high temperatures were achieved; the process and products have

certain limitations, namely:

- reproducibility of structure and properties is a problem
- scale up for large batch or continuous operation is a serious inhibition
- preparation of special master alloys for complex compositions entails high costs of production, and more complex alloys will present greater problems.

Strengthening Parameters in OD Alloys

The effects of oxide particle size, interparticle spacing and volume fraction on stress-rupture strength values have been reported for a number of OD systems. Various formulations relating the size, spacing, and volume fraction of the oxide to strength have been suggested and studied. Due to variations in grain size, the grain aspect ratio, grain texture, the amount of cold work or recrystallization, and because of differences in the oxide size distribution, degree of dispersal, thermodynamic stability, and shape, no single structural relationship has thus far adequately described the strengthening of OD alloys. An attempt is made here to enumerate some of the more plausible relationships.

Grant and co-workers (21,29) have shown that rupture strength is a reciprocal function of interparticle spacing for fine grained, cold worked OD alloys. Assuming that interparticle spacing, particle size and volume

fraction are uniform and can be interchanged (46), the above relationship can be restated in terms of volume fraction or average particle size. In general, stress rupture strength increases as the volume fraction of the dispersoid increases and as the interparticle spacing decreases. Grant et al (14) demonstrated that for oxide dispersion stabilization of iron which contain 4 to 10 volume percent Al_2O_3 or MgO, the stress rupture strength increases with volume fraction of the oxide. Additionally, the iron-alumina alloys were considerably stronger than iron-magnesia alloys at equivalent volume fraction of dispersoid. This was attributed to finer particle size and smaller spacings of alumina.

Gatti (13) reported a higher stress rupture life for an internally oxidized iron-alumina alloy as compared to an alloy prepared by mixing iron and alumina powders. Improved strength was attributed to a finer and more uniform oxide particle spacing. Similarly, Hunkeler (42), and Grant and Wolf (6) found that iron-beryllia alloys produced by internal oxidation exhibited improved elevated temperature strength with higher oxide content.

Studies by Wilcox and Clauer (47) suggested that the creep rate of dispersion stabilized nickel is controlled by the function λ^2/d_v, where λ is the interparticle spacing and d_v represents the average oxide particle size. Later work by Wilcox and Clauer (48)

demonstrated that the grain aspect ratio (GAR), the length of the grain divided by its diameter, can be correlated to the stress rupture strength for both cold worked and recrystallized dispersion strengthened alloys up to GAR values of 14. Furthermore, work by Petrovic and Ebert (49) on recrystallized TD-Ni reported similar increases of elevated strength with GAR.

Additional work by Benjamin and Bomford (50) revealed a striking correlation between the 100-hr rupture strength and GAR. They found that for GAR values of approximately 6, rupture strength is strongly dependent upon GAR. For values above 6, rupture strength is relatively independent of this ratio. Their results were consistent with a model proposed by Fraser and Evans (51). In the latter model, dispersion stabilized alloys were treated as fiber composite materials with load being transferred from one fiber to another through the grain boundaries. When the shear strength of the grain boundary is much less than the tensile strength of the grain body, the strength of the dispersion stabilized material is controlled by the GAR and the grain boundary shear strength.

Directional Recrystallization

The high temperature strength of dispersion stabilized materials is limited by macroscopic yielding through

grain boundary sliding and rupture of transverse grain boundary segments. Intrinsic elevated temperature matrix strength of dispersion stabilized materials can be best utilized through development of materials with elongated grains of fibrous substructure to minimize grain boundary sliding (15,48). Both short and long time elevated temperature strengths have been quantitatively related to the degree of elongation of the structure parallel to the applied stress.

As a class, dispersion stabilized materials are difficult to recrystallize unless sufficient deformational energy from thermomechanical processing is stored in the substructure to overcome the barriers to grain growth. In general, thermomechanical processing introduces anisotropy in the worked microstructure. TD-Ni is used in this form and has fine elongated grains with a strong deformation texture which is resistant to recrystallization (52). Other dispersion strengthened materials such as TD-Ni-Cr recrystallize after working and are used in the recrystallized form.

The secondary recrystallization or grain coarsening behavior which forms very coarse elongated grains in dispersion stabilized superalloys is not well understood. This behavior of dispersion stabilized nickel-base alloys has been reviewed by Wilcox and Clauer (53). Their discussion suggested that the grain coarsening

behavior could be related to two separate effects. Firstly, the materials are extremely resistant to ordinary recrystallization or grain growth because the uniform, stable, oxide dispersion acts to pin the existing grain boundaries and to homogenize the deformation substructure. As a result there exist few locations where a sufficient energy gradient can promote grain boundary movement. In addition, the materials usually have fairly strong deformation textures which may further tend to homogenize internal shear strains and stored energy. As a result, the materials only recrystallize with difficulty and at very high temperatures in a strong temperature gradient.

Secondly, there are the considerations about the processing variable which can cause formations of a coarse elongated grain structure. In this regard, Wilcox and Clauer suggest that the preferred orientation which developed during rolling might lead to certain grain boundaries or particular orientations being more mobile than others. They also noted that the oxide particle distribution in some materials showing this behavior is not uniform. Stringers of particles aligned in the working direction would act to impede lateral grain growth.

It has long been known that massive grain coarsening, even growth of single crystals, can be achieved by passing material through a hot zone with a steep thermal gradient. This technique was originally invented by Andrade and has been reviewed in the literature (54). Work using this technique has been reported by others (55,56,57). Ni-base alloys combining oxide dispersion with γ' precipitation hardening have been developed (16-20). Extruded bar of these materials form an ultrafine (0.2 to 0.6μ) equiaxed grain structure when viewed in transverse direction (81). The materials undergo a process of secondary recrystallization when heat treated at high temperatures; complete recrystallization occurs over a narrow temperature range and in quite a short time.

The Effect of Thermomechanical Processing

In general, cold working with partial recovery (annealing) increases elevated temperature strength when the cold work structure is retained. Work by Yim and Grant (58) on nickel had no effect on the creep rate, whereas the creep resistance of prestrained nickel with carbon clusters was improved. This finding was associated with a stabilized substructure. Also, Chin and Grant (82), concluded that the high values of stored energy found in their investigation was evidence that high-temperature strength in metal-metal

oxide alloys requires a preformed substructure with a high and stable dislocation density.

Many researchers (5,6,10,42,43,59-61) of the behavior of ODS alloys have identified improvements in elevated temperature strength with substructure strengthening (stored energy). In these cases the oxide particle spacing became important because it defined the size of the substructure cells formed during initial processing. Furthermore, cold work with recovery anneals reduced the size of the cells, which resulted in smaller apparent particle spacing as proposed by Grant and co-workers (5,6,60). It was suggested that the function of the closely spaced oxide particles is to pin grain boundaries and cell walls and to prevent boundary shear and migration. This stabilization structure subsequently impedes dislocation motion, slows down the rate of recovery, prevents grain and subgrain boundary migrations, and improves elevated temperature strength.

Recently, Sherby et al (62) developed a model relating creep rate to subgrain size. They suggested that if a fine subgrain can be introduced and retained in an alloy, large increases in creep strength may result.

In addition, it has been demonstrated that mechanical properties of OD alloys vary with orientation from the

rolling direction or swaging axis (6,63,64). Grant and Wolf (6) determined that longitudinal stress-rupture strength values increased with cold rolling plus intermediate anneals while transverse strength remained unchanged. Furthermore, Doble and Quigg (63) also discovered an absence of strengthening in the transverse direction of swaged TD-Ni bars.

Yielding and Creep Models for Dispersion Stabilized Alloys

There are many models to explain the room temperature strength of recrystallized OD alloys where direct dislocation-particle interactions are possible. Most of these models invoke the early concept of Orowan (65) based on the stress required to bow a dislocation between two obstacles. Ansell (66) developed a model, which was subsequently modified by Ashby (67) that describes the yielding behavior of OD materials. This model relates the yield stress of a dispersion stabilized material to the oxide particle spacing and particle size. Recently Place and Lund (68) calculated yield stress values for Fe-ThO_2 alloys using the modified Orowan relationship. The calculated values were within 8 percent of the experimental results. Jones (69), and more recently Hildeman (41), using the same model, also reported close agreement between calculated and experimental

yield stress values for iron with dispersions of FeTa and BeO particles respectively.

Grain boundary sliding plays an important role in high temperature yielding. Wilcox and Clauer (52) suggested this to be the case for high temperature creep of TD-Ni bar and Doble et al (70) and Fraser and Evans (51) purported that grain boundary sliding was the predominant mechanism for yielding of Ni-ThO_2 alloys tensile tested in high temperatures. Dislocation climb over dispersed particles has also been proposed as a rate controlling step during creep. Ansell and Weertman (71) originally developed this model to explain the creep behavior of recrystallized SAP alloys. In their model, the stress exponent equalled 4 and the activation energy was that of self-diffusion of the matrix element. This relationship can be written in general terms as follows:

$$\dot{\varepsilon} = A\sigma^{\eta} \ (-Q_c/RT) \qquad (1)$$

where: $\dot{\varepsilon}$-steady state creep rate, η-stress dependent exponent, Q_c-activation energy for creep, A-material constant, R-gas constant and T-absolute temperature. Wilcox and Clauer (72) also used this equation to describe the steady-state creep behavior of highly cold worked TD-Ni alloys. It was determined that extremely large stress exponents on the order of 40 and activation energies three times that for self-

diffusion are required to satisfy the creep rate relationship.

McLean and Hale (73) first observed that the constant A for various metals and alloys depended systematically on their moduli of elasticity and Sherby (74) proposed the empirical modification of equation (1) to:

$$\varepsilon = \left(\frac{\sigma}{E}\right)^{\eta'} \exp\left(-Q_c/RT\right) \qquad (2)$$

and if $Q_c = Q_D$

$$\frac{\varepsilon}{D} = A'\left(\frac{\sigma}{E}\right)^{\eta'} \qquad (3)$$

where: E-modulus of elasticity, Q_D-activation energy for self diffusion, and D-the diffusion coefficient. Sherby has shown that these equations give good correlations of creep data on many materials, and recently Lund and Nix (75) and Malu and Tien (76) have established that if equation (2) is applied to data on OD alloys, Q_c=Q_D, apparently suggesting that anomalously high values of Q_c arise from the temperature dependence of E and the large value of η' in these alloys. Lin and Sherby (77) have subsequently shown that equation (3) gives good correlation of data for a number of ODS alloys.

CHAPTER III

Plan of Work

Germane to this research effort was concern regarding the high cost of processing OD Ni-base superalloys. In this program an OD Ni-base superalloy was cost effectively developed and processed, and then tested and characterized. The latter included ascertaining the oxide particle size, shape, and distribution, the oxide (and γ') volume fraction, and their respective interparticle spacings, the grain size, grain shape and grain texture, and the intragranular structure.

The plan of this experimental work was as follows:

A. Powder Processing and Alloy Development
   1. Selection of fully alloyed powders
   2. Attrition of powders
   3. Ball milling to distribute oxides
   4. Consolidation of composite materials

B. Evaluation of Structure and Properties
   1. Evaluation of as-extruded structures
   2. Phase extraction and analysis
   3. Texture determination
   4. Thermomechanical processing
      a. Swaging and annealing
      b. Recrystallization
         i. Standard annealing treatment

ii. Zone aligned polycrystals (ZAP)

i.e. directional recrystallization

5. Mechanical property determination

a. Room temperature tensile tests

b. Room temperature hardness and elevated temperature stability

c. Elevated temperature stress rupture strength

d. Stress rupture fracture

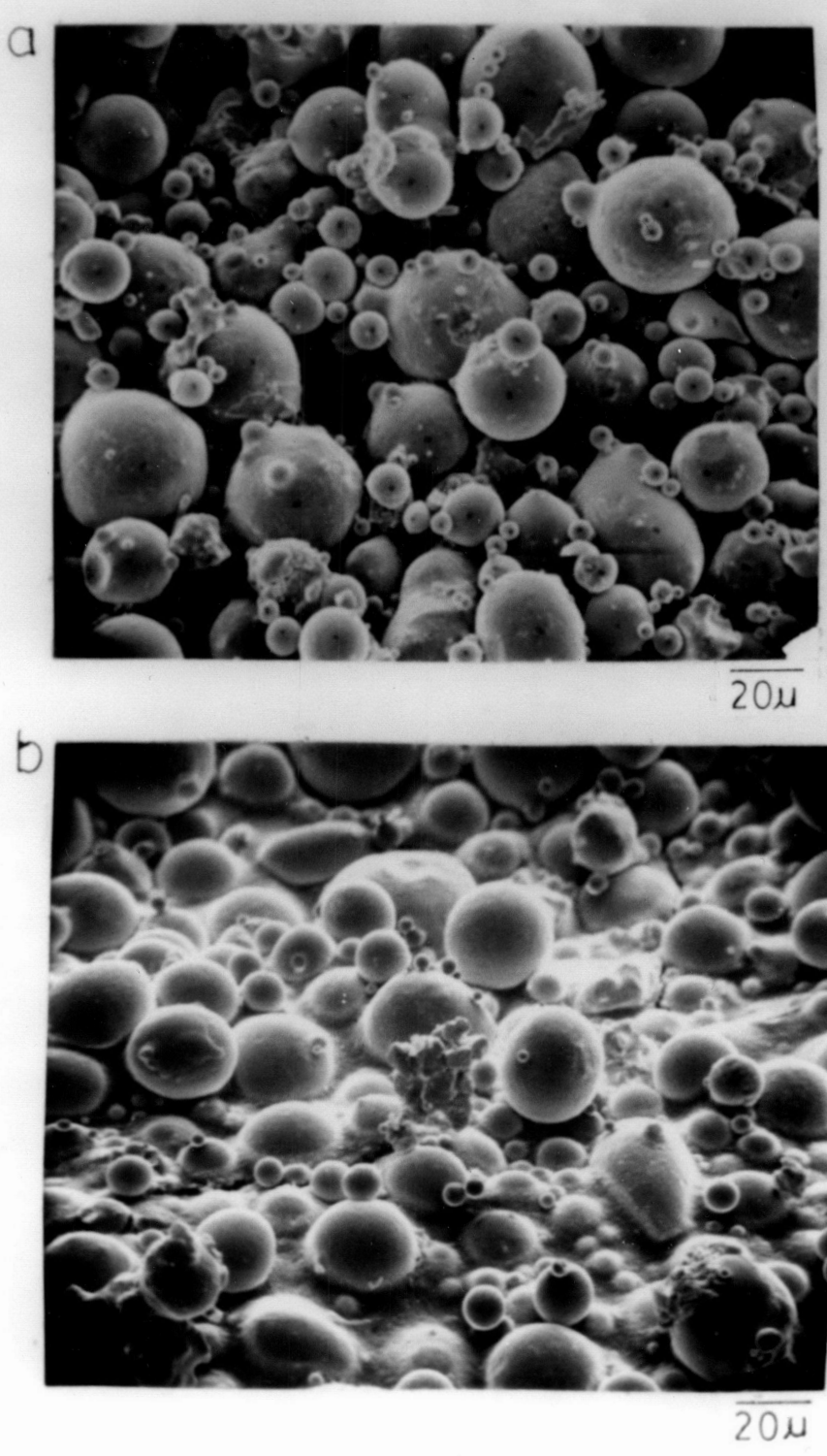

Figure 1. Scanning electron micrograph showing as-received powders: a. rapidly solidified powders (RSP) from Homogeneous Metals and b. RSP from Osprey Metals.

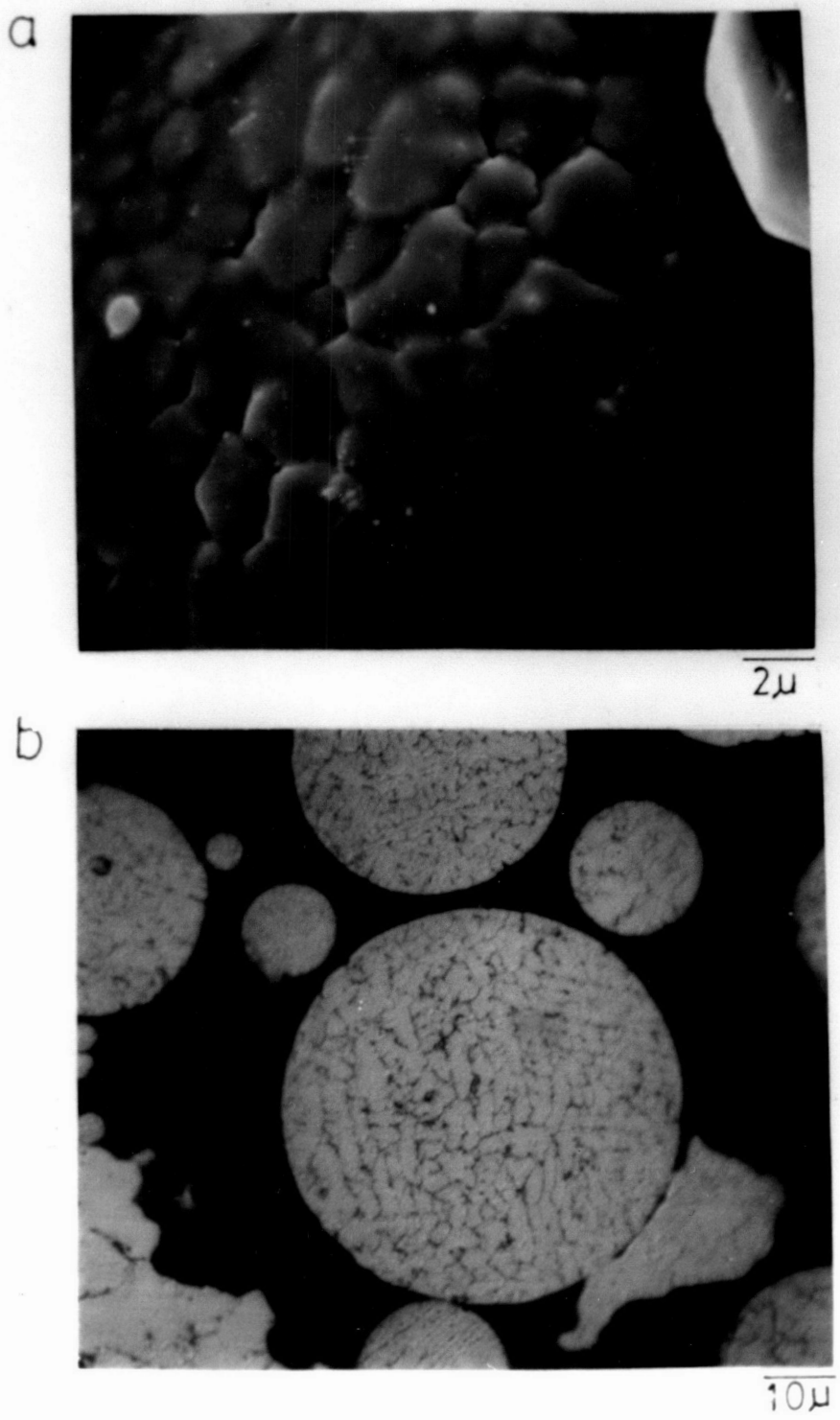

Figure 2. Photomicrographs showing dendrite arm spacing (DAS) of a. RSP powder particle from Homogeneous Metals and b. RSP powder particles (cross section) from Osprey Metals.

CHAPTER IV

EXPERIMENTAL PROCEDURE AND RESULTS

A. Powder Processing and Alloy Development

1. Selection of fully alloyed powders

Atomized prealloyed powders were supplied by Homogeneous Metals Inc. (vacuum atomization through hydrogen solubility) and Osprey Metals Limited (inert gas, RS). The chemical compositions are given in Table I as alloys N-1 to N-5. Alloys N-4 and N-5 represent the chemical composition of IN-100, and were supplied by Osprey Metals. The powders were manufactured from master remelt cast ingots via vacuum atomization (Homogeneous) and inert gas atomization (Osprey). Microstructures of typical as-received powders are shown in Fig. 1. With dendrite arm spacings (DAS) of 4μ (Homogeneous) and 3.5μ (Osprey) (Fig. 2), solidification rates (S.R.) were estimated to be 10^2°K/S<S.R.<10^3°K/S (98).

2. Attrition of powders

Attrition was accomplished in a 1 gallon Szegvari attritor. For all cases the attritor chamber was charged with 3 litres of ethanol (denatured alcohol), 11 kilograms of 3 mm. (0.12 inch) hardened steel balls, and 250 grams of alloy powders. The attritor

TABLE I

Compositions (Weight Percent) of Alloys Studied

Alloy		Ni	Co	Cr	MO	Al	Ti	W	Ta	C	B	Zr	Fe	Y_2O_3
N-1	(1)	bal	20	20	10	0.5	-	-	-	-	-	-	-	
N-2	(1)	bal	20	20	10	.5	-	-	-	-	-	-	-	1.18
N-3	(1)	bal	20	20	10	0.5	-	-	-	-	-	-	-	2.76
N-4	(2)	bal	14	10	3	5.5	4.6	-	-	0.16	0.012	0.04	0.1	-
N-5	(2)	bal	14	10	3	5.5	4.6	-	-	0.16	0.012	0.04	0.1	1.2
IN853	(3)	bal	-	20	-	1.2	2.4	-	-	-	0.007	0.07	-	1.3
MA6000E	(3)			15	3.5	4.5	2.0	4.0	2.0		0.01	0.15		1.1

(1) Solid solution strengthened: Homogeneous Metals Co.

(2) IN-100 type; γ-γ' with about 60 v/o γ': Osprey Ltd.

(3) Mechanically alloyed M-MO materials: Benjamin et al (19,81,83)

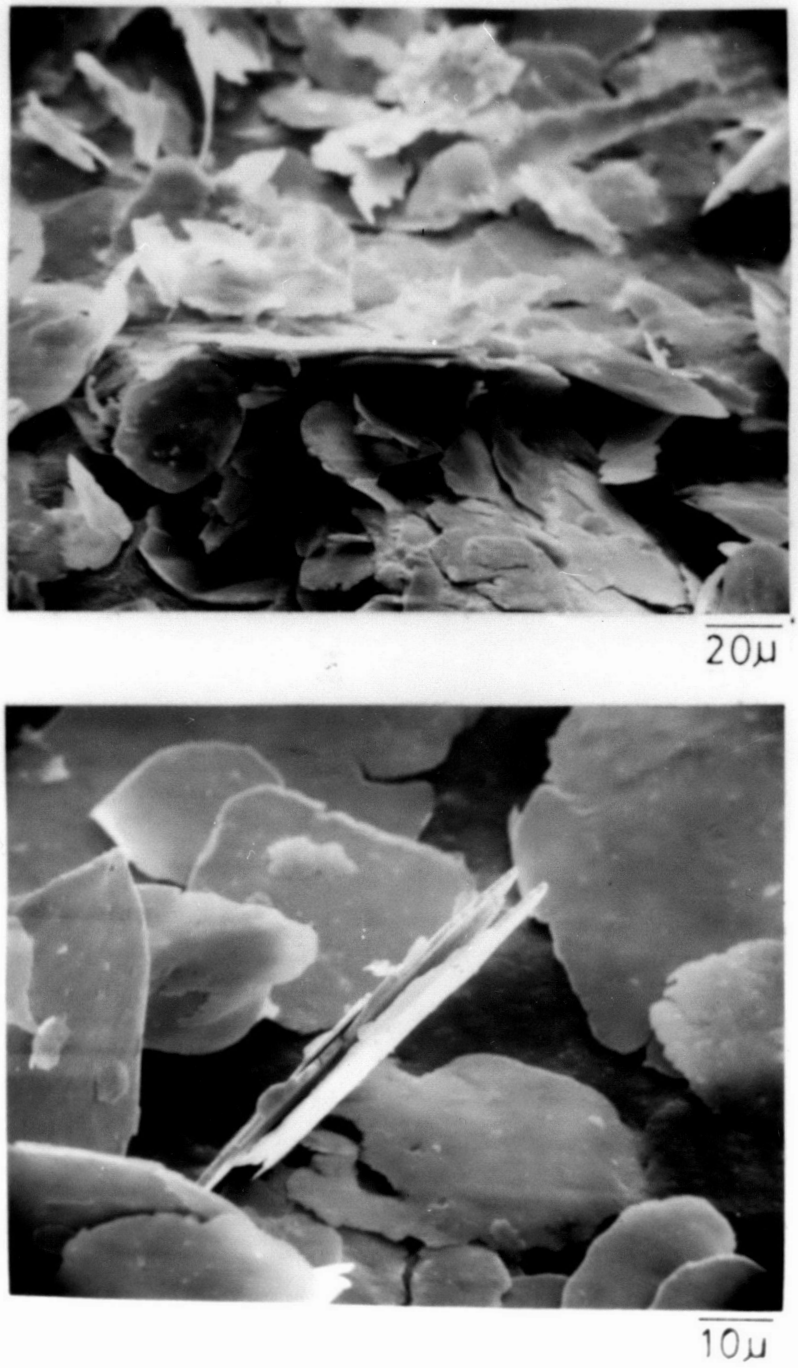

Figure 3. SEM micrographs of flakes resulting from seventeen hours of attrition.

operated at a rate of 250 rpm. Comminution time was varied with starting powder particle sizes. The details are given in Table II.

TABLE II

Processing Parameters-Comminution

Alloy	Powder Particle Size (μ)	Comminution Time (Hours)	Flake Thickness (μ)
N-1	<44	17	≤1.5
N-2	<75	20	≤1.5
N-3	50-104	36	≤1.0
N-4	<75	20	≤1.5
N-5	<44	17	≤1.5

Fig. 3 shows the shape and thickness of powder flakes after attrition.

Comminution of powders to flake was carried out for the following reasons:

a. Flaking effectively increased the surface area.

b. Attriting (in air) facilitates surface oxidation of aluminum, chromium and titanium.

c. The oxide interparticle spacing could be controlled more efficiently during the subsequent ball-milling stage.

Alloys N-1 and N-4 were utilized as-surface-oxidized alloys, i.e. no additional processing was required after attrition. The Al_2O_3 and Cr_2O_3 formed during

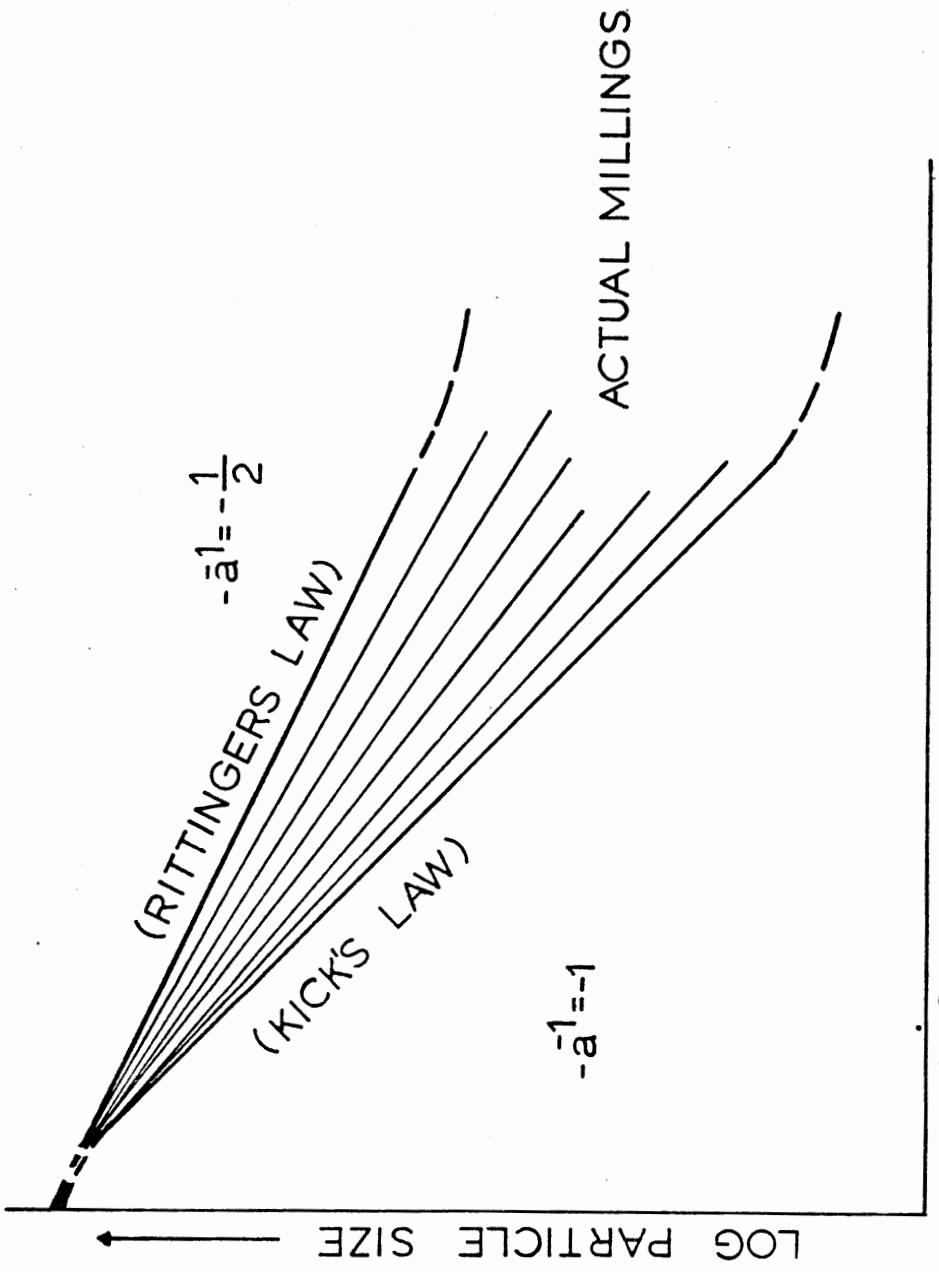

Figure 4. Ball milling of brittle materials (84).

comminution acted as the dispersoid for these alloys.

After attrition the balls were separated from the slurry by screening. The slurry was then transferred to an open plastic container and the flakes were allowed to settle, after which time the alcohol was decanted. Upon evaporating the residual alcohol, the flakes were transferred to a container filled with argon and stored in a high purity argon dry box.

3. Ball milling to distribute oxides

Theories for ball milling expressing the particle size as a function of milling time were given by Rittinger in 1867 and Kick in 1885. They assumed completely brittle materials. The theories were based on the idea that the energy supplied from the falling balls is absorbed as a corresponding increase in surface energy only (84). The energy balance can be described by the following equation:

$$E = c \cdot d^{-\alpha} \text{ or}$$

$$\log d = \frac{1}{\alpha} \log c - \frac{1}{\alpha} \log E \qquad (4)$$

where E-energy input, d-particle size, and c and α are constants. Consideration of log d versus log E, or that energy input increases linearly with time, a plot of log d versus log time should yield a straight line with slope $= -\frac{1}{\alpha}$. As shown in Fig. 4, the results from actual ball millings of brittle materials give

straight line segments for log d versus log t with slopes between $-\frac{1}{\alpha} = -\frac{1}{2}$ (Rittinger's law) and $-\frac{1}{\alpha} = -1$ (Kick's law) or $1 \leq \alpha \leq 2$. Coarse, brittle materials approach Kick's law, and brittle, very fine materials approach Rittinger's law in their behavior.

When ball milling ductile materials such as metals, the energy supplied from the falling balls is transformed into strain energy and heat as well as an increase in surface energy. None of the aforementioned theoretical considerations with respect to particle size are valid. However, as an approximation, after a significant milling time, the particles of ductile materials might be cold worked so much that they behave more like brittle materials.

That there are differences in processing rates between an attritor and a ball mill has been demonstrated (15). It is conceivable that processing times for this work could have been reduced further by using a high energy attritor. The conventional ball mill was selected because one was available, whereas a suitable attritor was not.

The maximum operating speed of a conventional ball mill is a function of the diameter of the mill. Centrifugal pinning of balls and powder charge occurs at higher rotating speeds (85). This pinning

phenomenon must be avoided at all times during operation. A ball mill rate of 55 rpm. was determined to be suitable.

Ball milling of alloys N-2, N-3 and N-5 was performed to incorporate a fine dispersion of the inert added oxide (Y_2O_3). A 17.5 cm. (6.9 inch) diameter by 26 cm. (10.2 inch) long ball mill was used. The hardened steel balls varied in diameter from 1.3 cm. (0.5 inch) to 3.2 cm. (1.25 inch). The ball mill was operated dry in an inert atmosphere at 55 rpm. More details of processing operations are tabulated below:

TABLE III

Processing Parameters-Ball Milling

Alloy	Final Flake Size(μ)	v/o Y_2O_3 (added)	Oxide Size(Å)	Charge(g)		Time of Milling (h)
				Flaked Alloy	Y_2O_3	
N-2	≤1.5	2	200-400	1010	12	60
N-3	≤1.0	5	same	250	8	48
N-5	≤1.5	2	same	250	4	48

Ball milling was a batch type operation. Typically, in the case of N-5, the charge of 250 grams of alloy flakes with 4 grams of Y_2O_3 were added to the mill, which was sealed (airtight), evacuated and then filled with argon. A positive overpressure was used in all cases. During grinding, the balls, when at the top

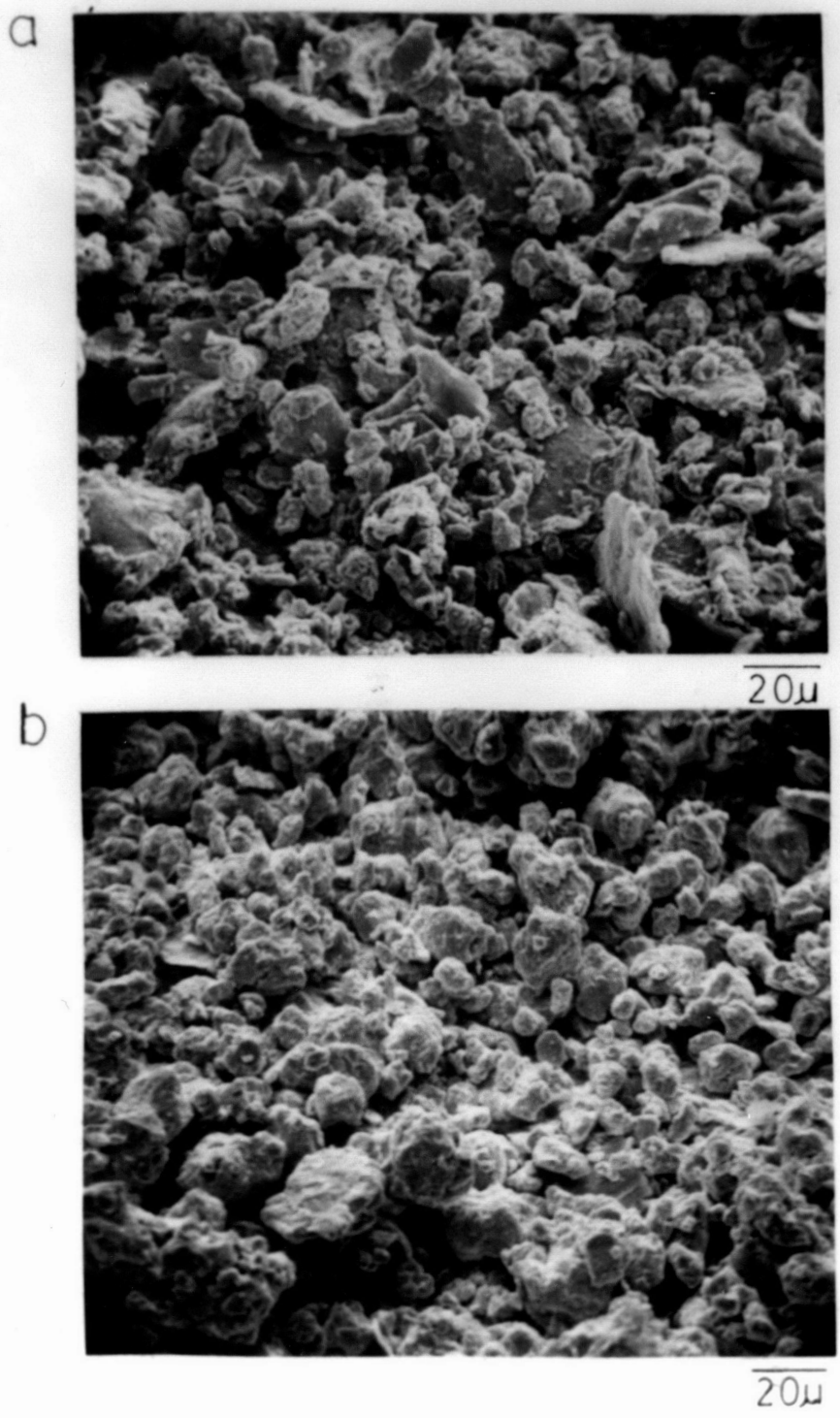

Figure 5. a. N-5 ball milled for 36 hours.
b. N-5 ball milled for 48 hours.

C

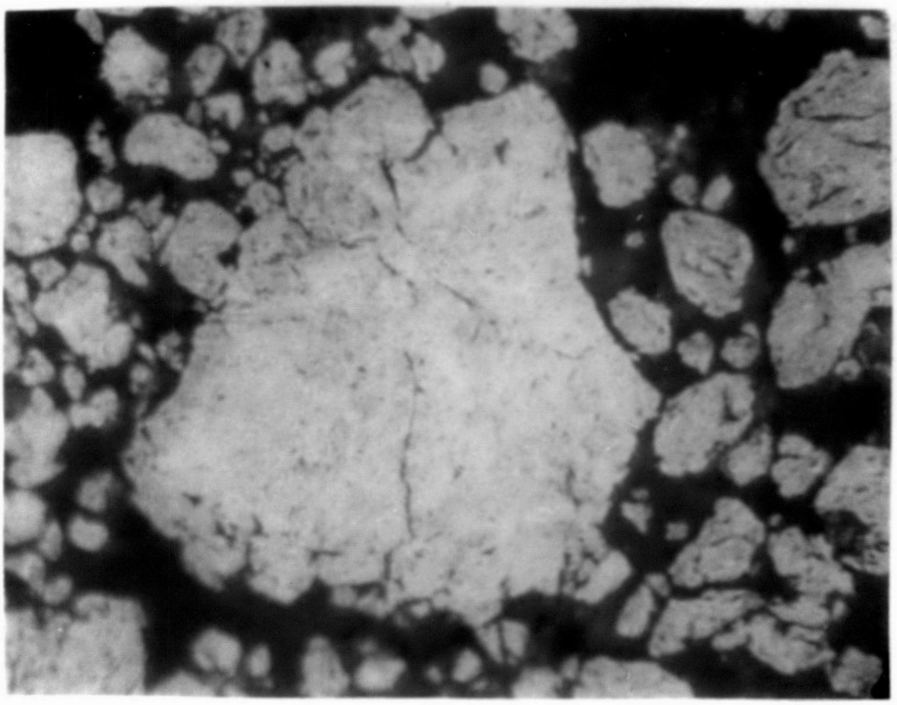

Figure 5. c. Cross section of composite N-5 particle.

of the mill revolution or when in their most thermodynamically unstable state, would fall. The falling balls on impacting other balls and flakes transfer their kinetic energy into strain energy and heat. This resulted in continuous kneading, agglomeration, fracturing and rewelding of the flaked material. Fig. 5 shows the agglomerated composite particles after 36 and 48 hours of ball milling; also shown is a cross section of one 48 hour ball milled flake. Voids are very apparent in this cross section, giving direct evidence of fracturing and rewelding process.

4. Consolidation of composite materials

A two step densification process of cold compaction and hot extrusion at Nuclear Metals Corporation was followed in order to approach 100% density after processing. In each case the blended material was transferred to a mild steel can. The material was compacted in increments of approximately 250 grams each at about 551.6 MN/m^2 (80 ksi). The density of the billet after cold compaction was approximately 80%. A plate with an evacuation tube was hermetically sealed to the open end of the can. The billet was then leak checked and evacuated. Table IV lists the important parameters relevant to evacuation and extrusion.

TABLE IV

Processing Parameters-Evacuation and Extrusion

Evacuation				Extrusion		
					Maximum Force (tons)	
Alloy	Temp (°C)	Time (h)	Pressure (μ)	Temp (°C)	Upset	Running
N-1	650	24	0.5	1093	800*	800
N-2	650	24	0.5	1066	290**	280
N-3	650	24	0.5	1149	290**	280
N-4	650	4	30.0	1149	330**	275
N-5	650	4	30.0	1149	300**	270

* 1500 ton press

** 300 ton press

B. Evaluation of Structure and Properties

1. Evaluation of the as-extruded structures

The general characteristics of the extruded alloys were determined by x-ray diffraction, optical and electron microscopy. The density was determined by water immersion. This consisted of obtaining the difference between the weight of a specimen in air and water, and dividing the difference into the product of its weight in air and the density of water. Table V lists important structural characteristics of each alloy.

TABLE V

Structural Characteristics of Nickel-Base Alloys

	N-1	N-2	N-3	N-4	N-5
Ext. Temp. (°C)	1093	1066	1149	1149	1149
Ext. Ratio	30:1	20:1	16:1	16:1	16:1
Theo. Density (g/cc)	-	8.42	8.33	7.75	7.75
Density (g/cc)	9.06	8.51	7.82	7.92	7.99
% Theo. Density	-	101	94	102	103
Volume % Y_2O_3 (added)	-	2.0	5.0	-	2.0
Avg. Grain Size (μ)	2.1	0.41	0.38	0.62	0.43
Avg. Oxide Particle Size (μ)	0.108*	0.079	0.034	0.112*	0.021
Grain Aspect Ratio (GAR)	2-3	1-2	1-2	1-2	1-2
IPS (μ)**	0.438	0.319	0.121	-	0.105

* Oxide particles from surface oxidation primarily in the form of Al_2O_3.

** $IPS = \left(\frac{A - n\,\bar{a}_p}{n} \right)^{1/2}$

where $\bar{a}_p = \frac{\pi \bar{d}^2}{4}$

$\bar{d}$ = mean oxide particle size

A = area on micrograph

n = number of oxide particles in A

*** Density of IN100 (cast)

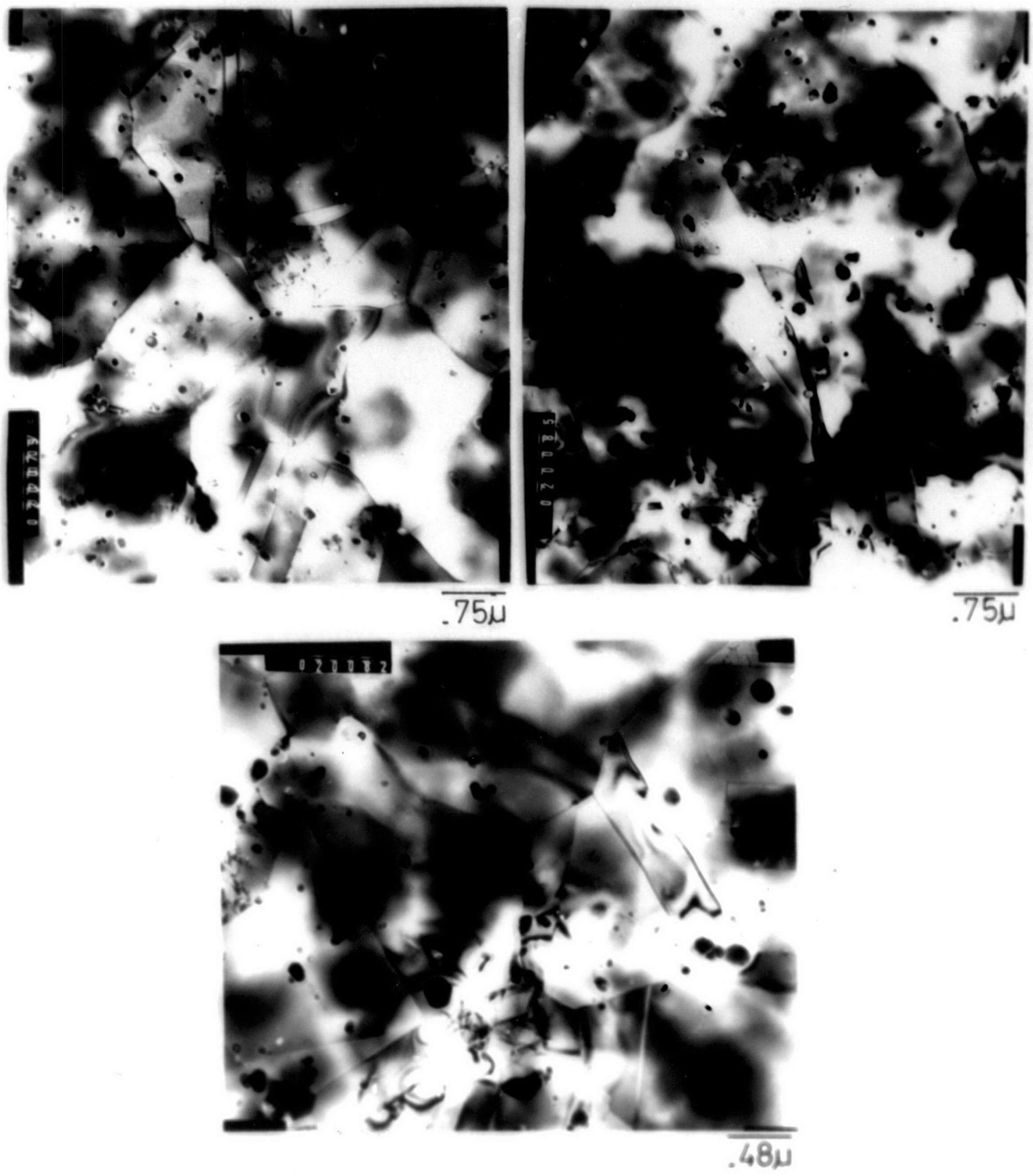

Figure 6. Transmission electron micrographs showing as-extruded structure of alloy N-1. There is evidence here for a recrystallized structure.

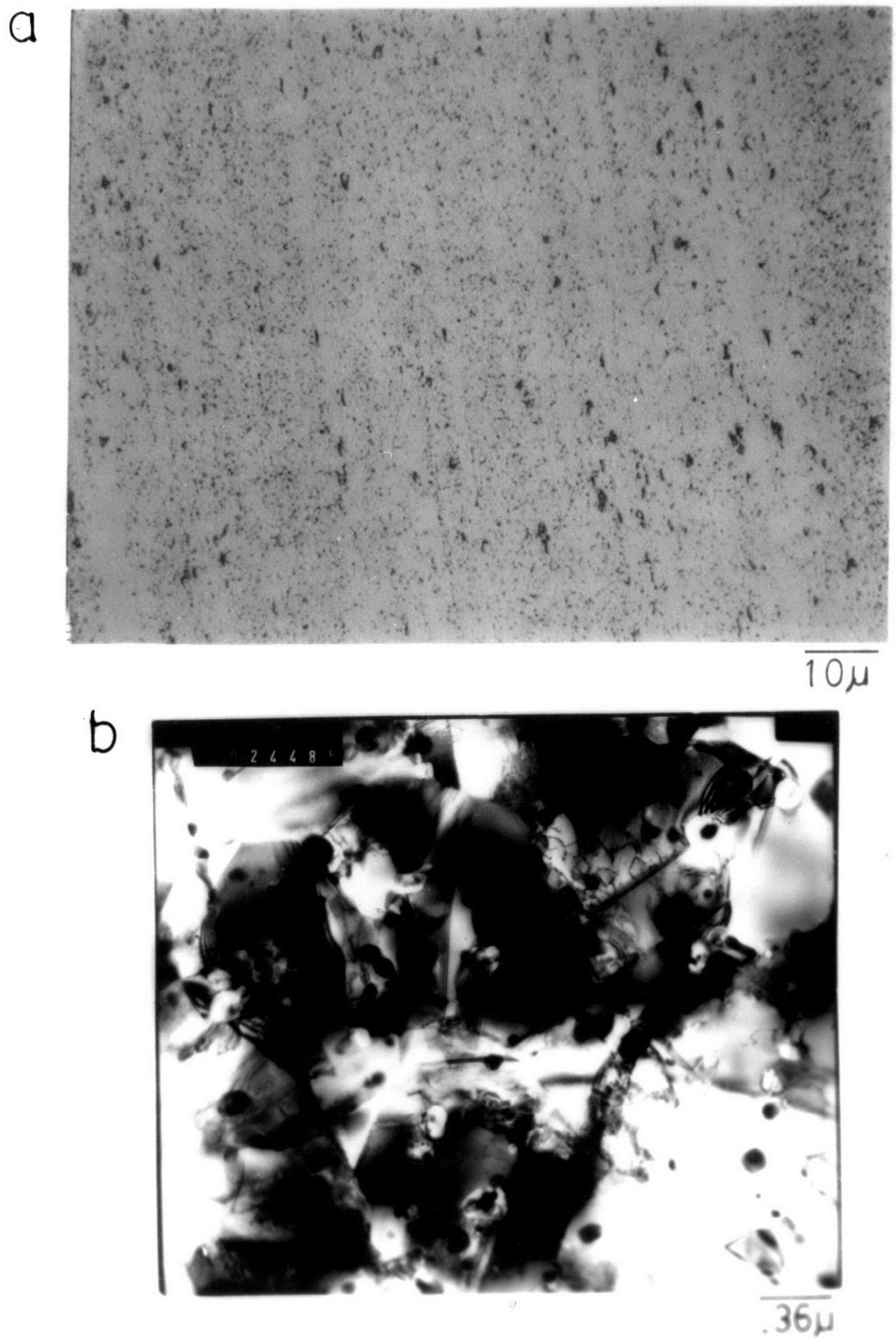

Figure 7. a. Photomicrograph of alloy N-2 (as-extruded).
b. TEM micrograph of alloy N-2 showing as-extruded grain structure.

C

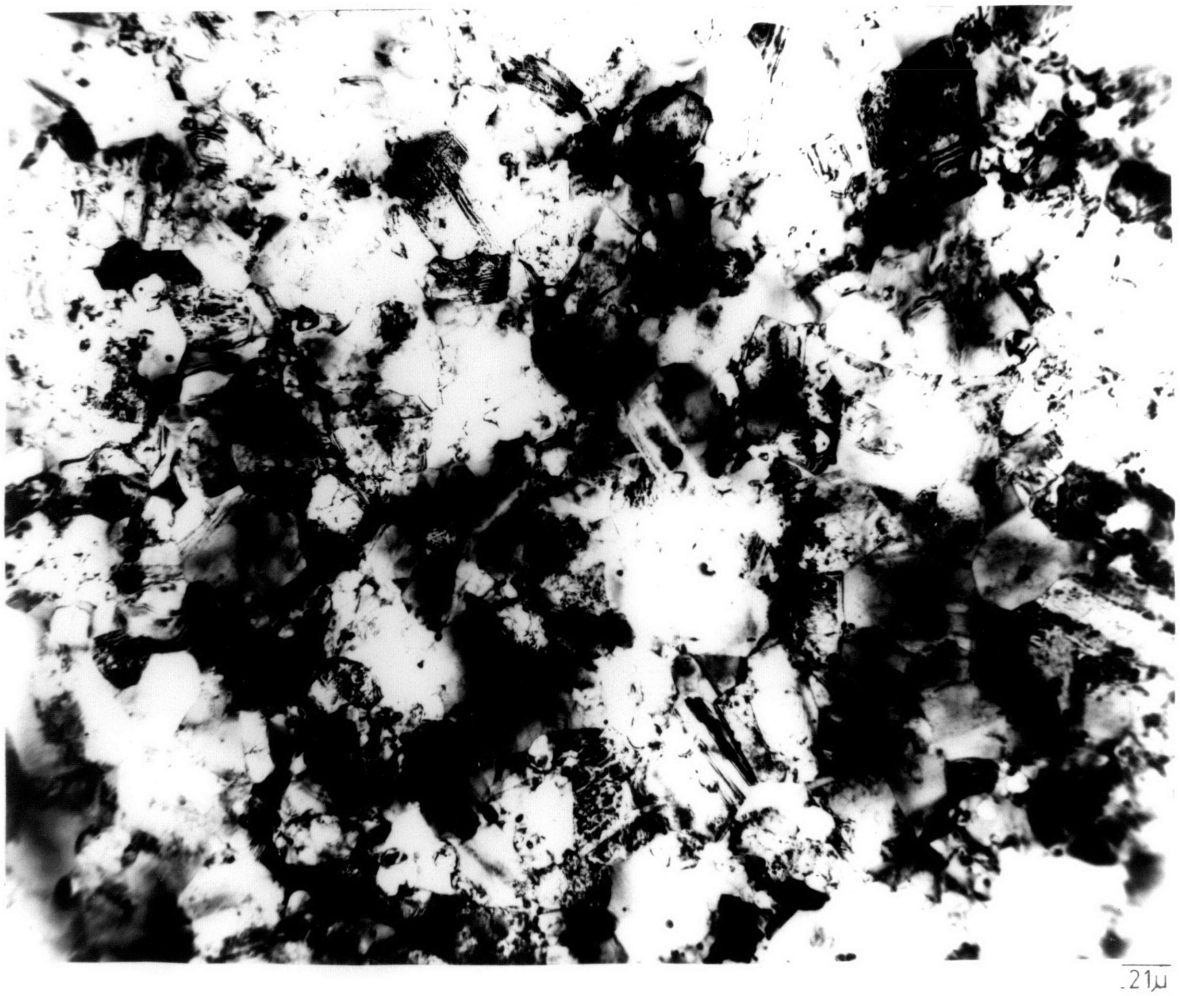

FIGURE 7. c. TEM MICROGRAPHS OF ALLOY N-2 SHOWING HIGHLY WORKED STRUCTURE.

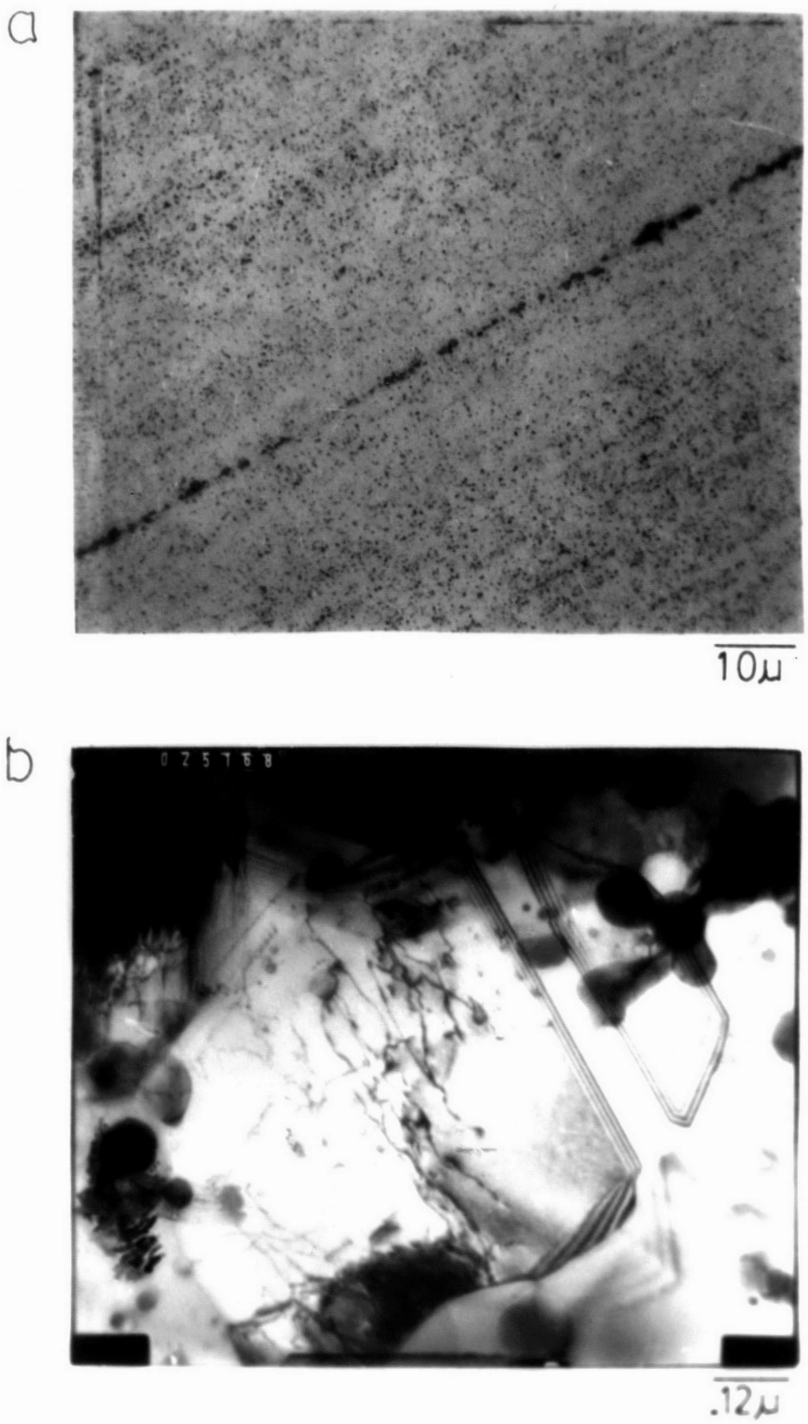

Figure 8. a. Photomicrograph of alloy N-3 (as-extruded).
b. TEM micrograph of alloy N-3 showing as-extruded structure.

C

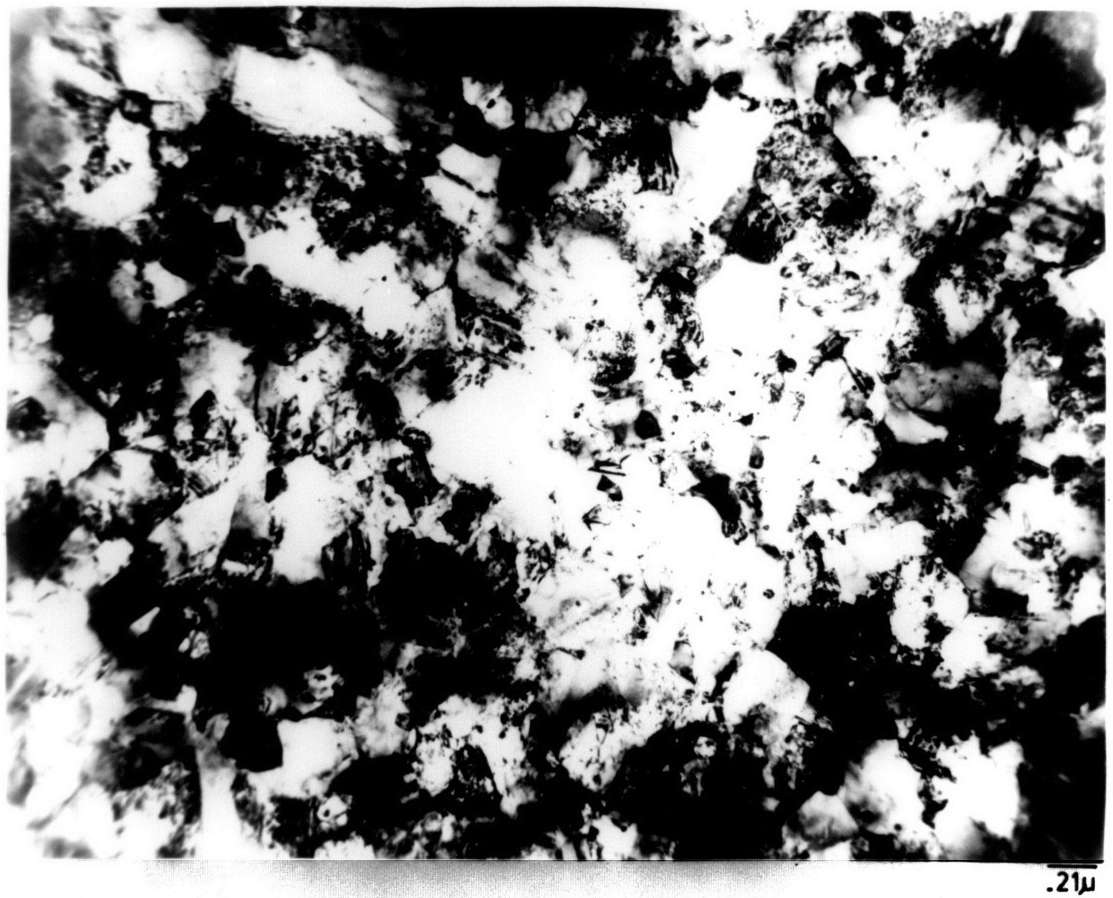

FIGURE 8. c. TEM MICROGRAPH OF ALLOY N-3 SHOWING HIGHLY WORKED STRUCTURE.

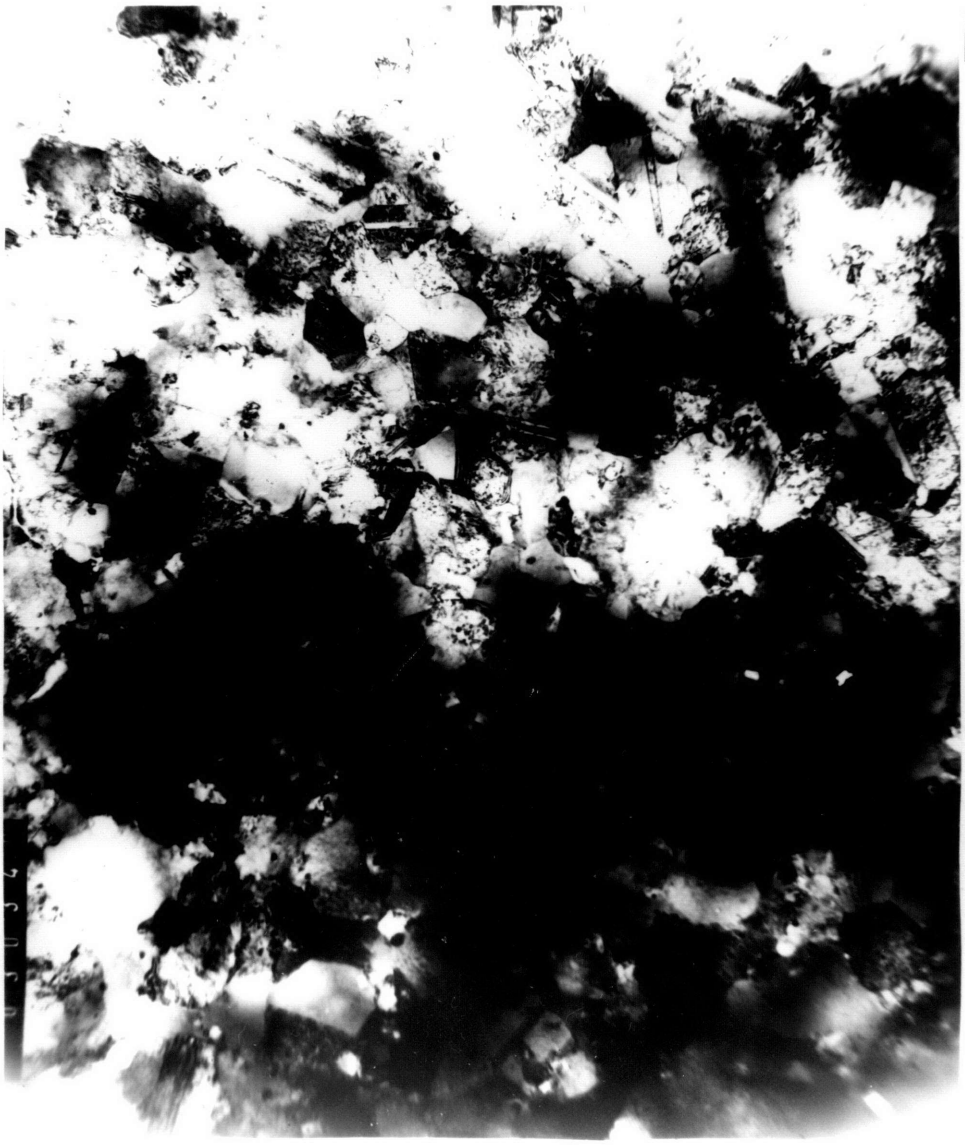

FIGURE 9. A. TEM MICROGRAPH OF ALLOY N-5 SHOWING AS-EXTRUDED STRUCTURE (TRANSVERSE).

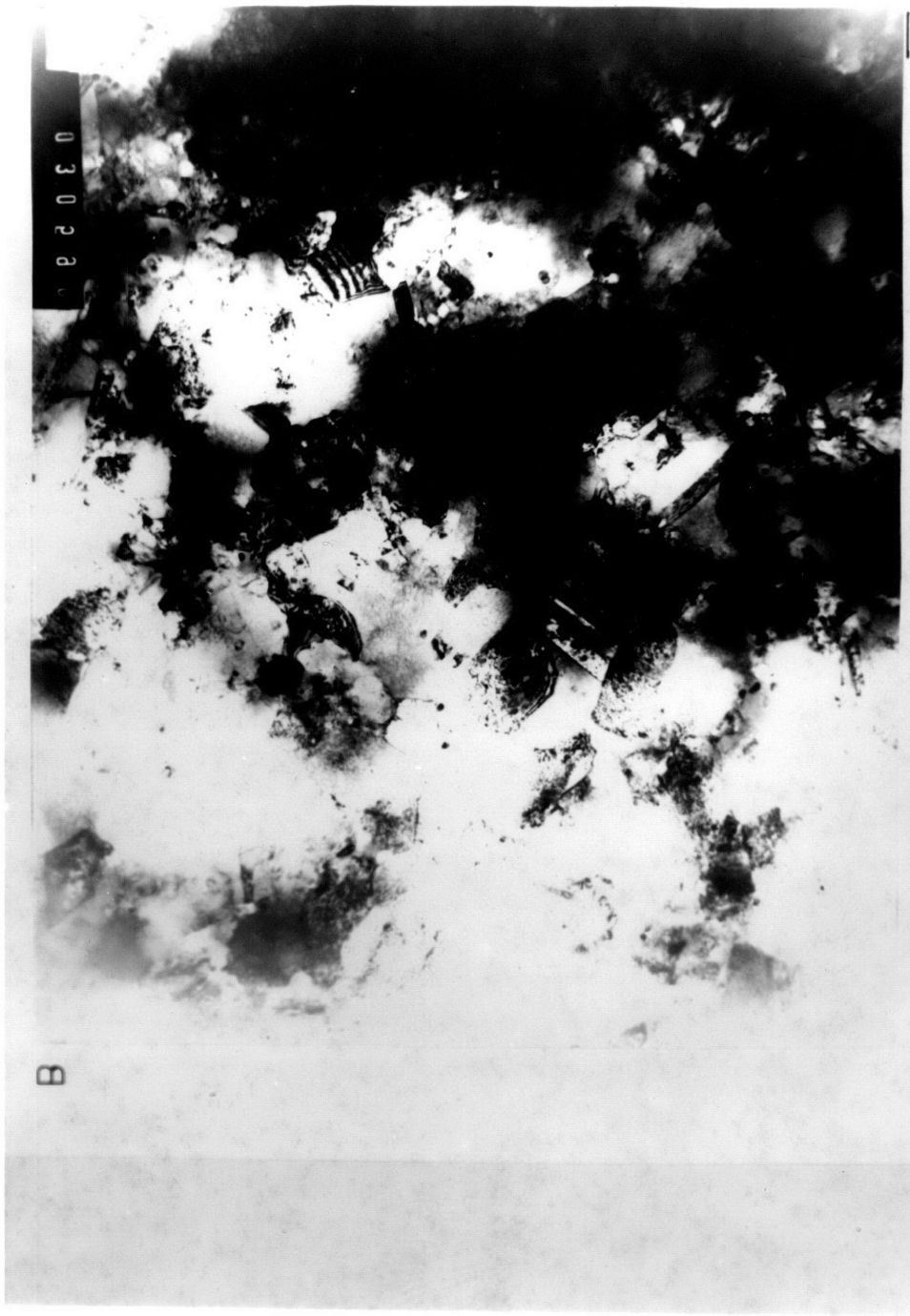

FIGURE 9. B. TEM MICROGRAPH OF ALLOY N-5 SHOWING AS-EXTRUDED STRUCTURE (LONGITUDINAL).

The as-extruded structures are shown in Figs. 6 to 9. The optical photomicrographs were taken on an American Optical Metallograph. A Phillips EM-300 Electron Microscope operating at 100 kv was used to examine the alloys' grain and particle size and dislocation structure. The details of the specimen preparation for optical and transmission electron microscopy (TEM) are given in Appendix I.

With the exception of alloy N-1, the grains of extruded bars were of submicron dimensions and essentially equiaxed. Some reports (81,83,92) have claimed that ODS alloys recrystallize after extrusion to submicron sized equiaxed grains yet retaining a high dislocation content. It is difficult to conceptualize a fully recrystallized structure having a high dislocation content. The TEM micrographs of Figs. 7 through 9 show highly deformed substructures with submicron grains containing a dislocation substructure. The dislocation content was estimated to be greater than 10^9 cm/cm^3. These alloys did not recrystallize during extrusion. Alloy N-1, Fig. 6, did recrystallize. Grain sizes as measured by the linear intercept method yielded values of 2.1μ for N-1, 0.4μ for N-2, 0.4μ for N-3, 0.6 for N-4 and 0.4 for N-5.

Transverse to the high angle grain boundaries in alloys N-2, N-3 and N-5 are bands of dislocation

FIGURE 10. A. TEM MICROGRAPH OF AS-EXTRUDED N-2 SHOWING CELL FORMATION.

FIGURE 10. B. TEM MICROGRAPH OF AS-EXTRUDED N-5 SHOWING CELL FORMATION.

tangles which define a cellular type of structure. Cell sizes vary as follows: alloys N-2: 0.013μ to 0.042μ, N-3: 0.013 to 0.042μ, and N-5: 0.009μ to 0.039μ. Fig. 10 demonstrates that cell walls along the grain's high angle boundary are thin and well defined while the cell walls across the grain width are thick and irregular. Like most oxide dispersion stabilized alloys, the processing route of alloys in this work has a major effect on the particle distribution and on the structure of the matrix. As illustrated in Figs. 6 to 9, the particle distribution is heterogeneous on both the optical and the electron microscope scales.

Since cost effective processing and development of an ODS alloy was a major objective of this project, it is imperative at this point to sketch laconically the sequence of steps that led to its development. Accomplishing this depended on the oxide particle size being close to ideal as possible, 100°A/200°A, but sizes up to 1000°A are acceptable, and an IPS less than 0.2μ. Particular attention was given to these parameters. Alloy N-1 was processed via surface oxidation with no Y_2O_3 added. Unsatisfactory oxide particle distribution based on IPS, particle size (PS) and content resulted in poor mechanical properties. A decision was made to add 2% Y_2O_3 to the alloy, and

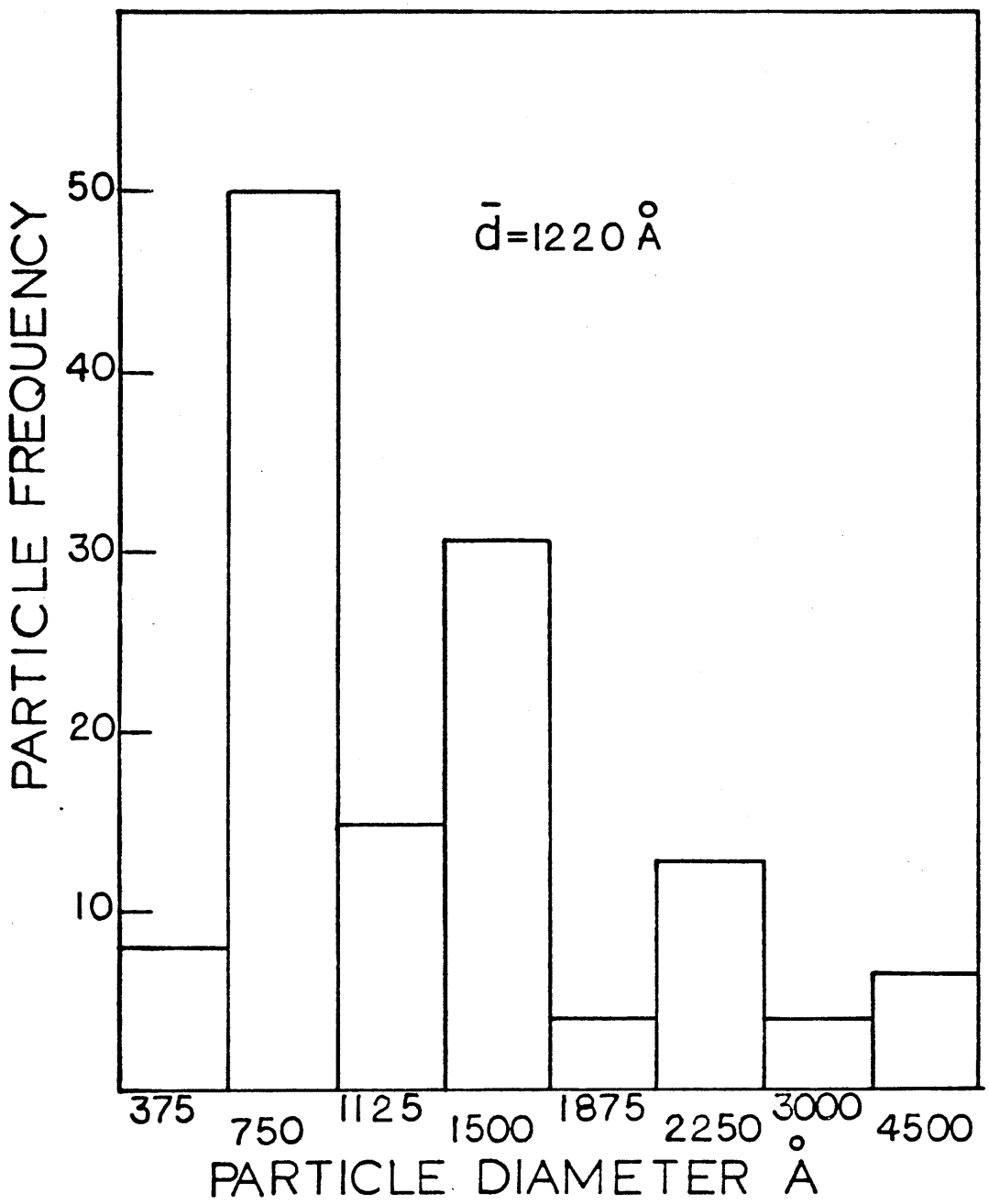

Figure 11, A-1. Particle size distribution of experimental alloy N-1.

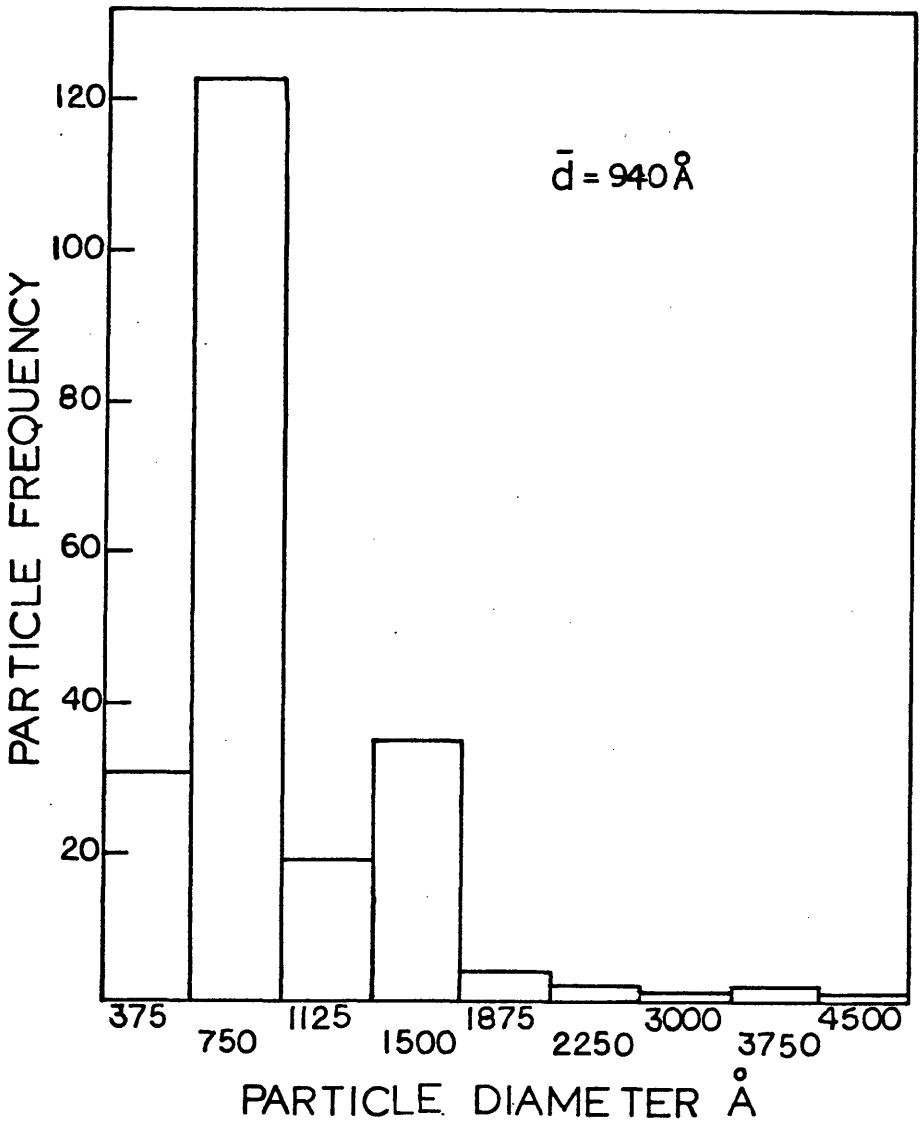

Figure 11, A-2. Particle size distribution of experimental alloy N-1.

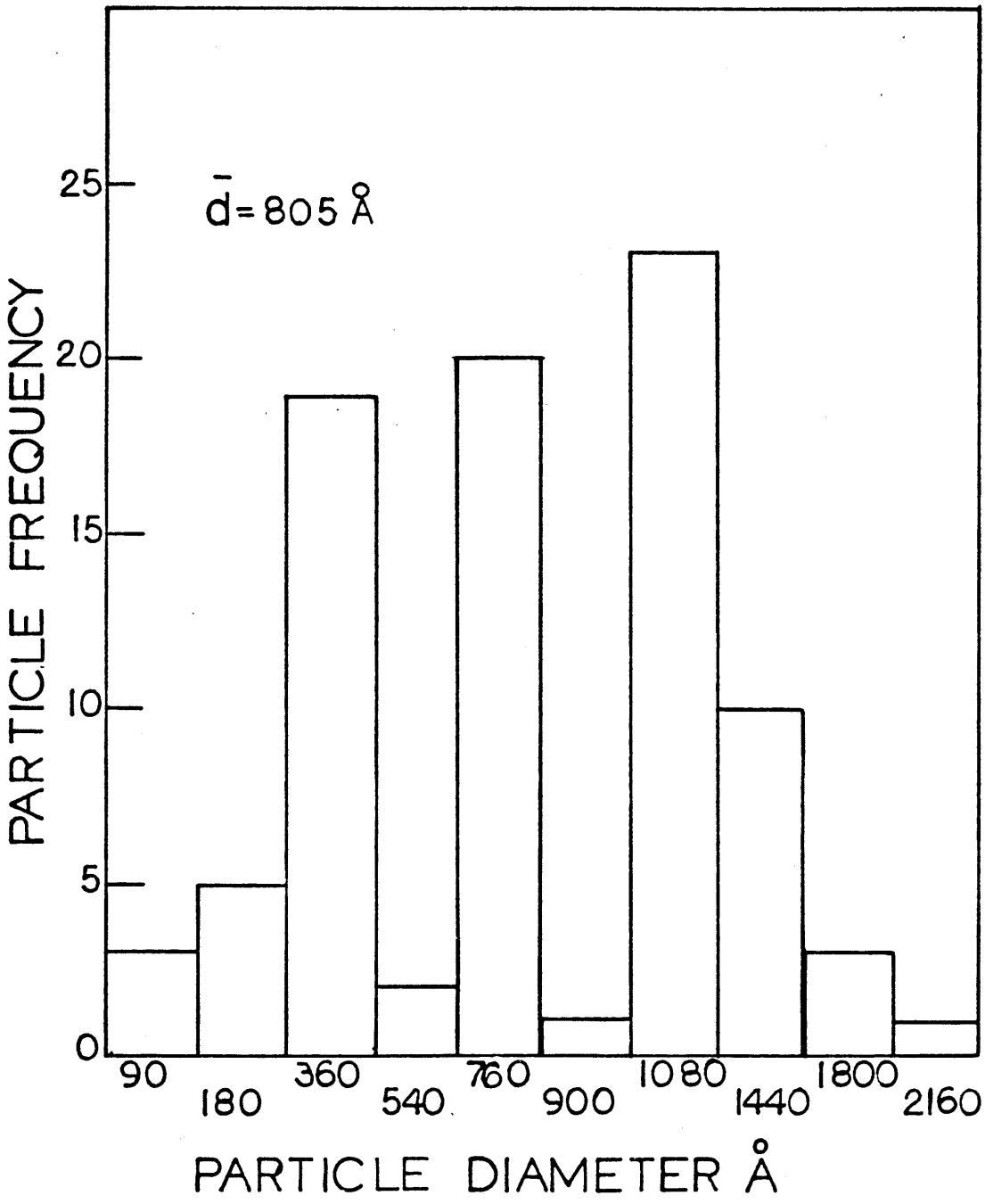

Figure 11, B-1. Particle size distribution of experimental alloy N-2.

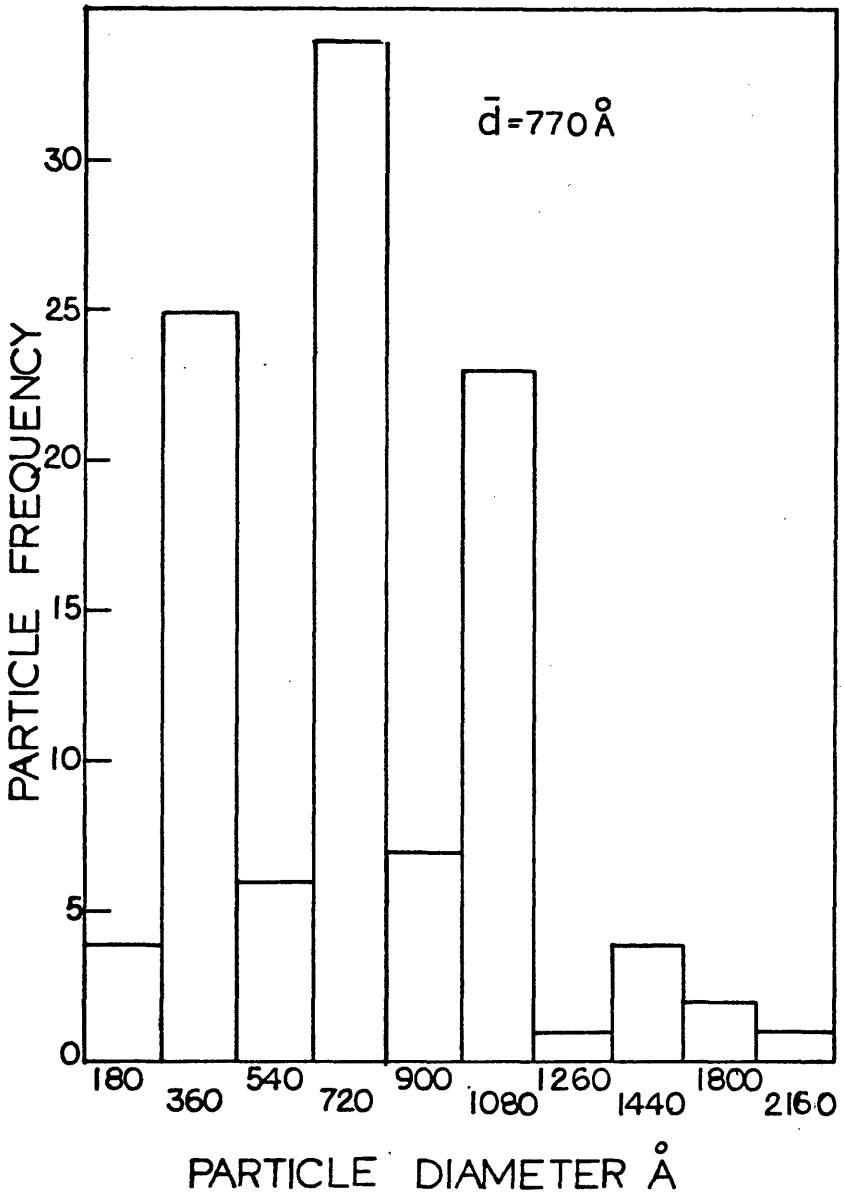

Figure 11, B-2. Particle size distribution of experimental alloy N-2.

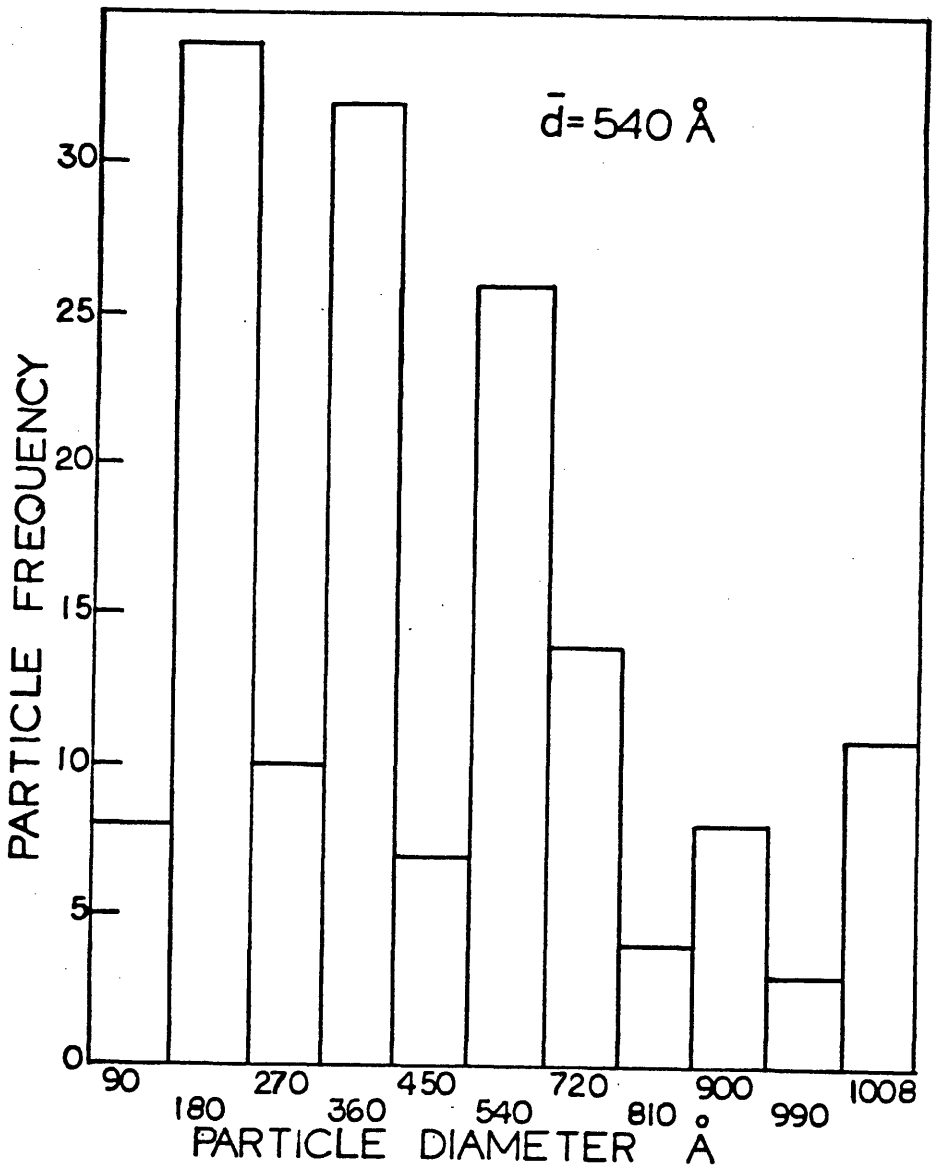

Figure 11, C-1. Particle size distribution of experimental alloy N-3.

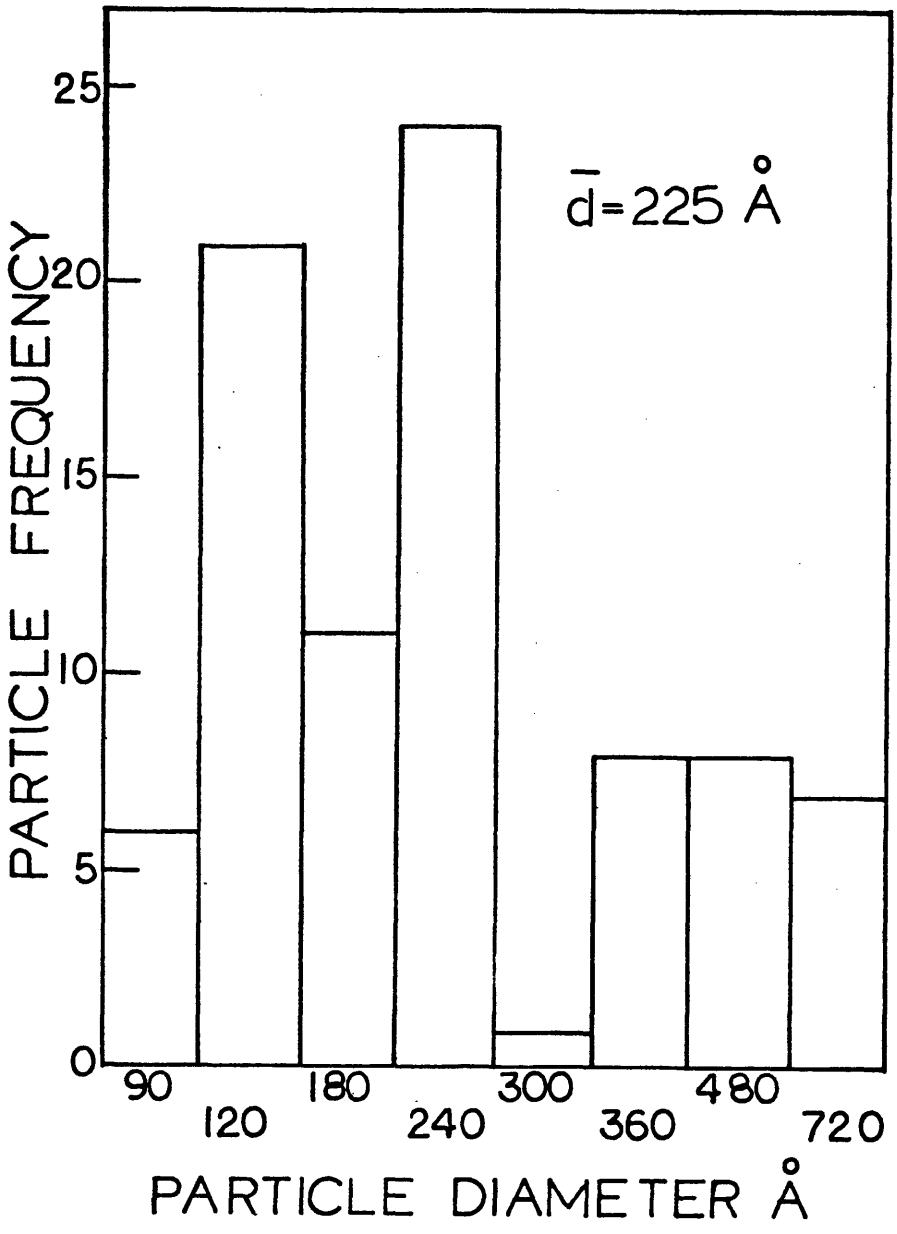

Figure 11, C-2. Particle size distribution of experimental alloy N-3.

identified as alloy N-2. Characterization of this alloy indicated somewhat more satisfactory structural parameters. Both the IPS and PS decreased, however, the former was still greater than 0.2μ. Next, 5 v/o Y_2O_3 was added to alloy N-3; this resulted in satisfactory particle size (PS) and distribution. The wide range of particle sizes are illustrated quantitatively in Fig. 11 and Table VI. Alloy N-5 with 2 v/o Y_2O_3 added was then processed.

TABLE VI

Range of Oxide Particle Sizes

Alloy	Amt. of Y_2O_3 Added (v/o)	Analyzed Amt. of Y_2O_3 (w/o)	Range of Particle dia.(°A)	Avg. Particle dia.(°A)	IPS (°A) (calc.)
N-1	-	0.9*	375-4500	1080	4380
N-2	2.0	2.24	90-2160	790	3195
N-3	5.0	2.96	90-1008	341	1210
N-4	-	0.85**	-	-	-
N-5	2.0	2.65	120-400	210	1050

* Oxide from surface oxidation and analyzed as primarily Al_2O_3

** Oxide from surface oxidation estimated by point counting

2. Phase extraction and analysis

It has been demonstrated that γ', oxides, carbides and borides can be extracted by using anodic dissolution in an electrolyte consisting of 1% ammonium sulfate and 1% citric acid in water (86). When separating γ' by anodic dissolution it is desirable to work in a region of high current density so that a reasonably large amount of sample can be collected for analysis in a comparatively short period of time. Golubtsova (87) showed that an effective separation of γ' from Russian superalloys can be made at high current density by separating at potentials about, or slightly above, that required for oxygen evolution (1.1 to 1.4 volts versus a calomel electrode). A calomel electrode consists of a mercury electrode in a molar potassium chloride solution saturated with mercurous chloride. Its potential is 0.28 volts versus a standard hydrogen electrode at 25°C.

Extractions were carried out on all alloys except N-4. For N-5, the γ' precipitates were extracted from a sample of heat treated (1260°C/2 hr/AC + 1232°C/0.5 hr/AC + 954°C/2 hr/AC + 843°C/24 hr/AC) bar. The technique used was the same as that discussed in reference (86): the 6.35 cm (0.25 inch) thick sample was suspended from the anode by a fine platinum wire spot welded to the sample, while platinum foil (88)

served as the cathode. The electrolyte volume was about 300 ml., the current during electrolysis was 250 ma., the potential was 1.1 volts versus a calomel electrode in the same solution. Electrolysis was continued for 3.5 hours at ambient temperature. The w/o γ' (contaminated) was determined to be 61.74%.

Some γ' particles remained on the surface of the specimen, but most of it was recovered from the electrolyte by centrifuging. Carbides and oxides were also extracted with the γ'. A correction was made for this contamination by performing a second anodic dissolution on N-5 using 300 ml. of a 10% hydrochloric acid-methanol solution containing 1% tartaric acid (86). A current of 250 ma. was applied for 4.5 hrs. at room temperature. The w/o contaminant calculated was 2.65%. Hence the γ' content was determined to be 59.1 w/o.

For alloy N-3, the weight percent oxides calculated was 2.96. Values for N-1 and N-2 are given in Table VI. The type of oxides extracted was determined on a Diano diffractometer using nickel filtered copper kα radiation of 35 kv and 15 ma. X-ray diffraction patterns showed the oxides to be Y_2O_3, Al_2O_3 and Y-Al-O_3 and insignificant amounts of Cr_2O_3 and $Cr_{23}C_6$ were also observed to be present. γ, O and η-Al_2O_3 were observed by Schilling and Grant (89)

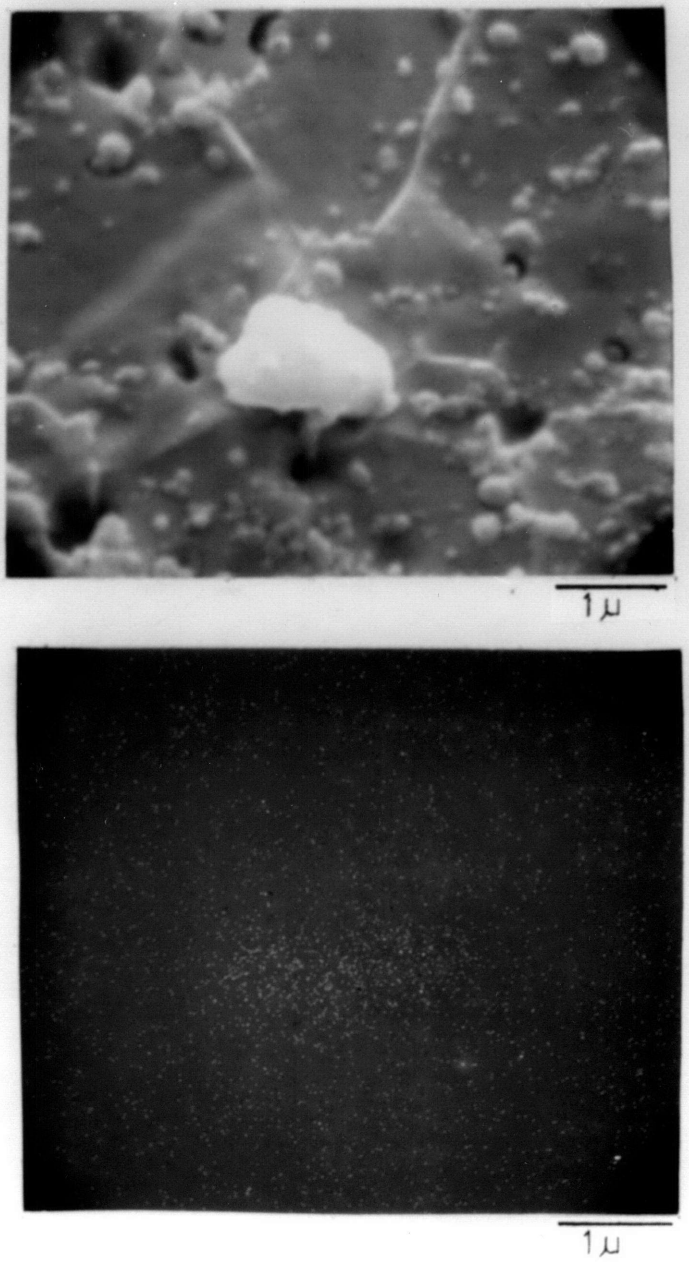

Figure 12. X-ray mapping of particle believed to be Al_2O_3 particle in alloy N-1.

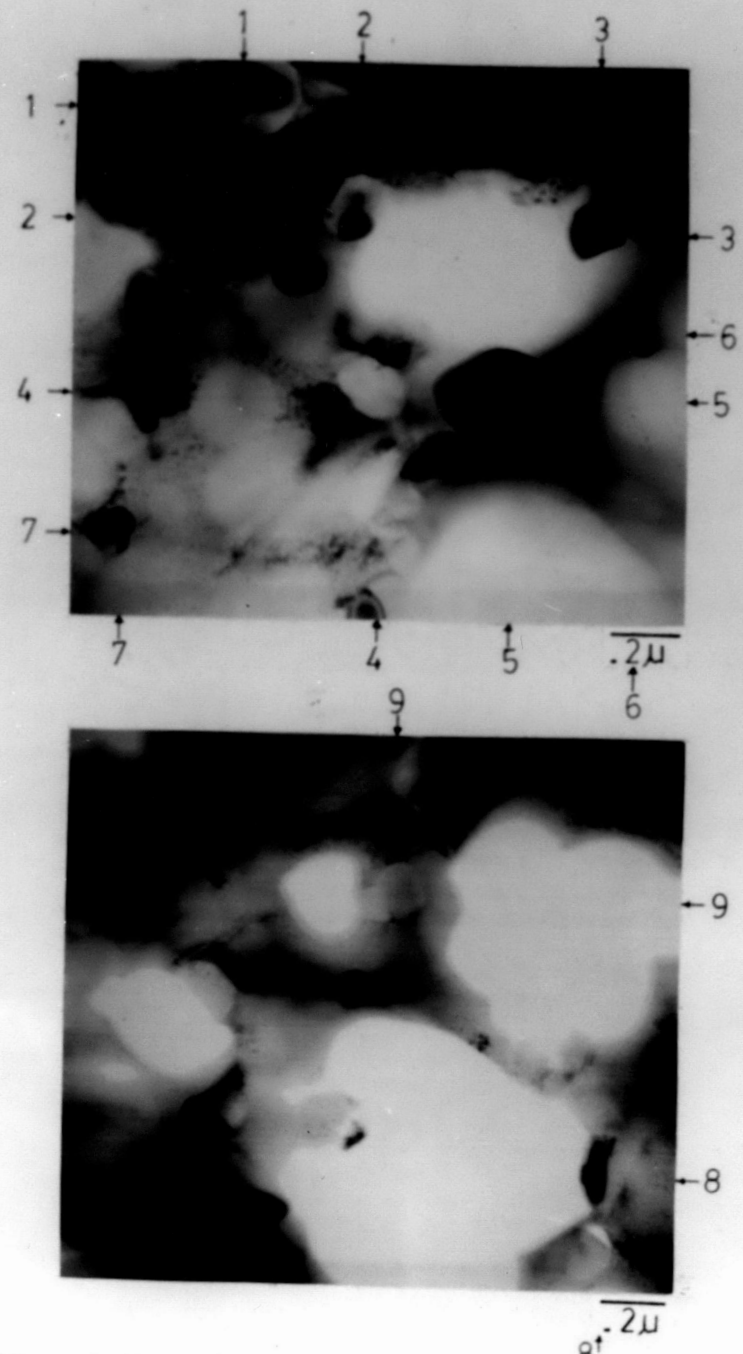

Figure 13. Showing particles identified by STEM analysis: 1-Al_2O_3, 2-Y_2O_3, 3-Y_2O_3, 4-Y-Al-O_3, 5-Al_2O_3, 6-Y_2O_3, 7-Y_2O_3, 8-Y_2O_3, 9-Ni_3Al.

A

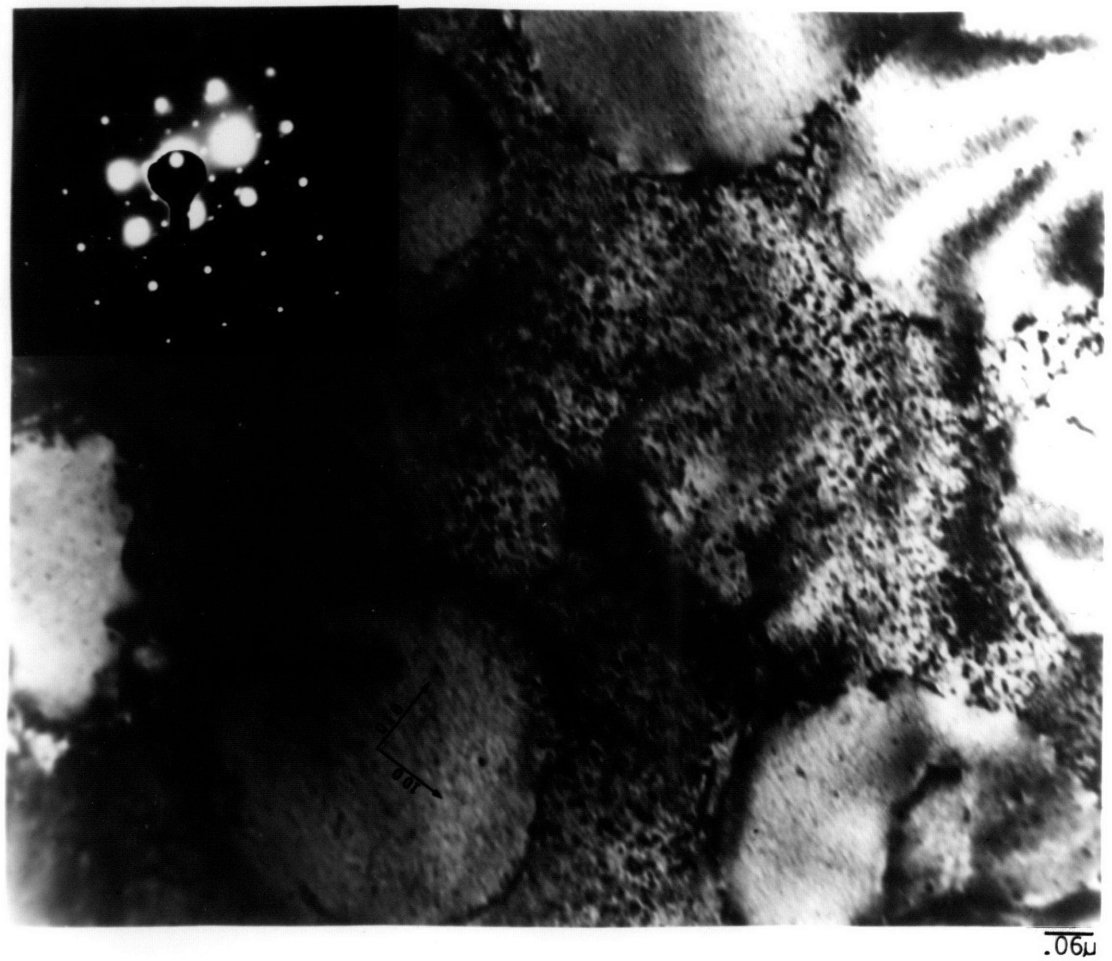

FIGURE 14. A. TEM MICROGRAPH OF γ' PRECIPITATES OF ALLOY N-5 AFTER ZAP TREATMENTS WITH CORRESPONDING (100) ZONE SAD PATTERN SHOWING γ' SUPERLATTICE REFLECTIONS.

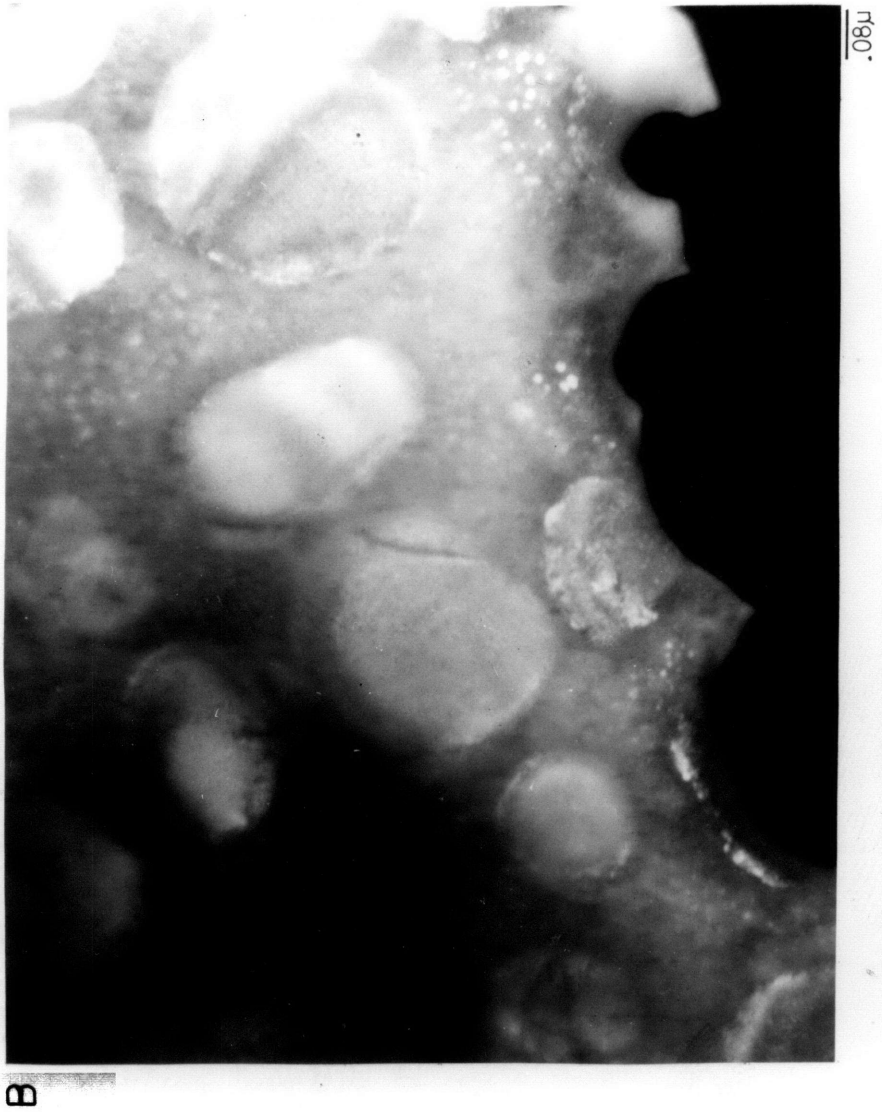

FIGURE 14. B. DARK FIELD USING A (100) γ' SUPERLATTICE REFLECTION.

FIGURE 14. C. DARK FIELD USING γ- γ' (200) REFLECTION, SHOWING CONTRAST RESULTING FROM DIFFERENCES OF ORIENTATION OF DIFFERENT PARTICLES INSIDE FOIL.

in their surface oxidized Cu-Al-Al_2O_3 and Cu-Ni-Al_2O_3 alloys. Schilling (57) observed complex Y-Al-O compounds in surface oxidized Fe-Cr-Al-Y_2O_3 alloys. Fig. 12 is a SEM micrograph of one of the many particles in alloy N-1 determined to be an alumina particle by x-ray mapping. An important observation here is the fact that fully alloyed powders can be attritor processed as a slurry in air without significant Cr_2O_3 contamination. Schilling's work (57) supports this fact. Furthermore, the high weight percent of γ' extracted is indicative of the absence of excessive oxidation of aluminum and titanium.

These findings were supported by scanning transmission electron microscopy (STEM) and TEM studies. STEM was used to identify particles in a way similar to the SEM. As shown in Fig. 13, particles were recognized as Al_2O_3, Y_2O_3 and Y-Al-O_3 type dispersoids. Gamma-prime (γ') precipitates were also identified. TEM studies revealed three types of precipitates. γ' precipitates, varying in size from 0.1μ to 0.4μ, are dispersed throughout the matrix. The latter are surrounded by hyperfine 200°A γ' particles. Both types of precipitates appear to have more or less spherical morphologies. These precipitates are displayed in Fig. 14. The micrographs are representative of alloy N-5 stress rupture

FIGURE 15. TEM MICROGRAPH OF EXTREMELY FINE PRECIPITATES INSIDE LARGER γ'.

tested at 1093°C. Other investigations (94) recognized a very coarse primary eutectic gamma prime that can reach several tens of microns, and that formed during solidification of powders. The subsequent heat treatments of this work effectively solutionized this coarse γ', reprecipitating finer γ' during aging at 843°C (1550°F).

Both fine and hyperfine γ' precipitates are coherent, and their LI_2 ordered structure introduces superlattice reflexions in the selected area diffraction patterns. This is shown in Fig. 14 for a (100) zone pattern. These precipitates have been identified in dark field TEM in Fig. 14 using a (100)γ' superlattice reflection.

Fig. 15 exhibits a uniform distribution of dark and extremely fine particles inside the fine γ'. This phenomenon has been characterized (94,95,96) as the precipitation of γ within γ' precipitates.

3. Texture determination

When metals with fcc structures are deformed by extrusion without the occurence of recrystallization, fiber textures are formed with (111) and (100) directions aligned close to the rod axis. X-ray diffraction studies with a Diano diffractometer using vanadium filtered chromium k_α radiation at 35 kv and 15 ma. revealed strong deformation textures for

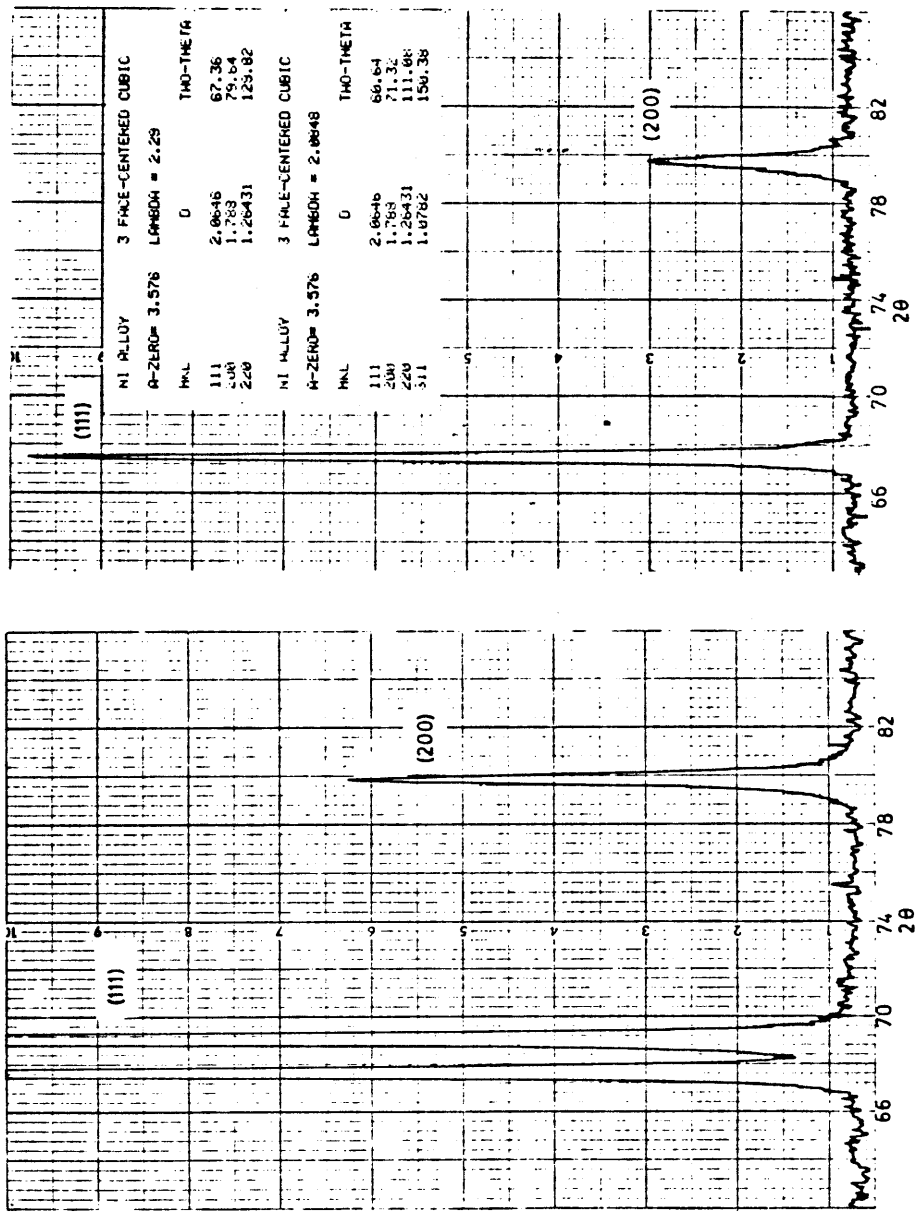

Figure 16. X-ray diffraction patterns showing duplex (111)-(100) fiber textures of alloy N-5: a. as-extruded b. as-extruded and annealed (1243°C/2 hour/AC + 1232°C/0.5 hour/AC + 954°C/ 2 hour/AC + 843°C/ 24 hour/AC).

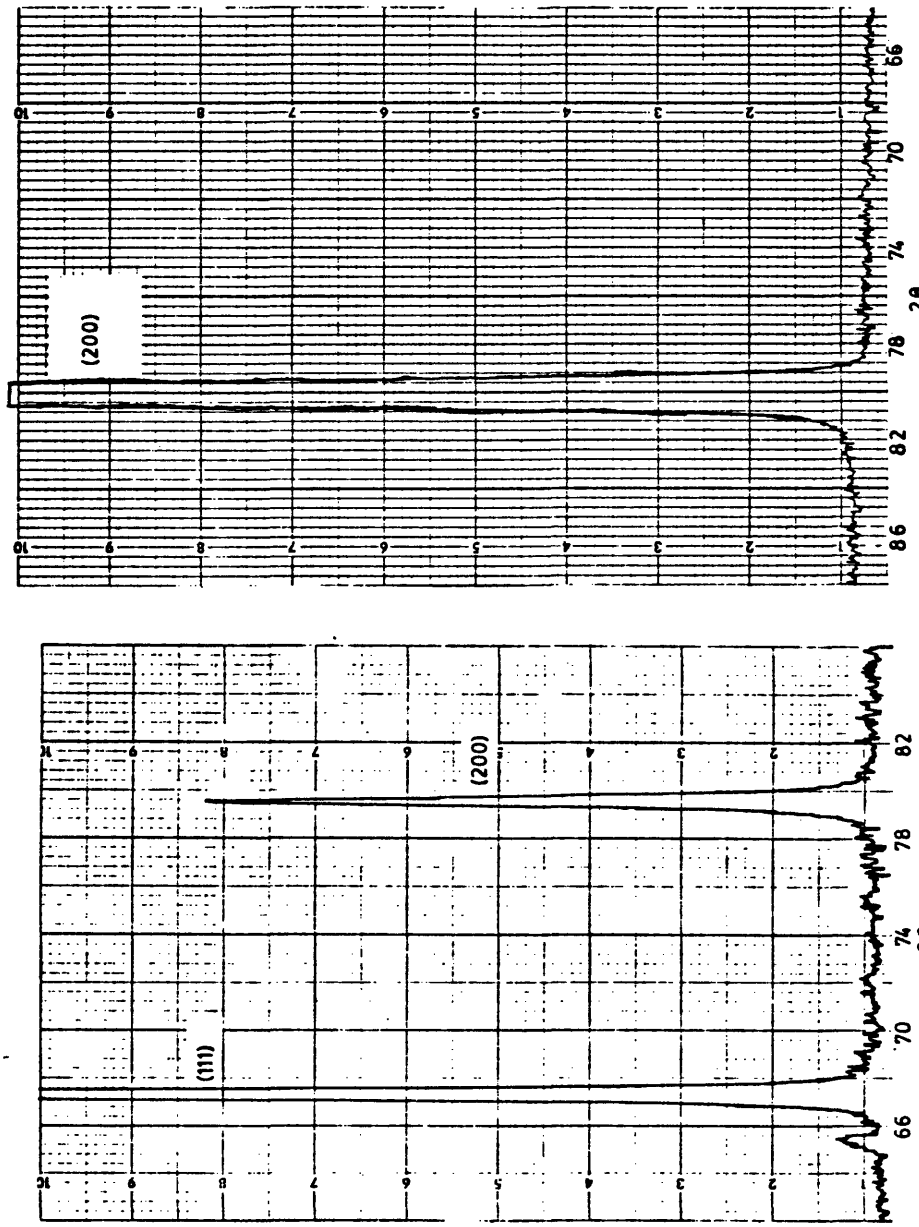

Figure 16. X-ray diffraction patterns of c. as-extruded N-3 showing duplex (1$\bar{1}$1)-(100) fiber texture and b. N-5, as-extruded and ZAP 7.6 cm. (3 inch)/hour at 1260°C showing strong (100) recrystallization texture.

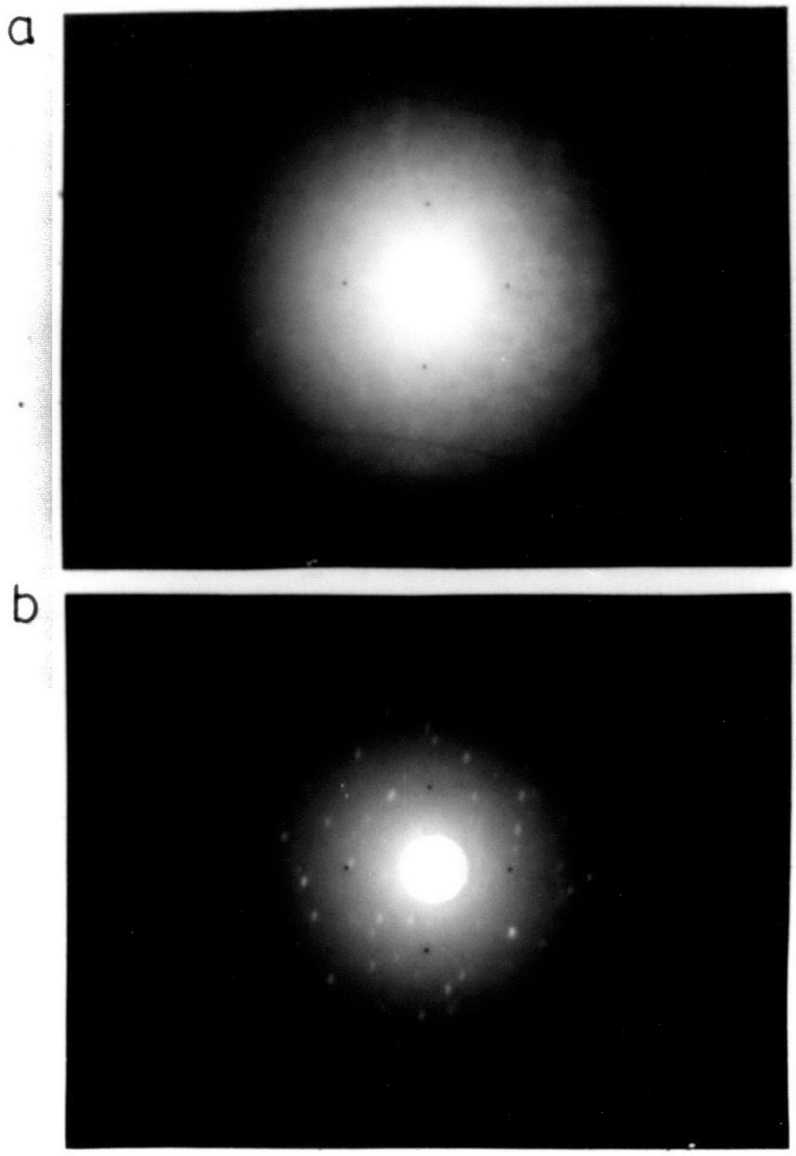

Figure 17. Laue back reflection patterns of: a. as-extruded alloy N-5 and b. N-5 ZAP at 7.6 cm. (3 inch)/hour showing (100) oriented crystal.

all the alloys in their as-extruded state. As depicted by diffraction patterns in Fig. 16, duplex (111)-(100) textures were observed, with the (111) texture dominating. Other investigations (4,43,53, 89,90) have found the (100) to be the major component in as-extruded dispersion stabilized Ni-base alloys. Wilcox and Hutchinson (89) and then Allen (55) found little or no deformation texture in extruded TD-Ni-Cr alloys, but after recrystallizing, either by ZAP or standard heat treatment, the latter found that his alloy contained a strong (100) recrystallization fiber texture.

Thermomechanical treatment of alloys N-1 and N-2 enhanced and stabilized the (100) texture at the expense of the (111).

Recrystallization by ZAP and by standard heat treatment, Fig. 16d, resulted in alloys with very strong (100) recrystallization fiber textures. Certainly (100) is a commonly observed recrystallization texture in fcc metals (91), and once formed it is stable during high temperature deformation.

Laue back reflection studies were made using vanadium filtered chromium k_{α} radiation. The specimen to film distance was 3 cm. A typical pattern of the as-extruded alloy N-5 is shown in Fig. 17a. The faint but broadened diffraction line indicated belongs to the

(110) reflection with $2\theta = 129.82$. Diffraction lines belonging to the strong (100) and (111) reflections ($2\theta = 79.64$ and 67.36, respectively) do not show up since their 2θ values are acute angled. All the extruded alloys had unresolved k_α doublets. This fact is taken as evidence of cold worked structures with high amounts of stored energy. Identical back reflection patterns were obtained from several grains of ZAP product, one of which is shown in Fig. 17b. After applying the method for orienting a single crystal (93) to this pattern, the crystal orientation was determined to be (100).

4. Thermomechanical processing

a. Swaging and annealing

Thermomechanical processing involved swaging with intermediate anneals with the final step being swaging. The intent was to determine how this in turn affects mechanical properties. The amount of deformation introduced during swaging was based on reduction-in-area compared to the initial as-extruded diameter. This was accomplished by swaging at room temperature; the intermediate anneals were carried out for 1 hour at various temperatures between 750°C (1382°F) and 1260°C (2300°F). Each as-extruded alloy was initially swaged with no anneals until cracking at its ends ensued. Alloys N-1 and N-2 were invest-

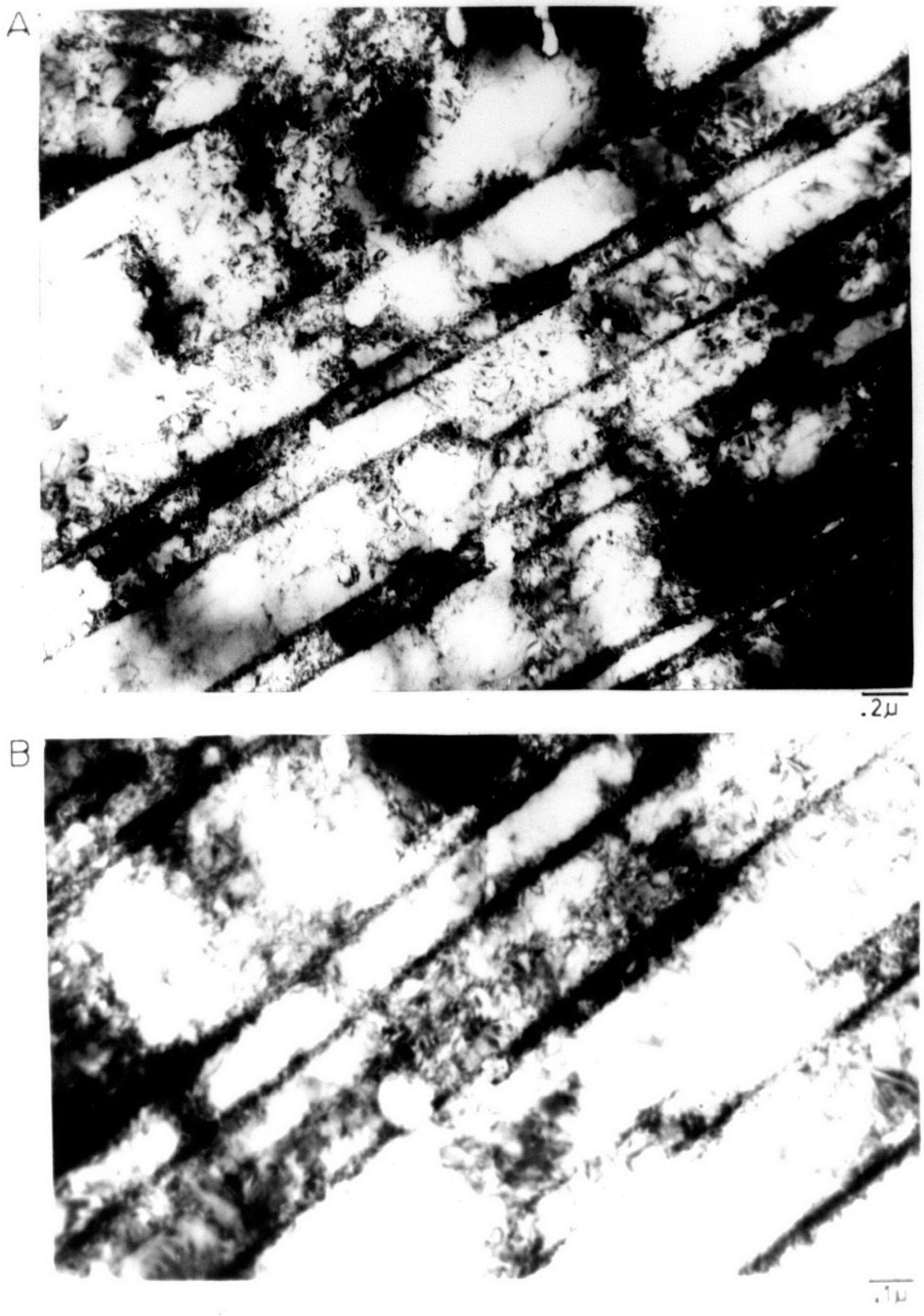

FIGURE 18. TEM MICROGRAPHS (LONGITUDINAL) SHOWING CELL FORMATION WITHIN SUB-BOUNDARIES RESULTING FROM TMT OF A. N-1 AND B. N-2

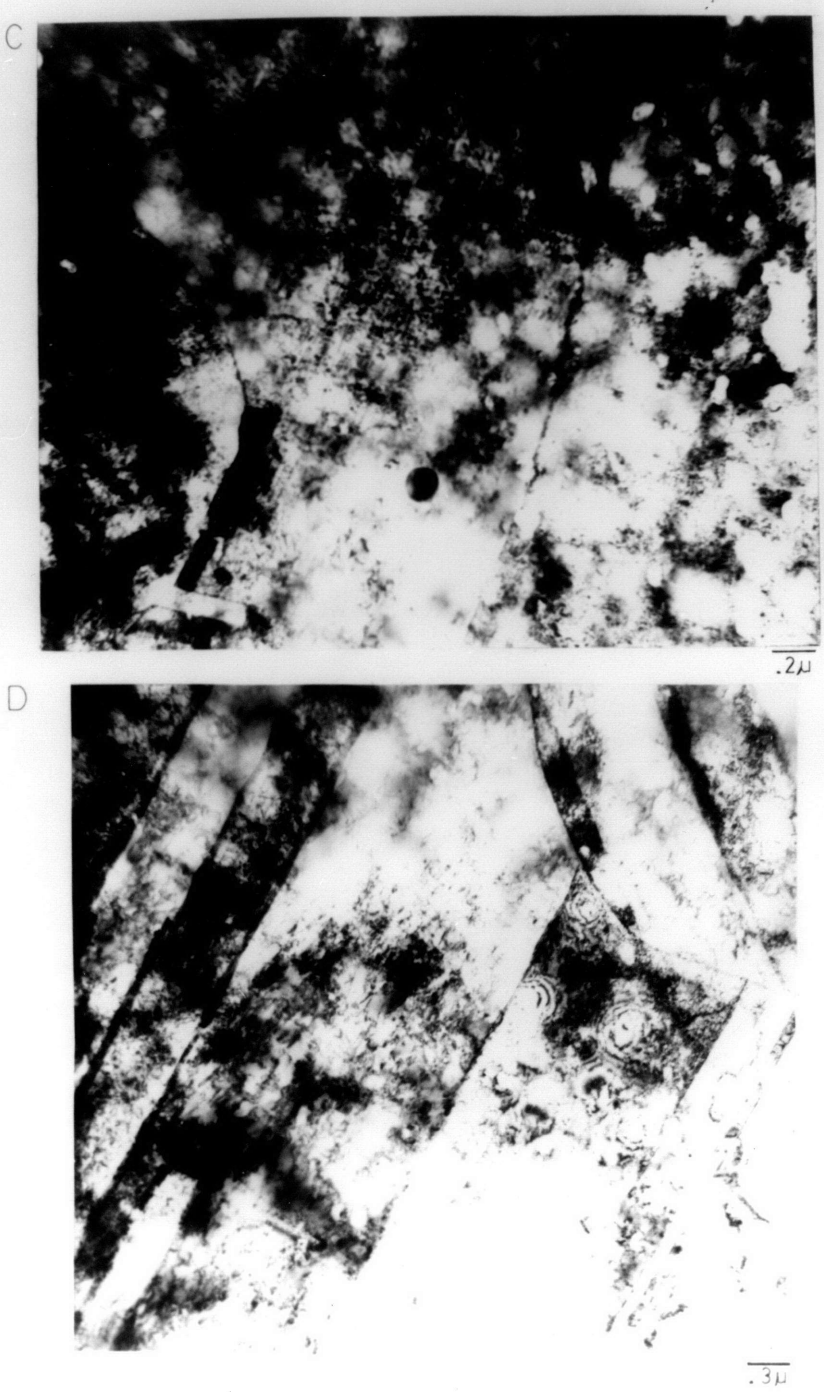

FIGURE 18. TEM MICROGRAPHS (LONGITUDINAL) SHOWING RECRYSTALLIZED GRAINS IN TMTED: C. N-2 AND D. N-1.

igated. N-1 took 13% R.A. before cracking while N-2 cracked after 5% R.A.

Previous research (5,39) has demonstrated that an optimum intermediate annealing temperature exists for nickel base alloys. Consequently, for N-1 intermediate annealing temperatures of 750°C (1382°F), 815°C (1500°F) and 982°C (1800°F) were investigated. The alloy was annealed after each 10% R.A. Alloys N-3 and N-5 were not thermomechanically treated (TMT) since any attempt at swaging resulted in cracking. Their strength values, derived from the residual strain energy obtained through processing made TMT impossible.

Microstructurally, N-1 and N-2 responded well to TMT. The dislocations arranged themselves into a regular network of cells as depicted in Fig. 18. Cell sizes vary from 490°A to 1700°A for N-1 and 208°A to 850°A for N-2. Alloy N-2 had an IPS smaller than alloy N-1, which accounted for the smaller cell size. Grant et al (5) attributed smaller cell sizes to a decrease in IPS. The dislocation density in the network was large for both alloys. Such arrangements are typical of recovered structures. These findings agree with the work of Grant et al (5), where most of the mechanisms important to TMT are enunciated. The GAR for both alloys increased with TMT. When the

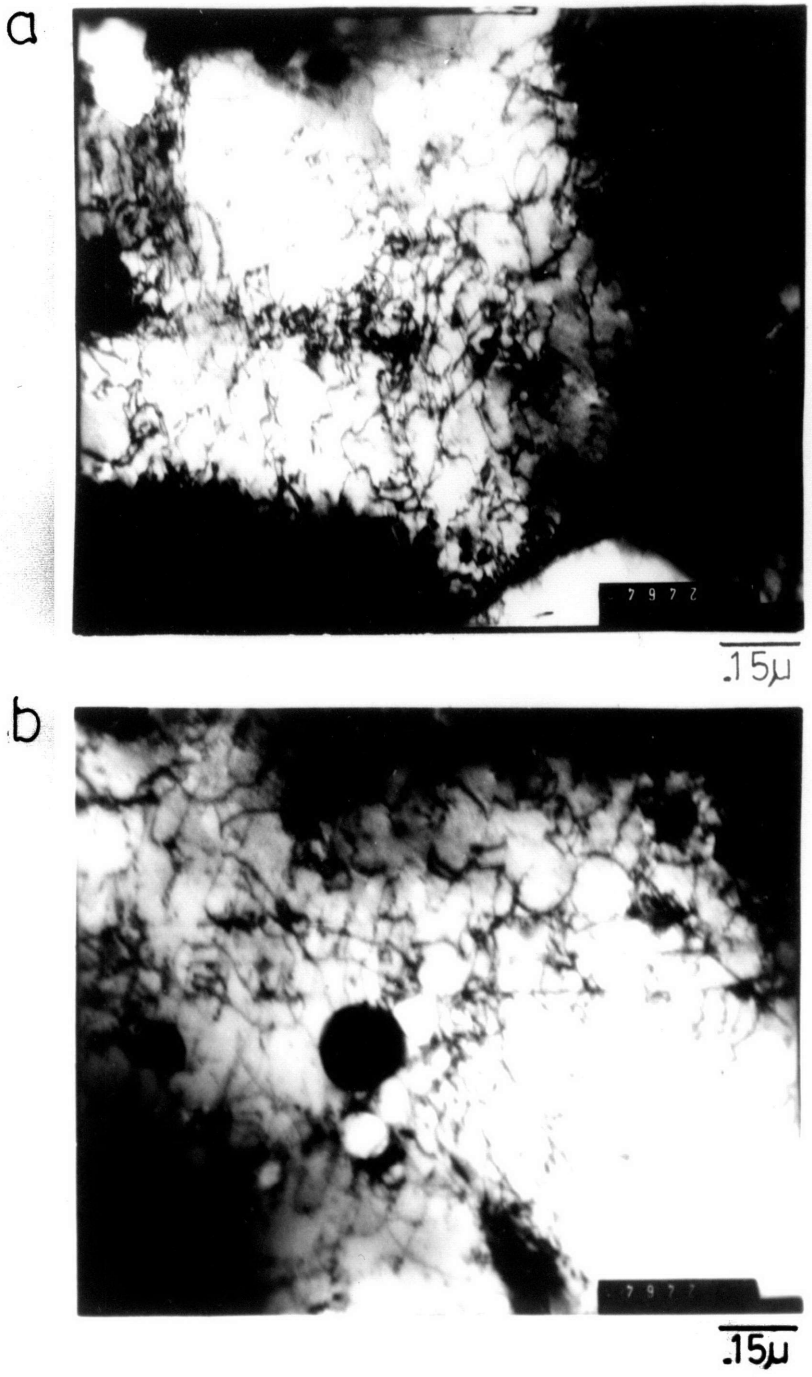

Figure 19. TEM micrographs (transverse) of: a. N-1 showing dislocation tangles and b. N-2 showing dislocation-particle interaction.

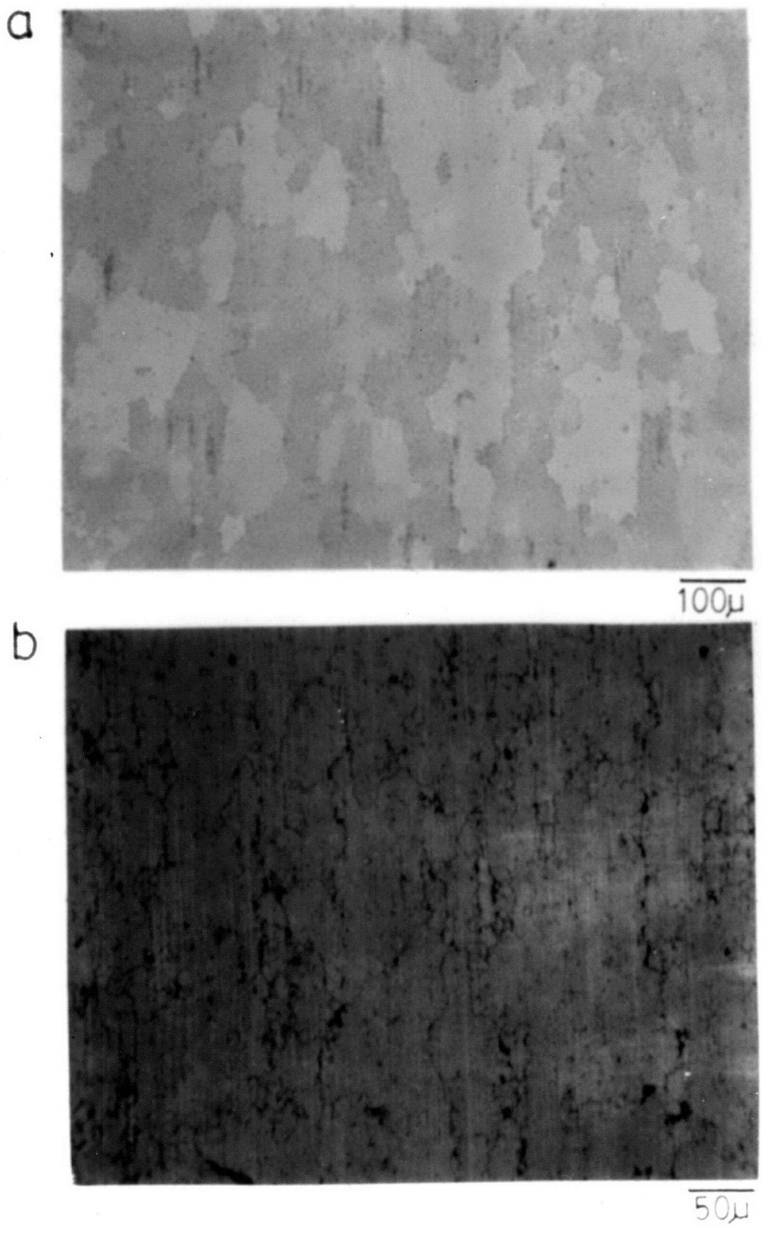

Figure 20. Photomicrographs (longitudinal) of: a. N-5 annealed at 1243°C (2270°F) for 2 hours and b. N-3 annealed at 1316°C (2400°F) for 0.5 hours.

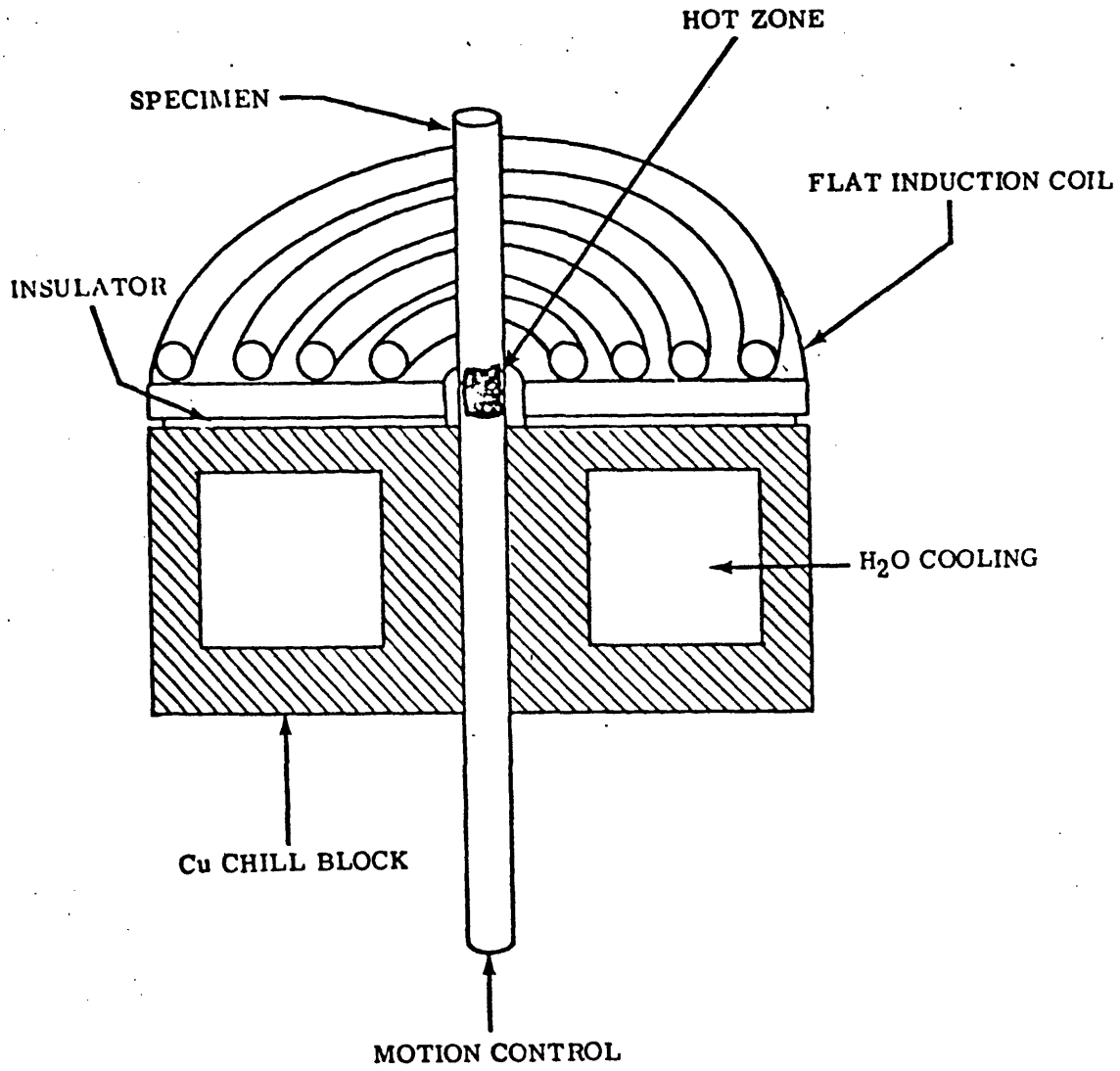

Figure 20. c. Schematic diagram of induction coil heat source and water cooled copper chill block combinations used to produce elongated microstructures in the ZAP process (55).

developed substructures and original grain boundaries are stabilized by the oxide particles, the grains do not recrystallize. The same cannot be said for both N-1 and N-2. Fig. 18 shows recrystallized grains in alloy N-1. The same was observed for TMT of N-2. The poor distribution of oxides could not effectively stabilize the substructures. Hence the alloys' poor mechanical properties were not unexpected. As depicted in Fig. 18, the GAR can be estimated to be greater than 10. Fig. 19 shows dislocation network formation and dislocation particle interaction. After TMT, all specimens displayed dual (100)-(111) textures with the (100) component becoming more dominant.

b. Recrystallization

Recrystallization was effected by standard annealing treatments and by zone aligned polycrystal formations (ZAP). Alloys N-3 and N-5 were the subjects of such treatments. Their recrystallization response was determined by standard heat treatments. For N-3, the best response was obtained at 1316°C (2400°F). Fig. 20 shows grain sizes of 300μ with GAR's that are sometimes greater than 10. For alloy N-5, the response was best at 1243°C (2270°F). Grain sizes as large as 810 with GAR's that are again greater than 10 were recognized, after annealing for 2 hours as depicted

in Fig. 20. Both alloys had smaller equiaxed grains among the larger grains. This arrangement of grains was detrimental to mechanical properties (83). The condition of the starting material for recrystallization differed in N-3 and N-5 primarily because of differences in their chemistries. Their working temperatures, strain rates and deformation symmetries were the same. The temperatures associated with the best recrystallization response were used for the ZAP treatments, i.e. for N-3: 1300°C-1316°C (2372°F-2400°F) and for N-5: 1243°C-1260°C (2270°F-2300°F).

The ZAP technique requires that the recrystallization process be controlled by passing highly cold worked, unrecrystallized material, with a suitable starting structure through a steep temperature gradient at a controlled rate. To achieve this experimentally, a heat source was positioned as close as possible to a heat sink, and the specimen was passed in a vertical direction from the heat sink into the heat source. A schematic of the apparatus used to produce this structure is shown in Fig. 20. The principal parts of the apparatus are shown. These include: a heat source (a flat induction coil) a heat sink (a water cooled Cu chill block) and a specimen motion controller (a variable speed motor and strip chart recorder). The specimen speeds

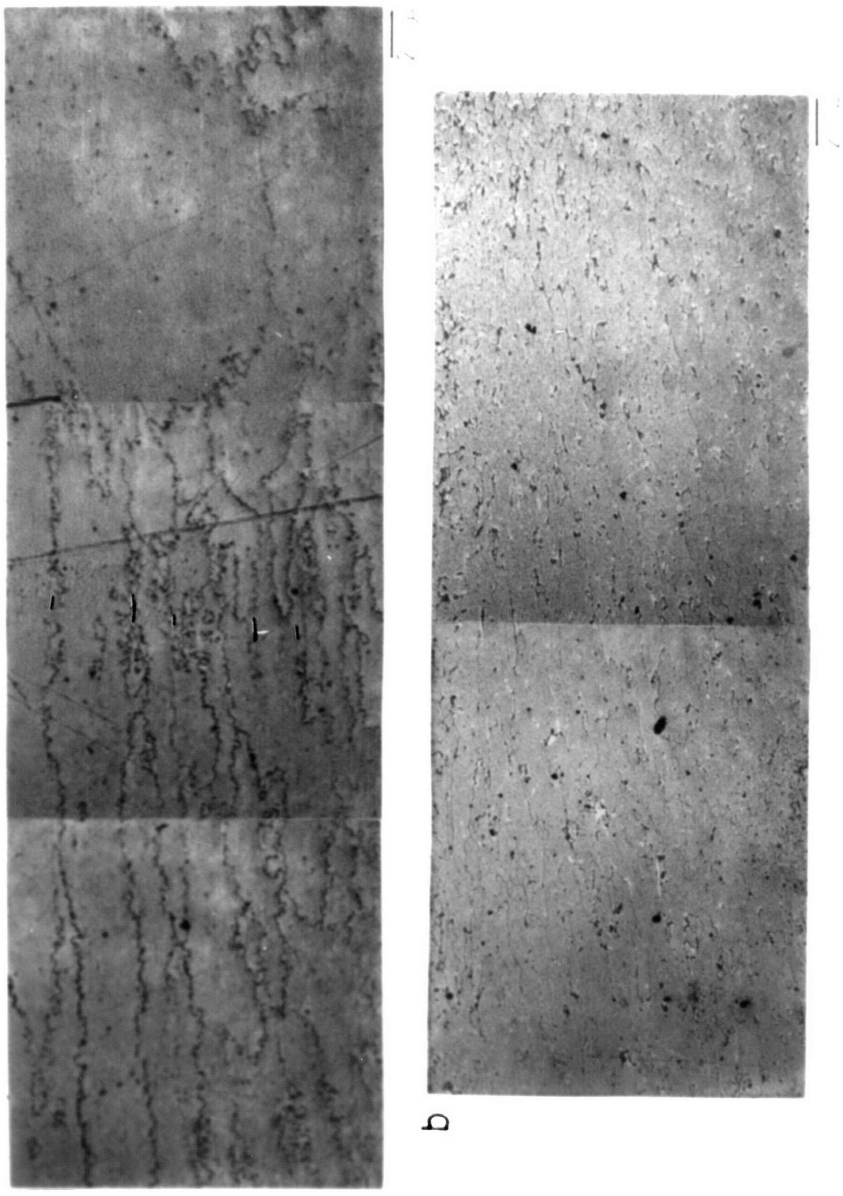

FIGURE 21. PHOTOMICROGRAPHS (LONGITUDINAL) OF N-3: A, ZAP AT 7.6 CM. (3 INCH)/HOUR AT 1300°C (2372°F) AND B. ZAP AT 15.2 CM. (6 INCH)/HOUR AT 1300°C (2372°F).

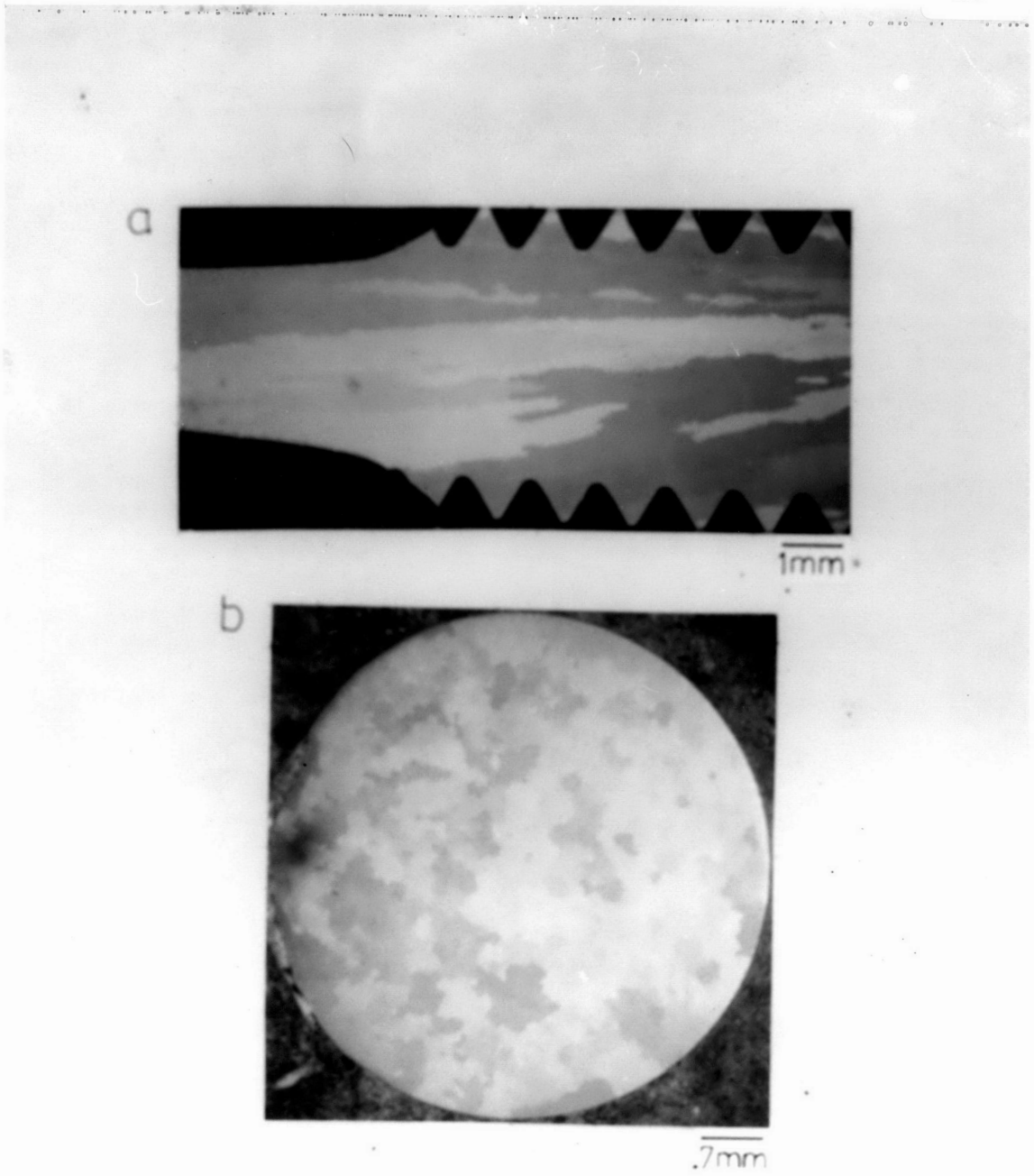

Figure 22. Photomacrographs of N-5. a. ZAP at 7.6 cm. (3 inch)/hour at 1260°C (2300°F) and heat treated (longitudinal) and b. ZAP at 7.6 cm. (3 inch)/hour at 1260°C (2300°F) and heat treated (transverse).

C

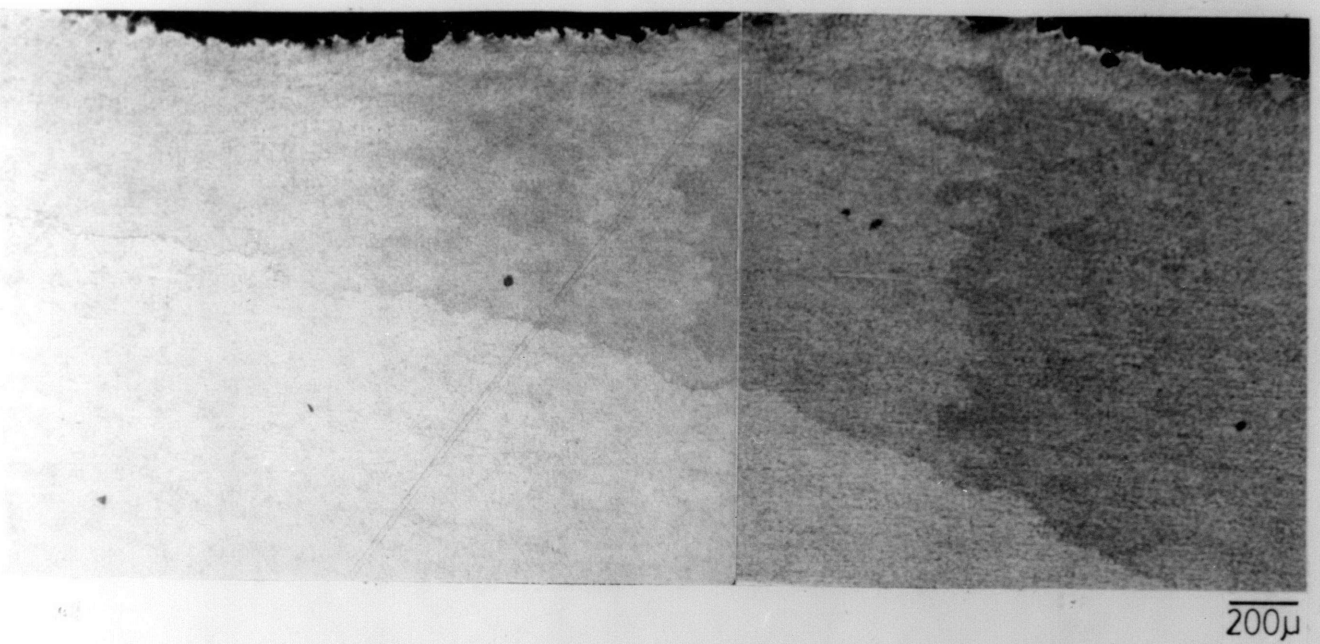

Figure 22. c. Photomicrograph of N-5 ZAP at 7.6 cm. (3 inch)/hour at 1260°C (2300°F) (longitudinal).

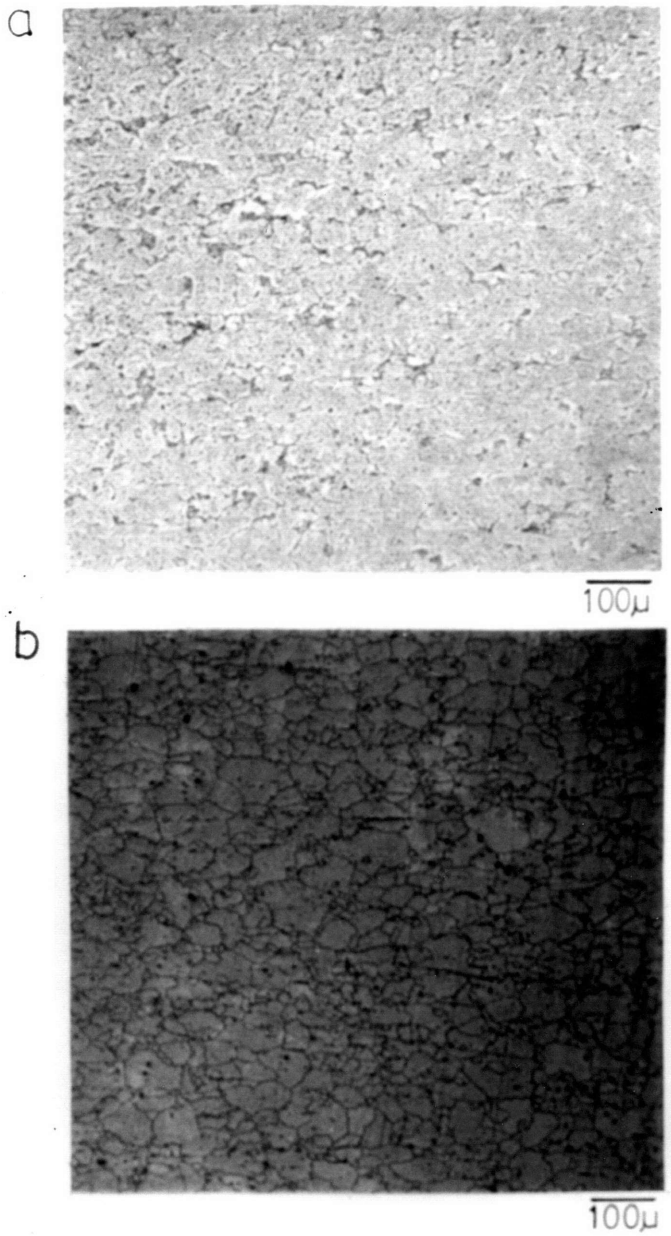

Figure 23. Photomicrographs (longitudinal) of N-3 ZAP at 1300°C (2372°F) at rates of: a. 30.5 cm. (12 inch)/hour and b. 3.8 cm. (1.5 inch)/hour.

achievable varied from 1.91 cm. (0.75 inch)/hour to 30.5 cm. (12 inch)/hour. Insulation was used to avoid arcing between the coil and chill block. A ZAP rate of 7.62 cm. (3 inch)/ hour gave the best results in terms of microstructure and mechanical properties for both N-3 and N-5. Figs. 21 and 22 show the microstructures of both alloys with GARs greater than 12. Exact numbers cannot be given for GAR values as it was difficult to determine the start and end points of individual grains.

The response to grain growth was not as ready at other ZAP rates attempted: 30.5 cm. (12 inch)/ hour, 15.2 cm. (6 inch)/hour, 3.8 cm. (1.5 inch)/hour and 1.9 cm. (0.75 inch)/hour were tried. Resulting structures are shown in Fig. 23. A rate of 3.8 cm. (1.5 inch)/hour was favorable for alloy N-5, developing microstructures similar to that for 7.62 cm. (3 inch)/ hours. Previous work achieved large columnar grains at ZAP rates of 13.5 cm. (5.3 inch)/hour (19,20), 122 cm. (48 inch)/hour (55) and 25.4 cm. (10 inch)/ hour and 45.7 cm. (18 inch)/ hour (83).

It is true that the average GAR increased as zone travel rate decreased (83), and that increasing ZAP rate through the temperature gradient decreased the GAR (55). For alloy N-3, rates of 15.2 cm. (6 inch)/hour and 7.6 cm. (3 inch)/hour resulted in GARs greater than 12. Comparable results were obtained

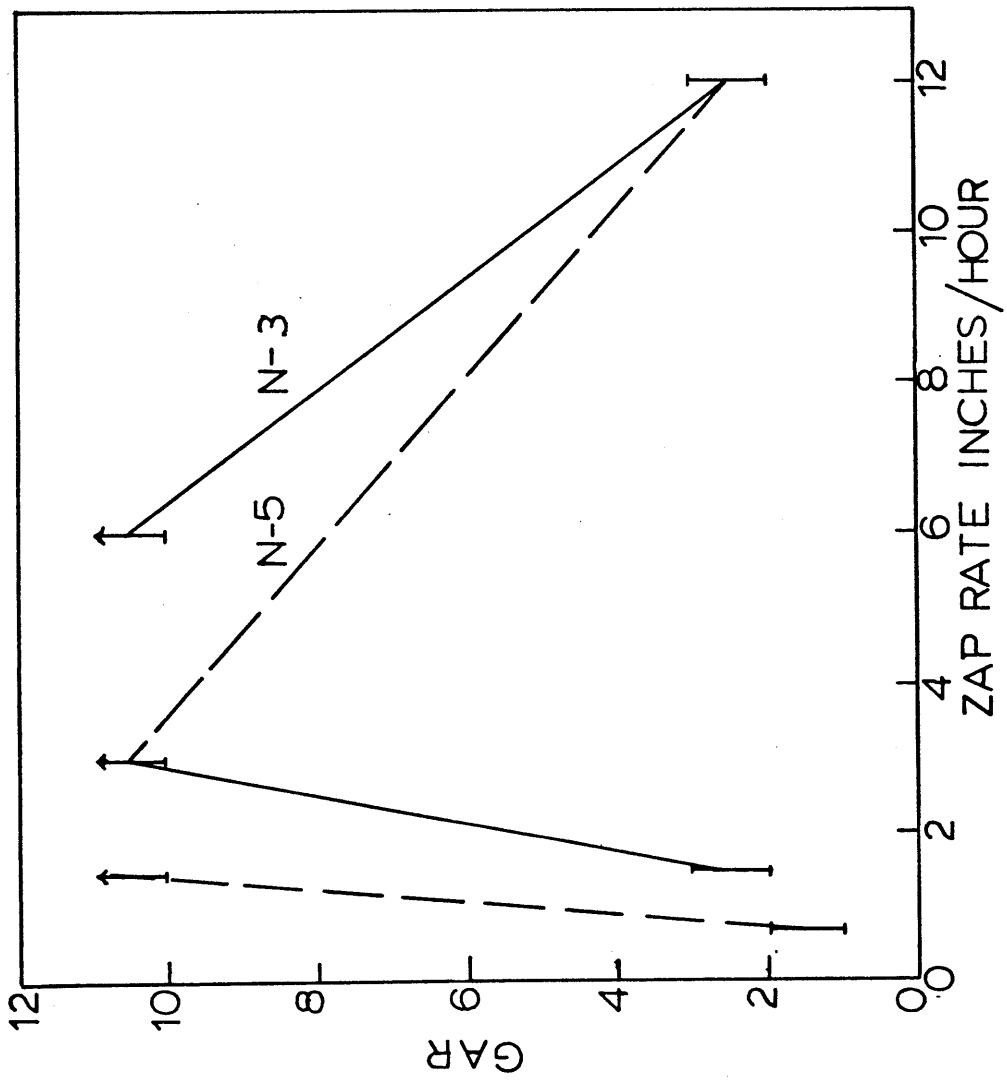

Figure 24. Schematic of ZAP rate versus GAR showing the optimum ZAP rate ranges for alloys N-3 and N-5.

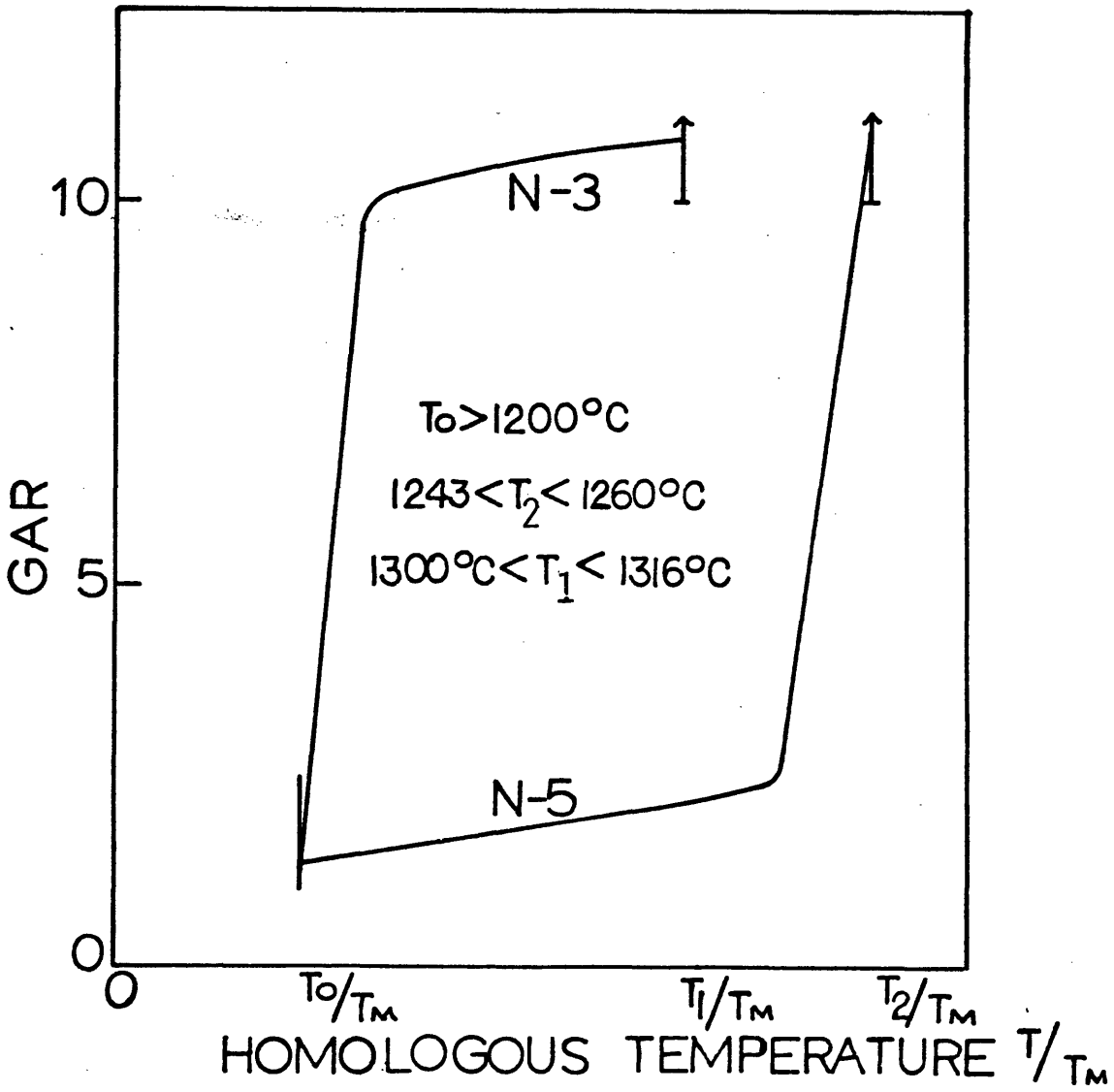

Figure 25. Schematic of Homologous Temperature versus GAR showing recrystallization responses of N-3 and N-5.

Figure 26. TEM micrograph showing oxide particle at grain boundary of alloy N-5.

for N-5 at 7.6 cm. (3 inch)/hour and 3.8 cm. (1.5 inch)/hour. Rates of 30.5 cm. (12 inch)/hour and 3.8 cm. (1.5 inch)/hour resulted in recrystallized equiaxed grains for N-3 as demonstrated in Fig. 23. In Fig. 24 the optimum ZAP rate range for each alloy is shown. This difference in response to ZAP rates and temperatures of recrystallization for N-3 and N-5 could be attributed to the peculiarities of the starting material (55,83). Furthermore, N-5 displayed a delayed response to recrystallization due to its ability to retain its higher residual strain energy content. This delayed response is illustrated in Fig. 25.

Fig. 26 shows how effectively grain boundaries can be pinned by oxide particles. After zone annealing, each specimen of alloy N-5 was given the following treatment: 1232°C (2250°F)/0.5 hour/AC + 954°C (1745°F)/2 hour/AC + 843°C (1549°F)/24 hour/AC.

Unsuccessful attempts were made to directionally recrystallize alloy N-4. This alloy had the same chemical composition as alloy N-5 with no Y_2O_3 added. Fig. 27 demonstrates N-4's response to this treatment. It is very different from that of N-5. Like alloy N-1, surface oxidation of aluminum to alumina resulted in a paucity of oxides in the alloy. It is believed that a sufficient volume of oxides with appropriate distribution will contribute to the storage of

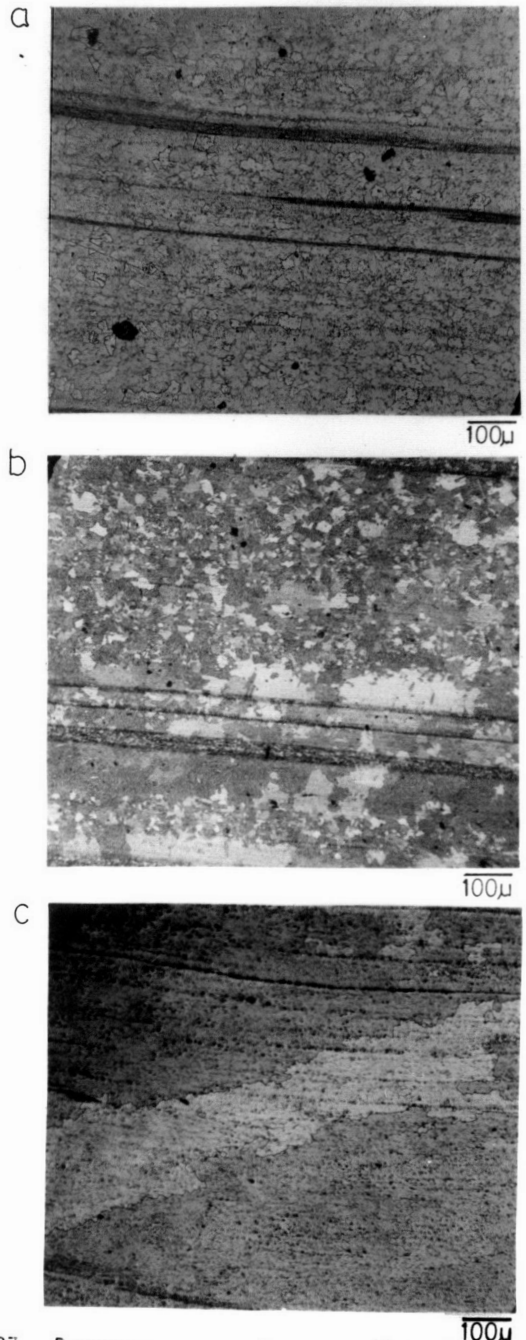

FIGURE 27. PHOTOMICROGRAPHS (LONGITUDINAL) OF N-4 ZAP AT 1260°C (2300°F) AT RATES OF: A. 7.6 CM. (3 INCH)/HOUR, B. 3.8 CM. (1.5 INCH)/HOUR AND C. 1.9 CM. (0.75 INCH)/HOUR.

significant energy which is then stored in the alloy's deformed substructure. It is this stored energy that provides the driving force for grain growth. Obviously, alloy N-4 lacked that important ingredient.

5. Mechanical property determinations

a. Room temperature tensile tests

Tensile specimens were machined to ASTM specifications. The test bars had a gage diameter of 0.406 cm. (0.160 inch) and a gage length of 1.905 cm. (0.750 inch). The tests were performed on an Instron tensile testing machine at a crosshead spead of 0.05 cm. (0.02 inch) per minute. During each test, load versus elongation was recorded.

The room temperature tension properties for the different alloys are listed in Table VII. Alloy N-1 was much stronger than similar Ni-base solid solution alloys (5,43,48,90). Thermomechanical treatment (TMT), i.e. swaging at room temperature with intermediate anneals at 815°C (1500°F) after each 10% R.A., increased the yield strength of this alloy over its as-extruded value; however, the ductility in the as-extruded condition was better. Indications are that N-1 saturates in strength with cold work. It was determined that the strength of ODS alloys increased with increasing volume fraction of the oxide (14). Therefore, the increase in strength of alloys N-2

TABLE VII

Room Temperature Tensile Data

Alloy	Condition	Ref.	Yield Strength ksi(MPa)	UTS ksi(MPa)	Elong. (%)	R.A. (%)
N-1	As Ext.		127(876)	167(1152)	18	22
N-1	As Ext.+13% R.A.		206(1419)	210(1455)	9	10
N-1	As Ext.+20 R.A. WIA 815°C		161(1111)	165(1136)	2	2
N-1	As Ext.+40 R.A. WIA 815°C		163(1126)	163(1126)	11	15
N-1	As Ext.+50 R.A. WIA 815°C		154(1061)	160(1105)	7	9
N-1	As Ext.+60 R.A. WIA 815°C		160(1105)	168(1162)	12	15
N-2	As Ext.		207(1427)	209(1441)	2	4
N-3	As Ext.		239(1648)	246((1697)	2	3
N-3	As Ext.+ ZAP 3"/ hr at 1300°C		114(789)	135(926)	3	3
N-4	As Ext.		223(1539)	223(1539)	2	4
N-5	As Ext.		326(2253)	326(2253)	1	2
N-5	As Ext.+ZAP 3"/ hr at 1260°C+HT		189(1302)	201(1389)	2	4
N-5	1243°C/2 hr/AC+ 1232°C/0.5 hr/AC +954°C/2 hr/AC + 843°C/24 hr/AC		156(1076)	174(1198)	3	4
IN853	As Ext. at 1066°C		295(2037)			

TABLE VII (continued)

Alloy	Condition	Ref.	Yield Strength ksi (MPa)	UTS ksi (MPa)	Elong. (%)	R.A. (%)
IN853	As Ext.+10 hr at 1177°C	81	176 (1212)			
IN853	As Ext.+10 hr at 1260°C	81	100 (689)	146 (1007)	12	16
MA6000E	As Ext. at 1038°C	20	186 (1284)	188 (1294)	2.5	3.0
MA6000E	As Ext. at 1010°C then hot rolled at 1010°C	20	185 (1275)	186 (1284)	2.0	6.0

and N-3 with 2 v/o and 5 v/0 Y_2O_3 added, respectively, was expected and so was the decrease in ductility. Alloy N-4 had strength values lower than N-3 and was also less ductile. The exceedingly high strength values of B-5 were a reflection of its high volume fraction of γ', determined to be 59%, and the 2 v/o Y_2O_3 added. The tensile behavior of these alloys is very typical of the more complex ODS Ni-base alloys in which the yield strength approaches the ultimate strength, indicating more brittle behavior. Perhaps of importance in understanding this behavior is the final material state which results from the interaction of such factors as the hot working temperature, working strain and strain rate with stored energy introduced during the attriting ball milling process. More severe working by extruding at a fixed strain rate and temperature lead to a submicron grain size and a higher level of residual strain energy stored within the substructure. Tensile data after ZAP and recovery heat treatments are also included in Table VI for N-3 and N-5. Values for IN853 and MA6000E are included for comparison.

Room temperature tensile fracture surfaces were examined by SEM. As seen in Fig. 28, alloy N-1 showed a typical dimples ductile fracture surface. For alloys N-2 to N-5, there was a mixture of brittle, i.e.

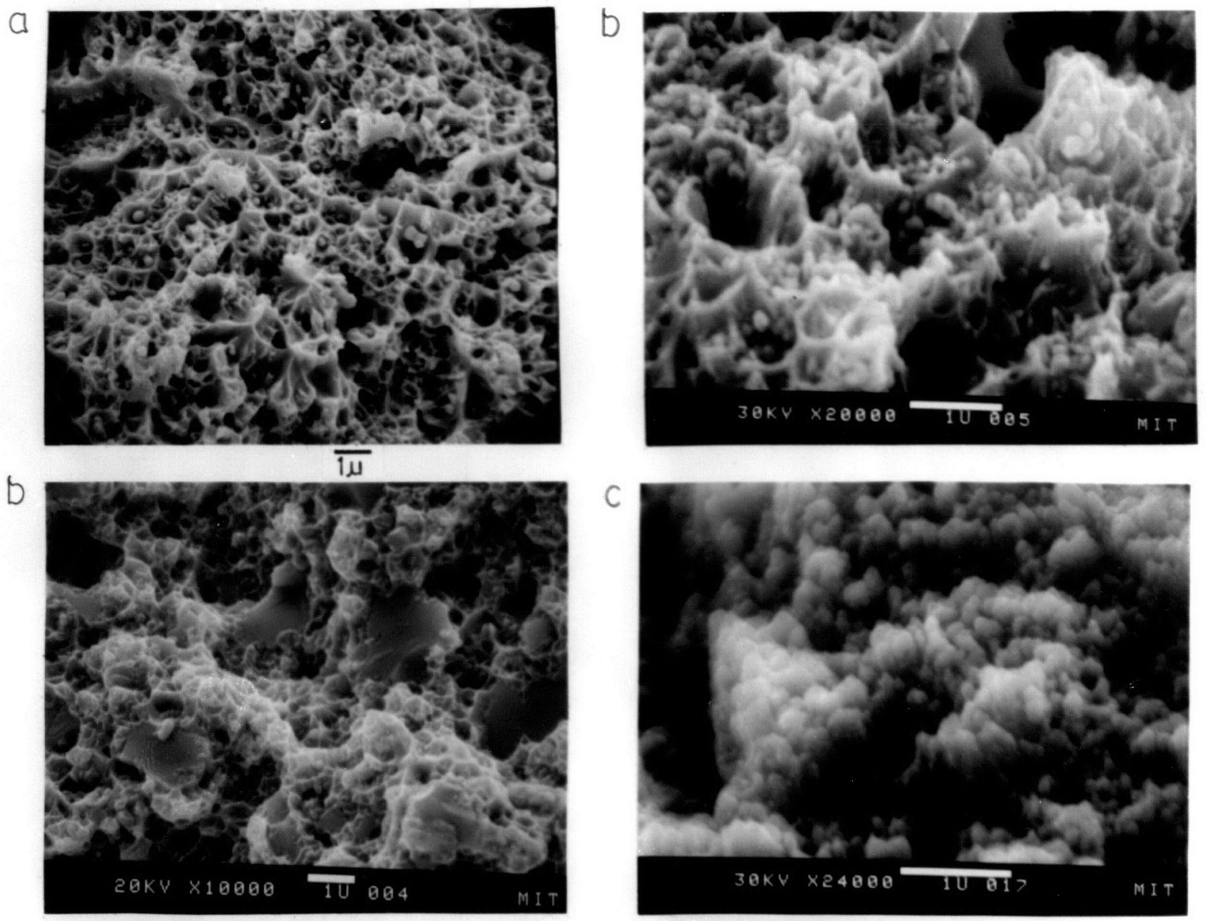

FIGURE 28. SEM MICROGRAPHS OF TENSILE FRACTURE SURFACES OF: A. N-1, B. N-2 AND C. N-3.

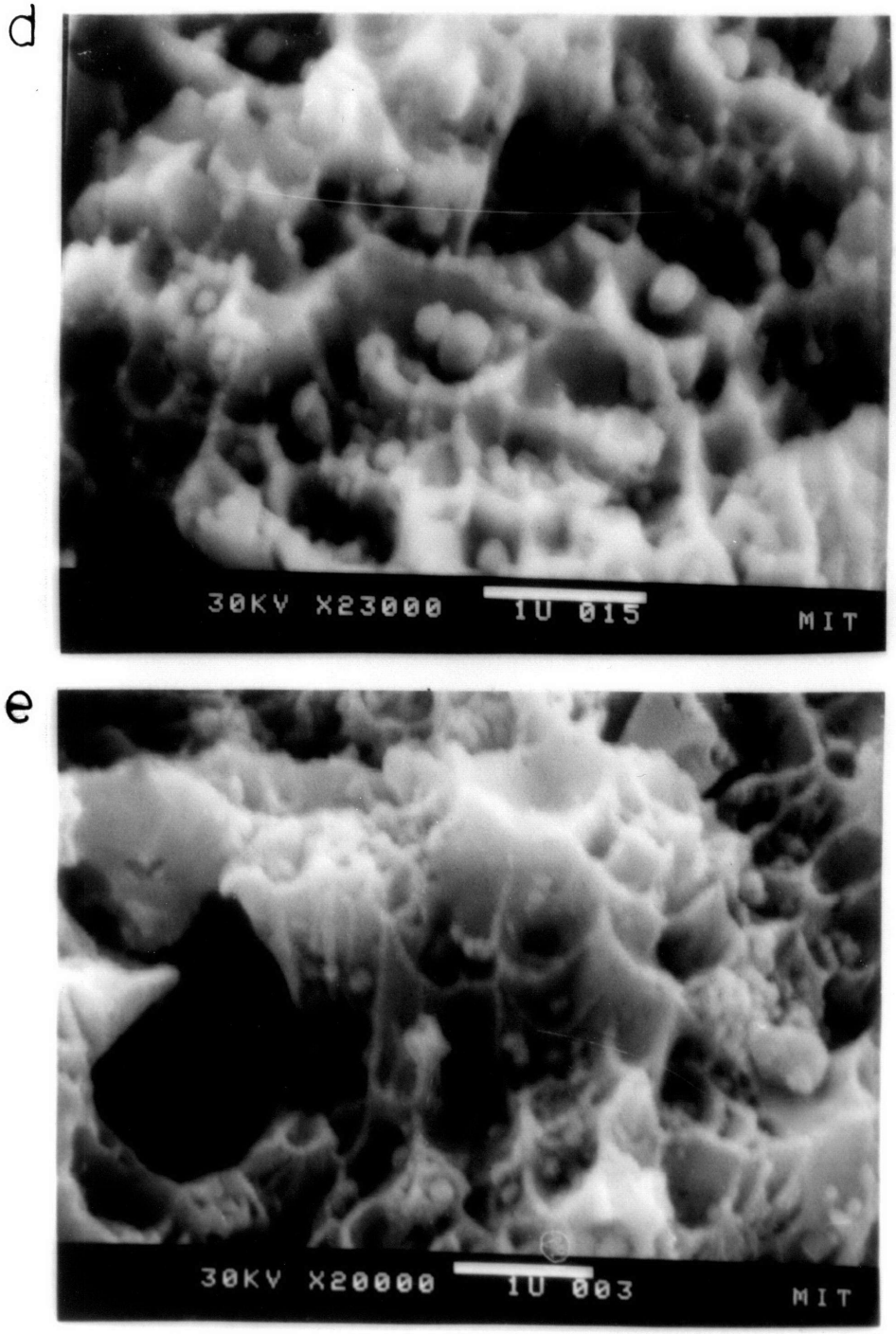

Figure 28. **SEM micrographs of tensile fracture surfaces showing oxide particles sitting in dimples of: d. N-1 and e. N-3.**

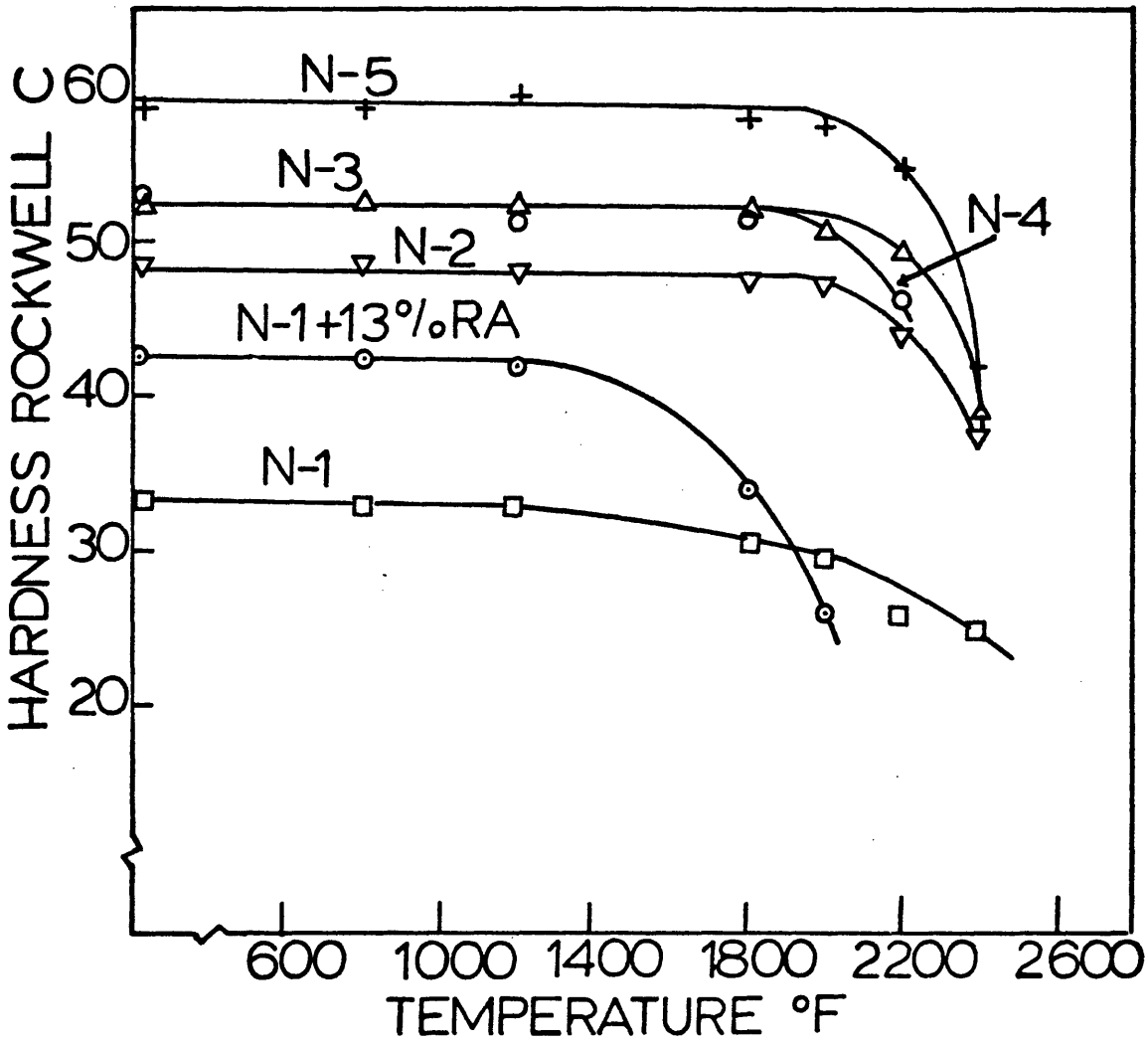

Figure 29. Hardness (Rockwell C) versus annealing temperature (°F) for alloys N-1 to N-5.

cleaved areas, and ductile fracture modes. Fig. 28a,b, & c show these characteristics. Close examination revealed that an oxide particle is located at the center of each void, quite spherical and clearly unbonded to the matrix (Fig. 28d & e). It has been proposed that these particles act as sites for initiation of cracks, which is not unreasonable. As the stress at the particle/matrix interface increases during plastic deformation, voids form normal to the particle perpendicular to the stress axis to relieve the localized stress concentration. Upon further straining, the ductile matrix among the particles necks and the voids coalesce. This reduced the effective cross-section and eventually caused failure.

b. Room temperature hardness and elevated temperature stability

The stability of each as-extruded alloy was determined by hardness measurements at 20°C after annealing for 1 hour at temperatures between room temperature and 1316°C (2400°F). Hardness values are given in Appendix II and shown graphically in Fig. 29. Alloy N-1 was the least stable, losing its energy above about 760°C (1400°F). The poor distribution of oxide which resulted from insufficient oxide volume was responsible for the onset of early recovery and recyrstallization. Alloys N-2, N-3, N-4 and N-5

maintained stability to much higher temperatures. Alloy N-4, with no Y_2O_3 added, was analyzed to have about 0.85 w/o oxide in the form of Al_2O_3 and some Cr_2O_3. This alloy derived its stability not only from Al_2O_3 dispersoids but from the γ' ($Ni_3Al(Ti)$) precipitates present. Interestingly, N-4 became less stable at a lower temperature 982°C (1800°F) than N-2, N-3 or N-5. The latter three alloys remained stable to 1093°C (2000°F). The drop in hardness after 1093°C is due to recovery and partial recrystallization. The ability of N-2, N-3 and N-5 to retain their stored energy is due to the contribution of the oxides to the development of a stable substructure during their processing.

c. Elevated temperature stress-rupture tests

The majority of stress rupture tests were performed at 982°C (1800°F). Other test temperatures were 815°C (1500°F) and 1093°C (2000°F). Specimens were tested in a loading train with Udimet 500 grips with universal joints at the top and the bottom. Load was applied by a lever arm and was constant throughout each test. A dial gage attached to the frame was used to measure the extension of the specimen with time. The stress rupture specimens were machined to the same specifications as the room temperature tensile test bars. The total elongation and reduction-in-area

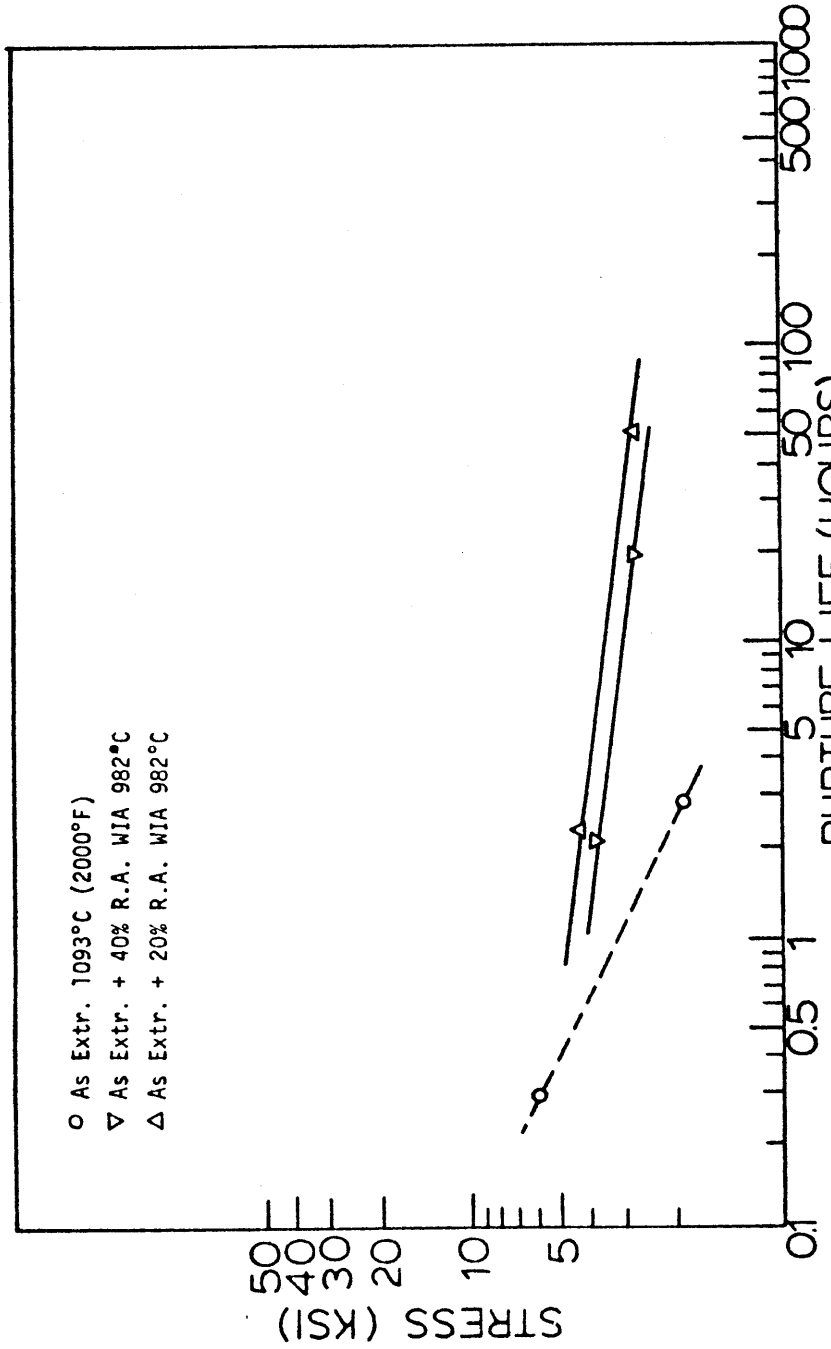

Figure 30. Log Stress versus Log Rupture Life at 982°C (1800°F) for alloy N-1.

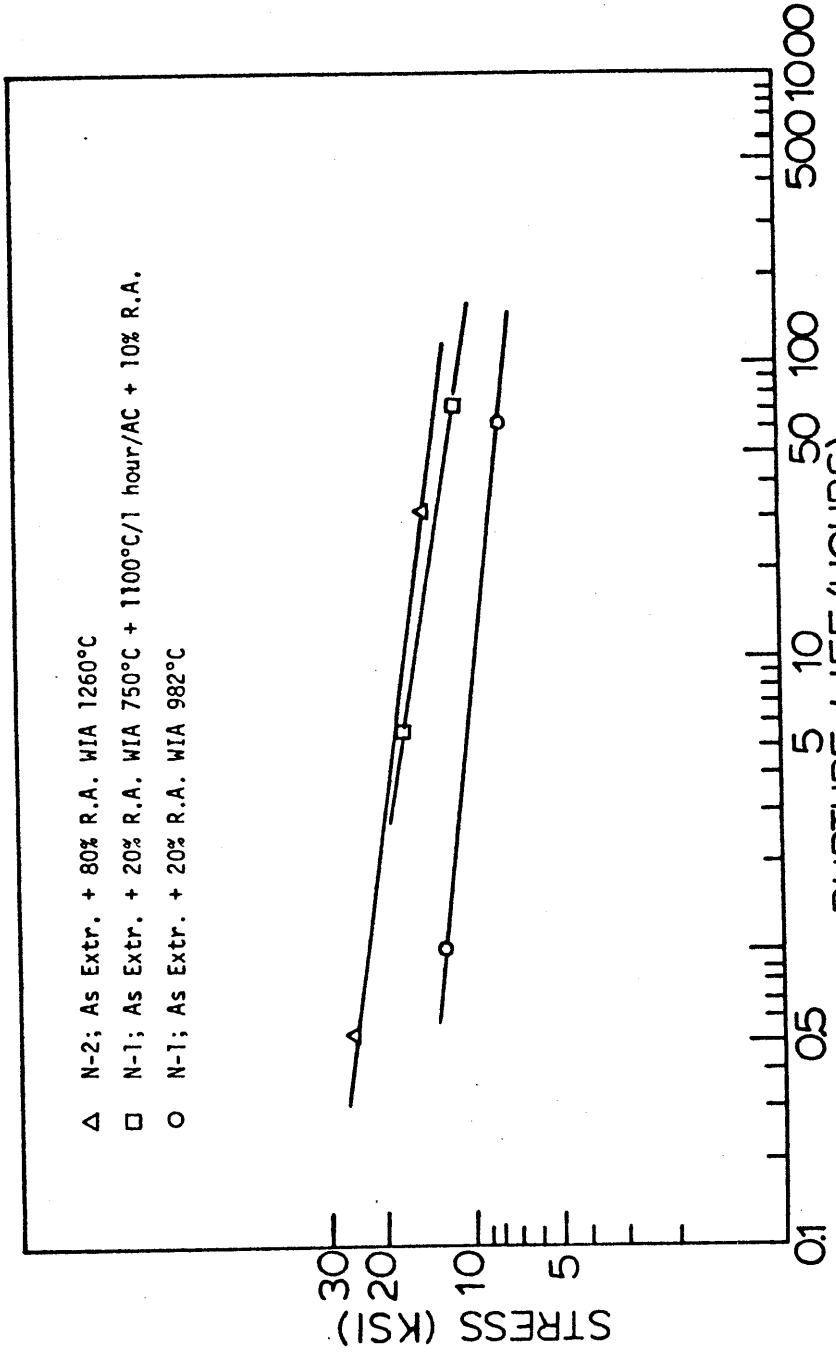

Figure 31. Log Stress versus Log Rupture Life at 815°C (1500°F) for alloys N-1 and N-2.

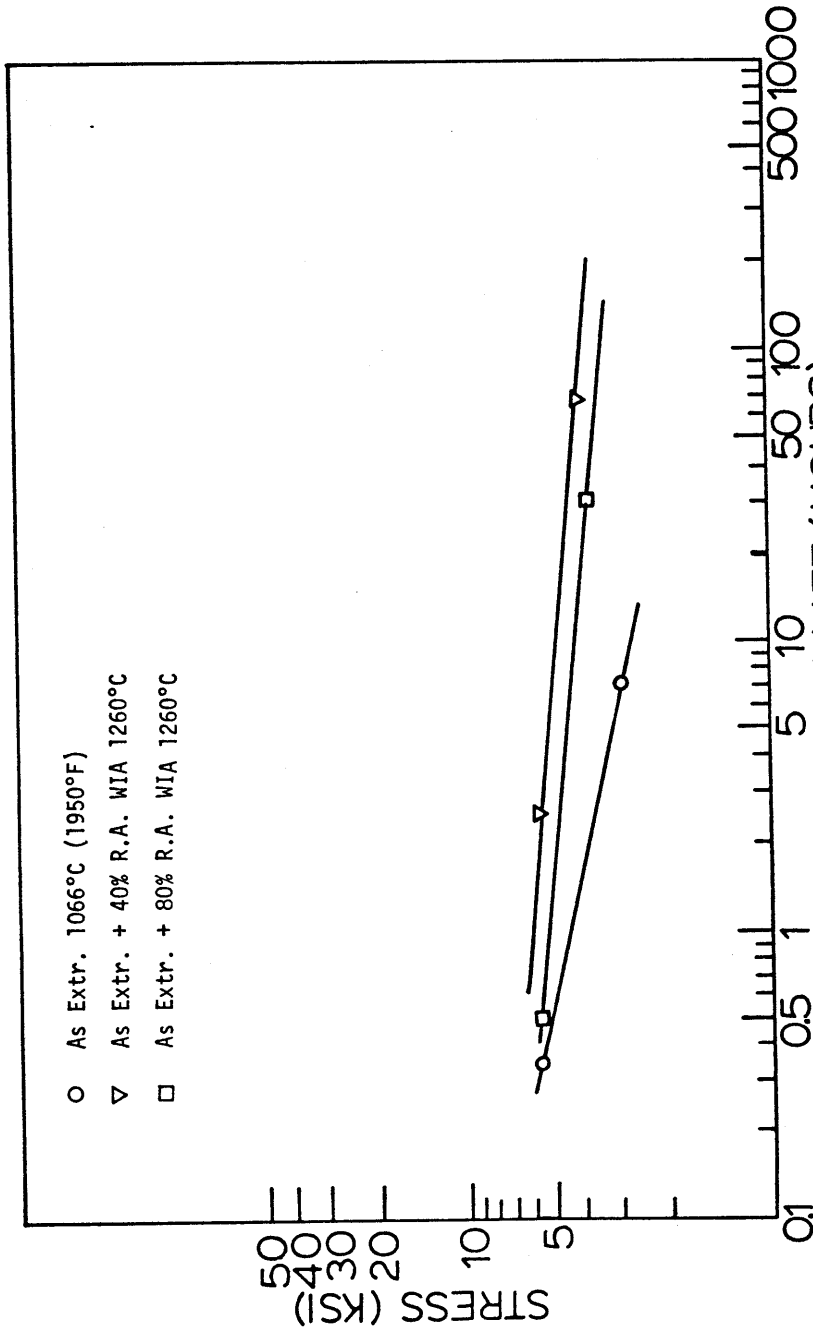

Figure 32. Log Stress versus Log Rupture Life at 982°C (1800°F) for alloy N-2.

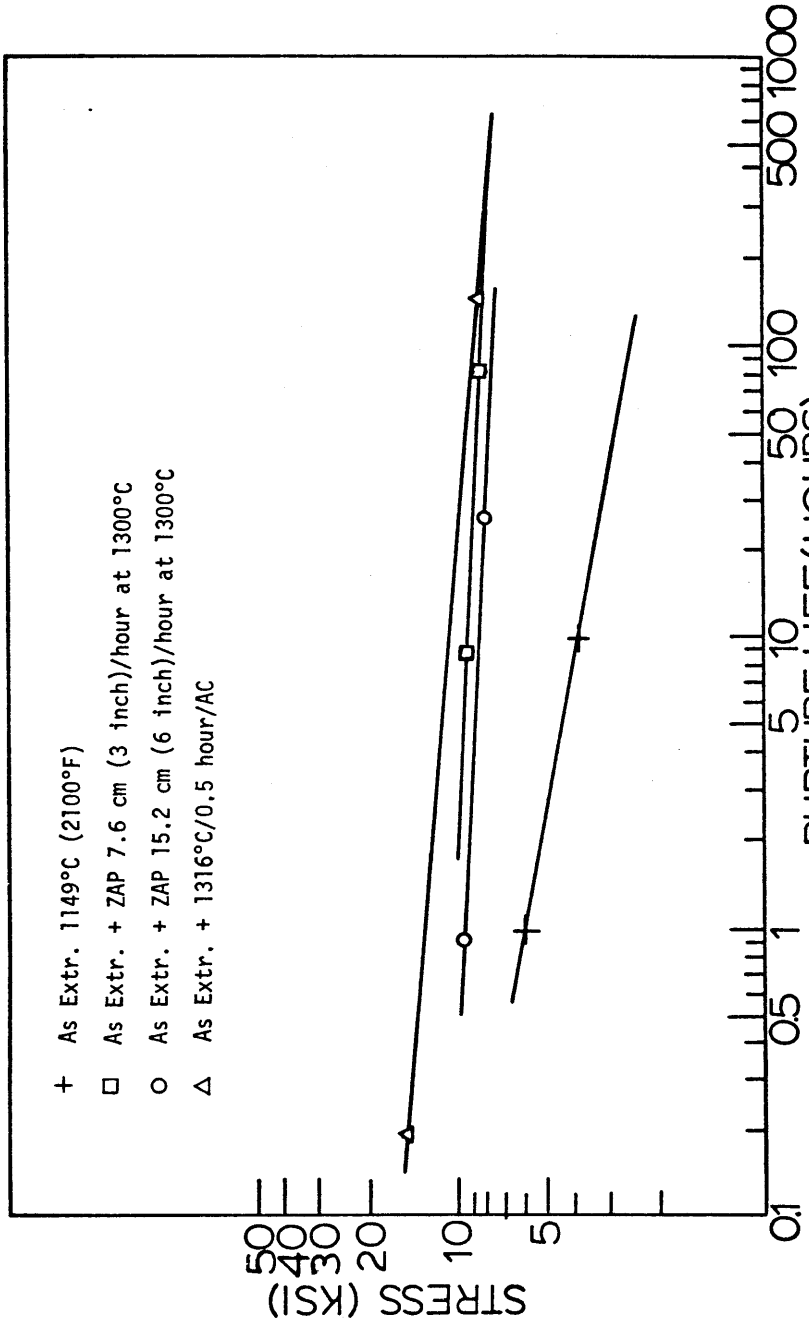

Figure 33. Log Stress versus Log Rupture Life at 982°C (1800°F) for alloy N-3.

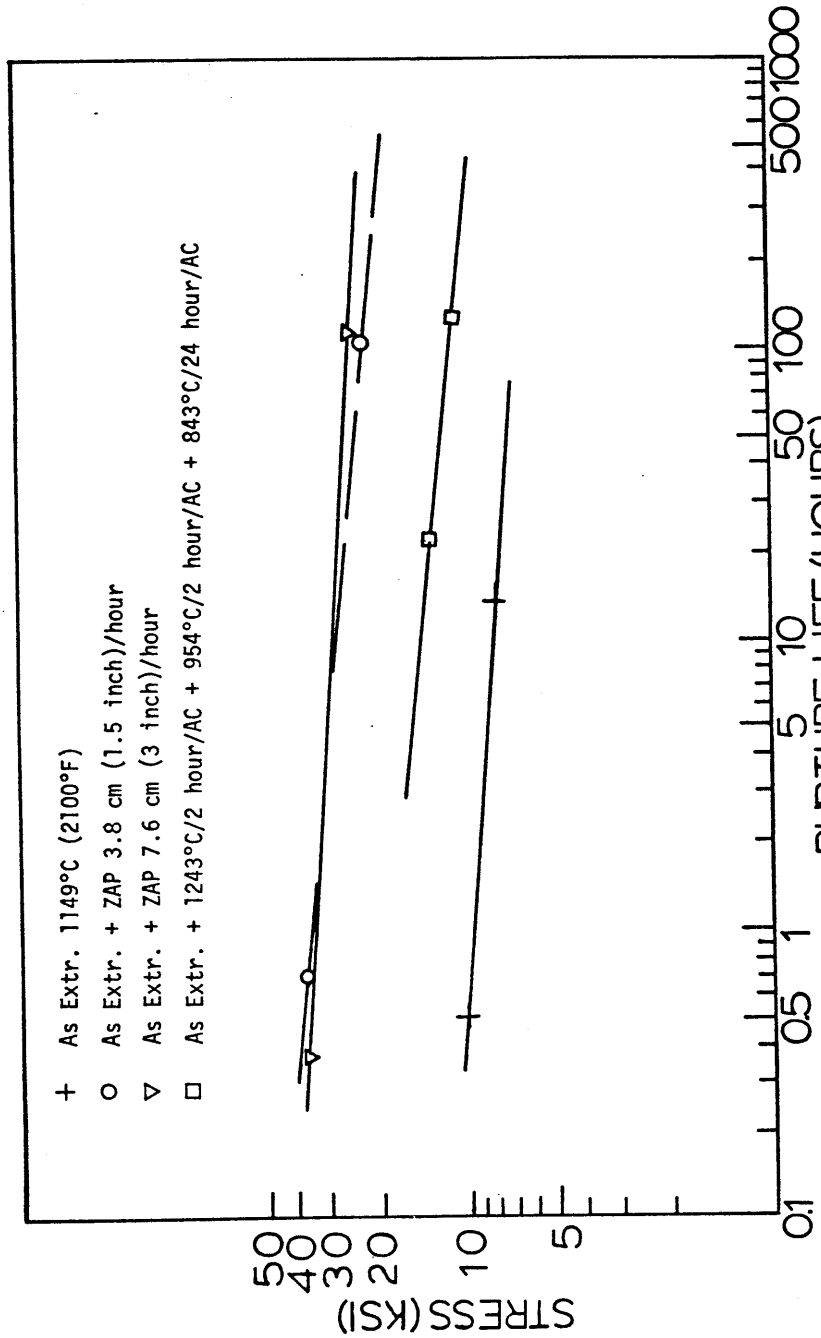

Figure 34. Log Stress versus Log Rupture Life at 982°C (1800°F) for alloy N-5.

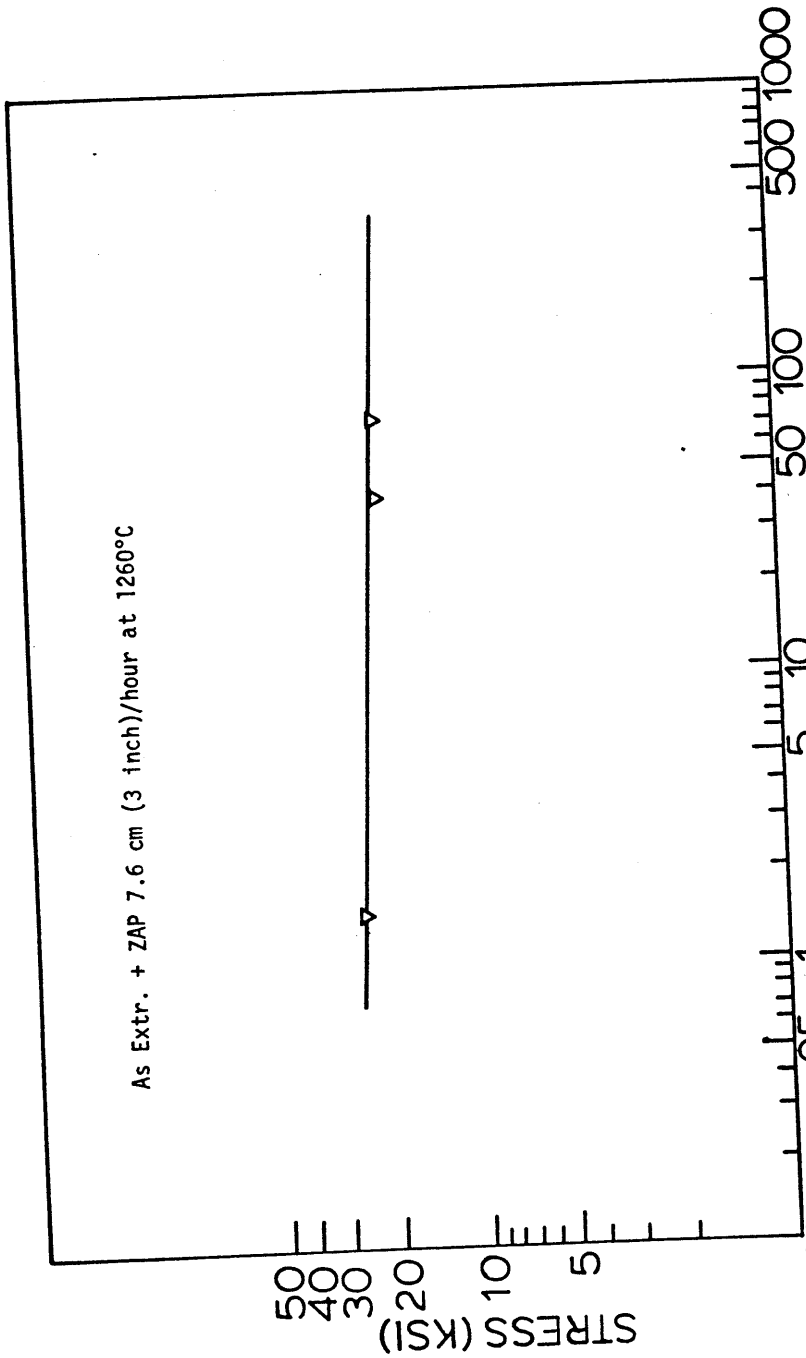

Figure 35. Log Stress versus Log Rupture Life at 1093°C (2000°F) for alloy N-5.

values were determined by comparing each specimen's initial length and diameter to its final length and diameter. The temperature of the specimen was controlled to $\pm$3°C along the gage length and monitored by two separate thermocouples located at the top and bottom of the gage length. The results of the stress rupture tests are plotted in Figs. 30 to 35. A compilation of all the stress rupture data is given in Appendix III.

The stress rupture properties for alloy N-1 were relatively poor. TMT markedly improved the alloy's performance. Many treatments were attempted as shown in Appendix II. The best properties were obtained at 20% R.A. WIA 982°C (1800°F) and 40% R.A. WIA 982°C (1800°F). The stress values for a life of 100 hours were 2.7 ksi and 3.0 ksi, respectively. TMT effectively flattened the slopes of the stress rupture curves compared to the as-extruded condition. The w/o oxide (0.9) oxide particle size (0.108μ) and IPS (0.438μ) were all illustrative of poor oxide distribution.

Alloy N-2, with the same composition as N-1 but with 2 v/o Y_2O_3 added showed improved strength over alloy N-1. Its stress for a 100 hour life at 982°C in the as-extruded condition was 2.0 ksi. TMT of 40% R.A. WIA 1260°C and 80% R.A. WIA 1260°C gave 100 hour

rupture life strength values of 4.5 ksi and 3.5 ksi, respectively. N-2 was very hard (R_c=48.5) and strong (Y.S.=207 ksi at R.T.) due primarily to the highly strained substructure developed during processing. This fact made annealing at a high temperature of 1260°C imperative. Annealing at this temperature for 1 hour did not interfere with the formation of a dislocation substructure associated with TMT as seen in Fig. 18. Furthermore, Wilcox and Clauer (48) annealed less complex solid solution dispersion stabilized Ni-alloys at 1200°C and obtained the same effect. Also, Grant et al (5) annealed internally and surface oxidized Ni-Co-Mo-BeO and Ni-BeO alloys at 815°C and developed similar dislocation substructures. What made N-2 differ from the above-mentioned alloys was its interparticle spacing, which was determined to be 0.32μ. Like N-1, the distribution of the oxides was inadequate to stabilize the dislocation substructure formed after TMT.

Alloy N-3 with 5 v/o Y_2O_3 added gave a stress for a 100 hour life of 3.0 ksi in the as-extruded condition. The extremely high hardness (R_c=52.3) and strength (Y.S.=239 ksi at R.T.) made TMT of this alloy impossible. It would crack at the ends when swaged to less than 10% R.A. after preliminary annealing at 1260°C for 1 hour. In the recrystallized condition, i.e. annealing at 1316°C for 0.5 hour,

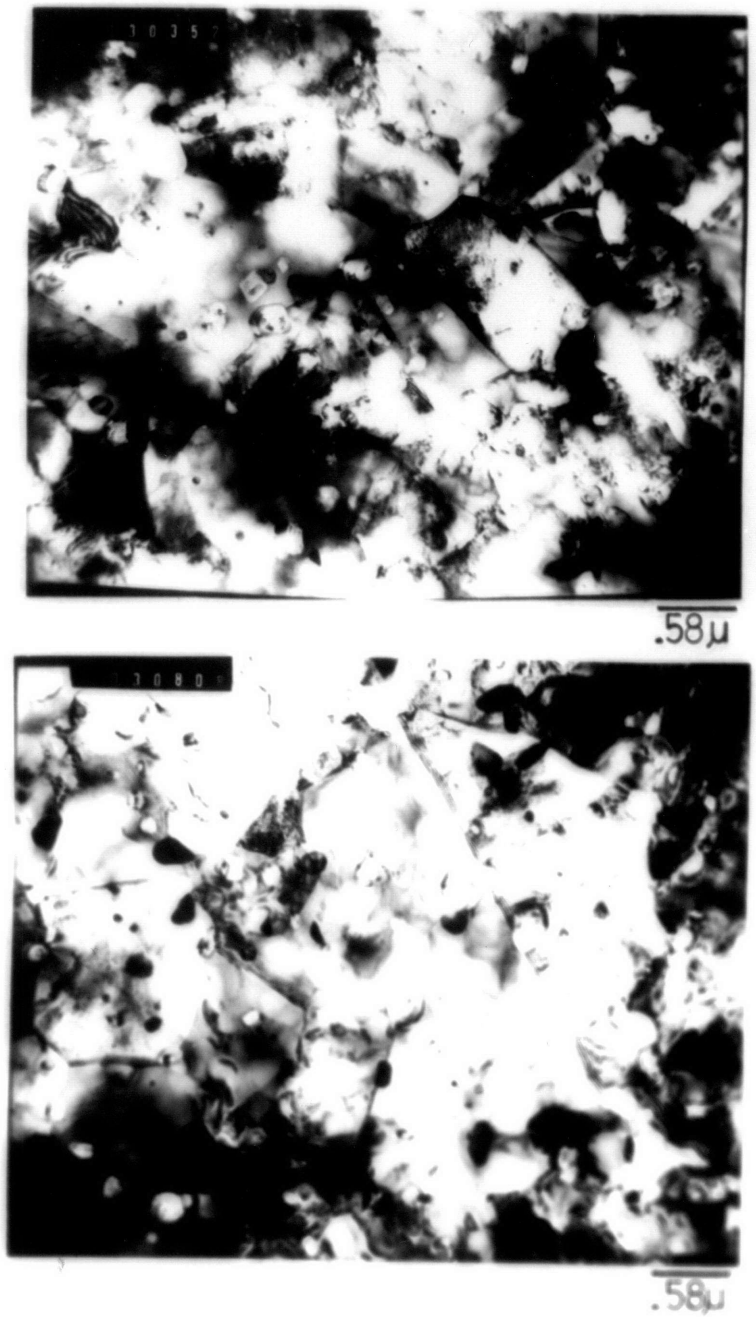

Figure 36. **TEM micrographs of heat treated (1243°C/ 2 hour/AC + 1232°C/0.5 hour/AC + 954°C/ 2 hour/AC + 843°C/24 hour/AC) alloy N-5 showing coarsened grain structure.**

the stress for a 100 hour life at 982°C was 10 ksi. This represented a considerable improvement over TMT treated N-1 and N-2. ZAP rates of 7.6 cm. (3 inch)/ hour and 15.2 cm. (6 inch)/hour resulted in stress values for a 100 hour life at 982°C of 9.7 ksi and 8.0 ksi, respectively. Shown in Fig. 33 is the impressiveness of the flattened stress rupture curves, indicating that the ZAP product will be much stronger in longer time tests than the annealed product.

The as-extruded N-5 alloy had stress for a 100 hour life of 7.5 ksi at 982°C. A recrystallization heat treatment was given to this alloy to effect grain growth and precipitation of γ'. The treatment was: 1243°C (2270°C)/2 hr/AC + 1232°C (2250°F)/0.5 hr/AC + 954°C (1749°F)/2 hr/AC + 843°C (1550°F)/24 hr/AC. Significant grain growth did not occur as is seen in Fig. 36. Grain sizes varied between 0.7μ and 3.5μ. Effective pinning of grain boundaries by oxide particles, Fig. 26, provided the resistance to grain growth. This heat treatment resulted in a stress for a 100 hour life at 982°C of 12 ksi. ZAP rates of 7.6 cm. (3 inch)/hour and 3.8 cm. (1.5 inch)/hour resulted in 100 hour life stressed of 27.5 ksi and 23.5 ksi.

Based on the latter values, tests at 1093°C were conducted on material ZAP treated at 7.6 cm.

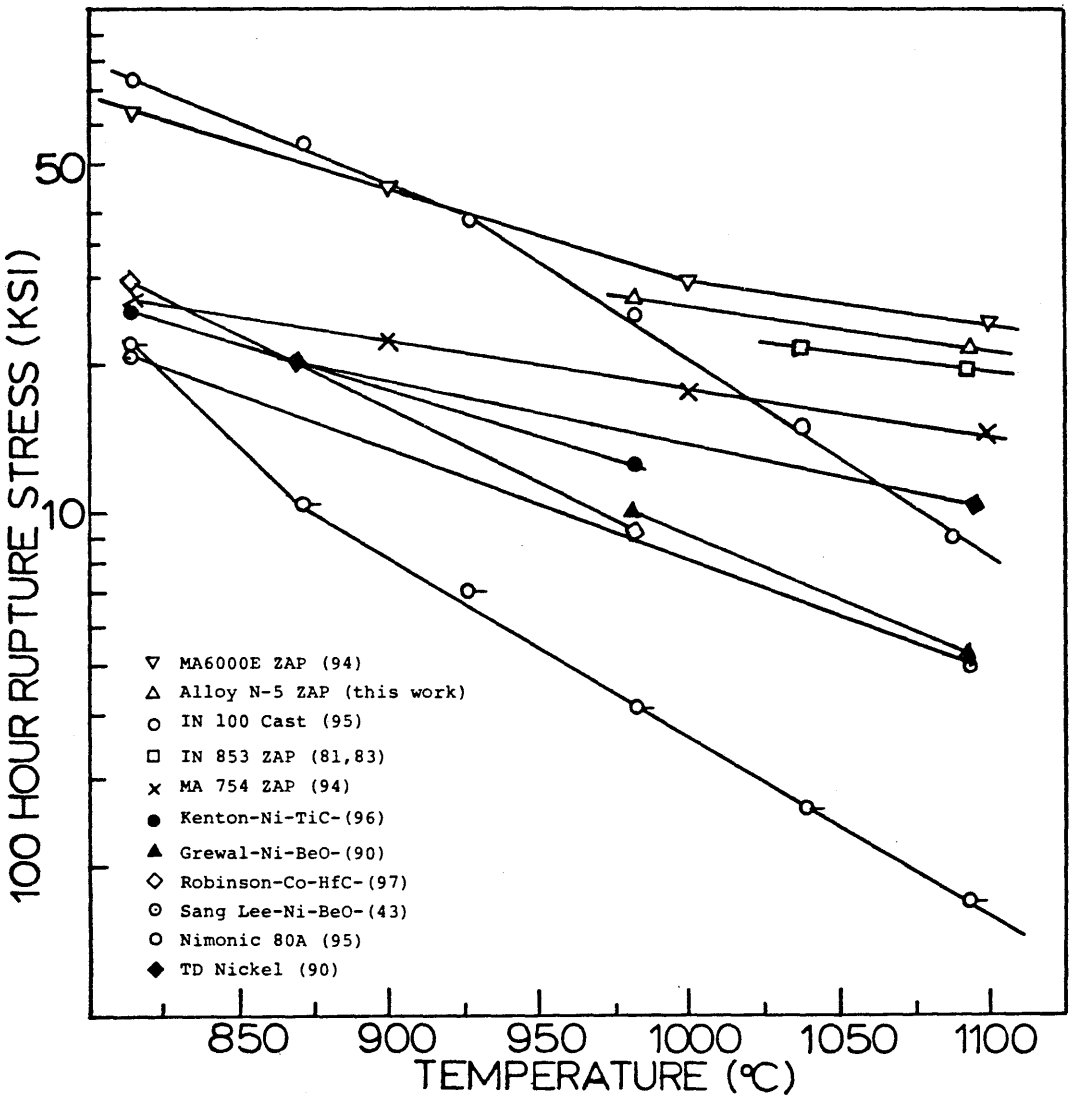

Figure 37. Comparison of stress for 100 hour rupture life of several Ni-base alloys.

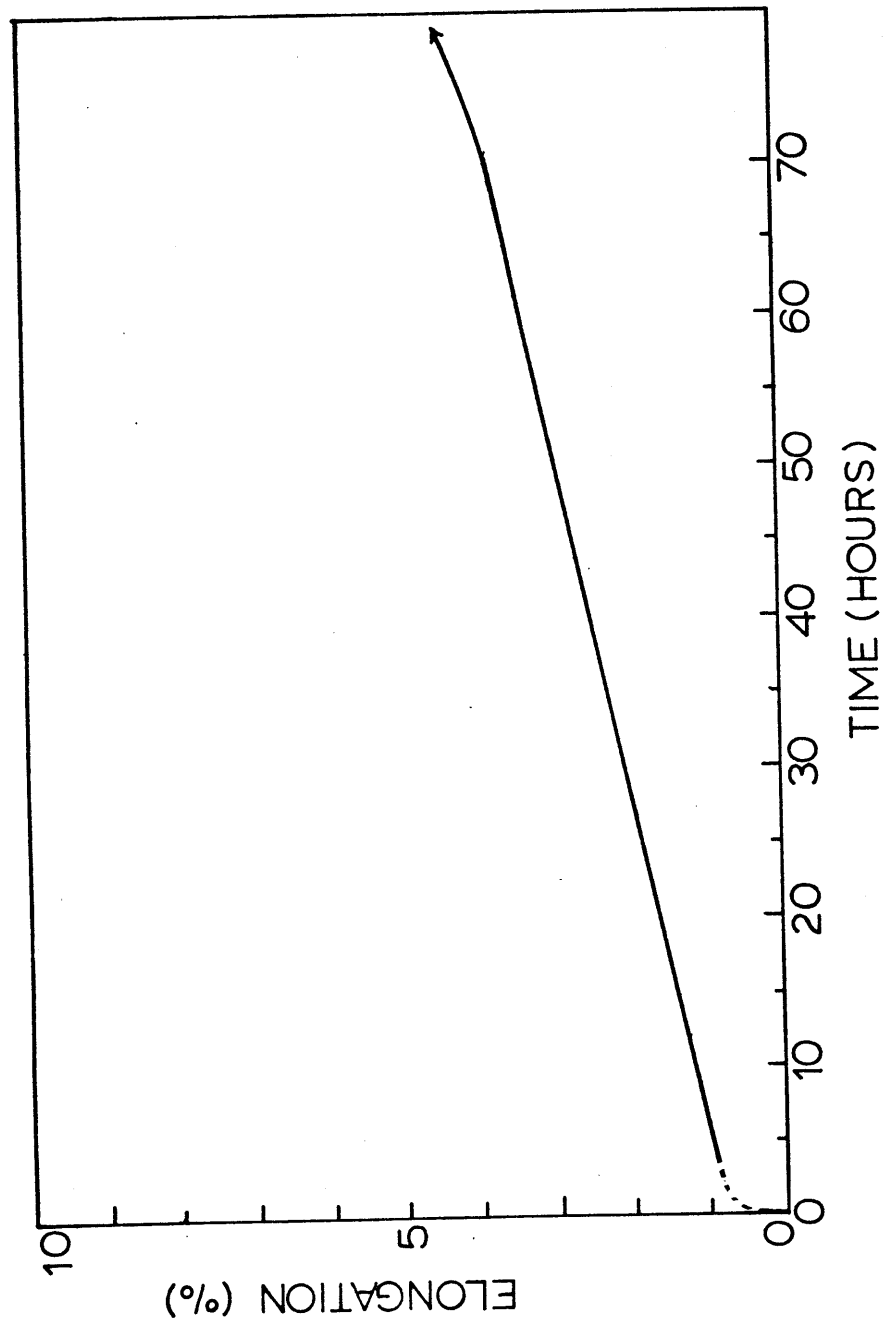

Figure 38. Creep curve at 24,000 psi and 982°C (1800°F) for N-5.

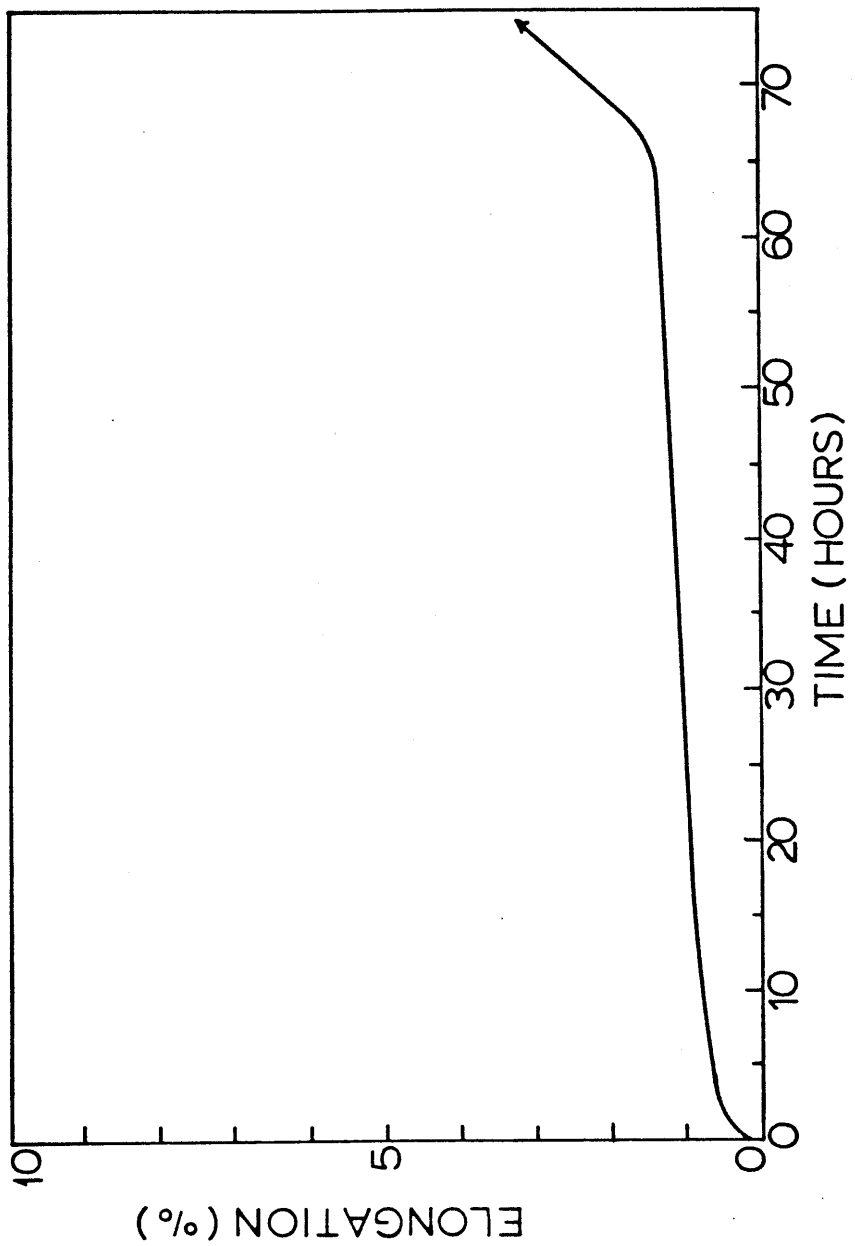

Figure 39. Creep curve at 22,000 psi and 1093°C (2000°F) for N-5.

(3 inch)/hour. A value of 22 ksi was obtained for the stress for a 100 hour life. This curve is shown in Fig. 35.

A comparison of the stress for 100 hour life of several Ni-base alloys is shown in Fig. 37. Alloy N-5 displays high temperature strength superiority over all alloys except MA6000E. (The latter is a mechanically alloyed ODS Ni-base superalloy (19). The disparity in strength between MA6000E.) The latter is a mechanically alloyed ODS Ni-base superalloy (19). The disparity in strength between MA6000E and N-5 is not significant especially when the cost savings incurred by the processing of N-5 is considered. The curves in Fig. 37 demonstrate succinctly the strength advantages obtained by combining the mechanisms of solid solution strengthening, precipitation hardening, and oxide dispersion stabilization in one alloy system.

Conventional creep tests were not carried out in this work, however, creep curves were generated from stress rupture data of alloy N-5. Typical creep curves at 982°C and 1093°C for N-5, ZAP treated at 7.6 cm. (3 inch)/hour plus heat treated are shown in Figs. 38 and 39, respectively.

The alloy displays typical three-stage creep behavior. The creep elongation at 982°C is about

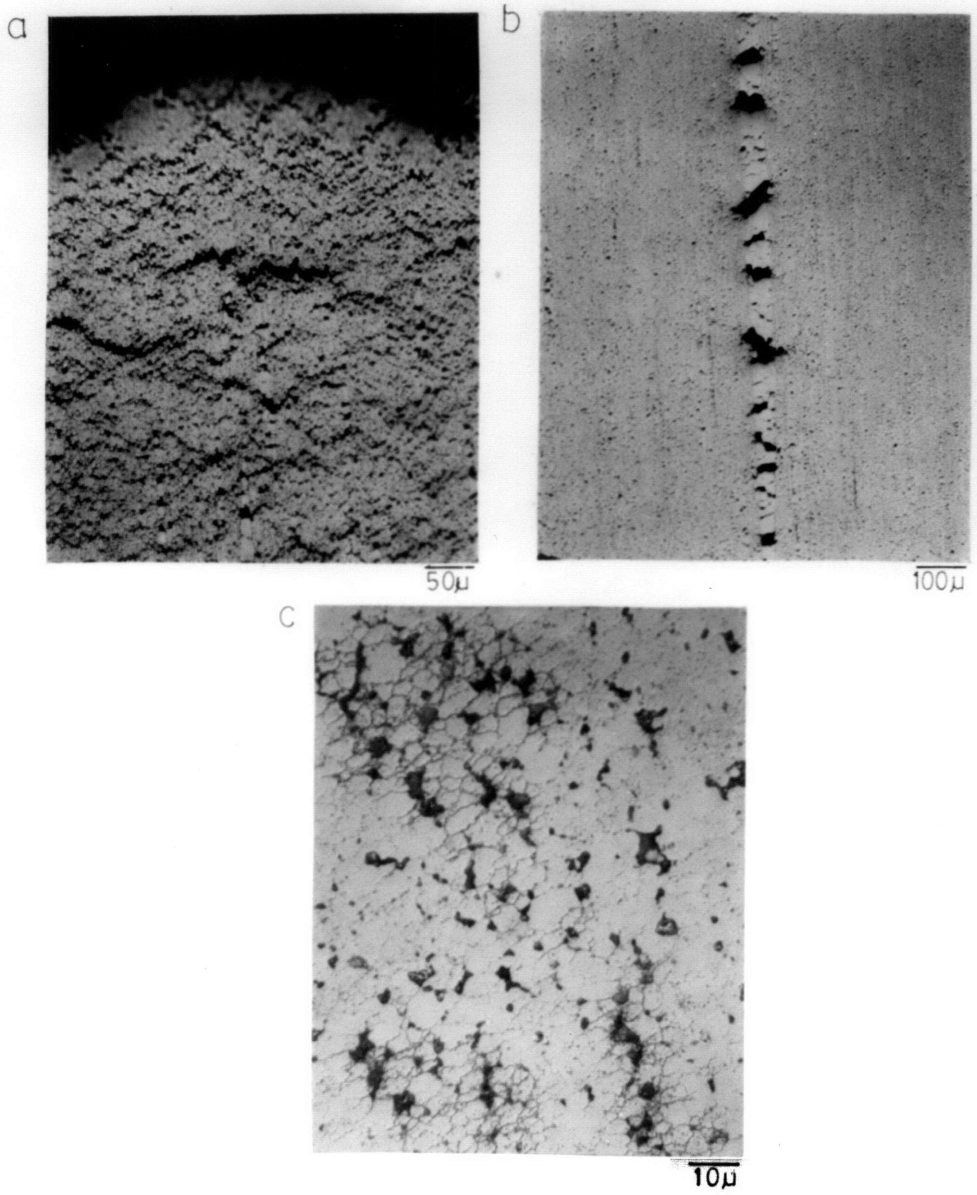

FIGURE 40. PHOTOMICROGRAPHS (LONGITUDINAL) OF STRESS-RUPTURE FRACTURE OF N-1, AS-EXTRUDED AND TESTED AT 982°C: A. AT FRACTURE SURFACE, B. SOME DISTANCE REMOVED FROM FRACTURE SURFACE AND C. ABOUT 2 MM. BELOW FRACTURE SURFACE.

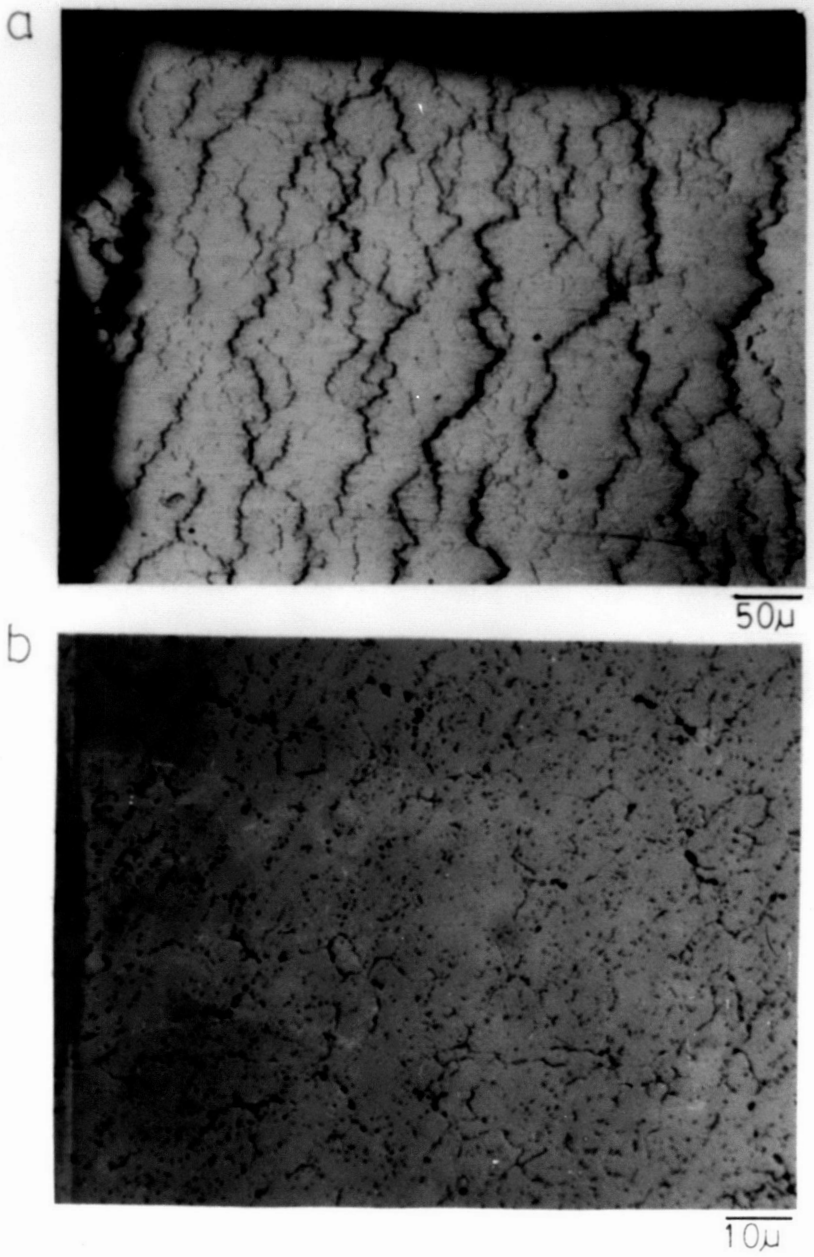

Figure 41. Photomicrographs (longitudinal) of stress-rupture fracture of N-1, as-extruded + 20 R.A. WIA 982°C (1800°F), and tested at 982°C: a. at fracture surface and b. about 2 mm. below fracture surface.

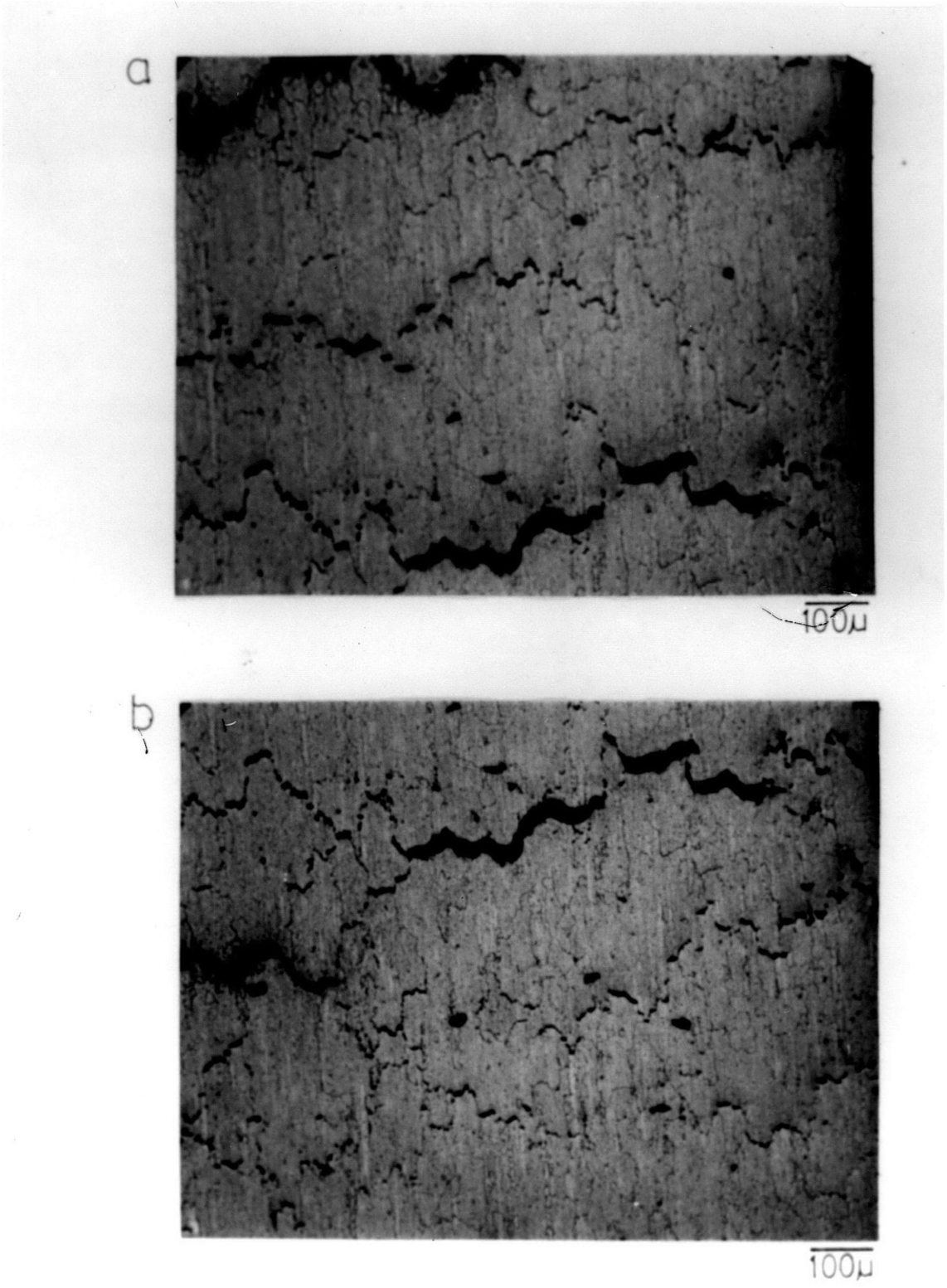

Figure 42. Photomicrographs of stress rupture fracture of N-3, as-extruded and anneal 1316°C (2400°F)/0.5 hour/AC, tested at 982°C (longitudinal).

5 percent and at 1093°C about 3.5 percent. MA6000E has a creep elongation at 760°C of about 3.5 percent and at 1093°C about 2 percent (20).

d. Stress rupture fractures

Alloys N-1, N-3 and N-5 were examined in an attempt to determine the mechanism of failure, and to compare qualitatively the extent of cracking that led eventually to failure. As shown in Fig. 40a, alloy N-1 had many small voids concentrated in the necked region near the fracture surface. Fig. 40b shows denuded regions of recrystallized grains with intergranular cracks, suggesting that cracks may have started in these regions. Void coalescence and intercrystalline cracking are shown in Fig. 40c.

Fig. 41a and b show that TMT decreases somewhat the severity of cracking over that of the as-extruded condition, and again cracking is intercrystalline. The wedge type morphology of cracks is more apparent here. Annealing so as to increase the grain size and decrease the grain boundary areas when applied to N-3 effectively impeded severe cracking. Fig. 42a and b shows that the extent of cracking in this alloy is not the same as N-1. It was determined in another study (83) that the presence of equiaxed grains among elongated, columnar, high GAR grains is pernicious to high temperature strength. This fact was apparent

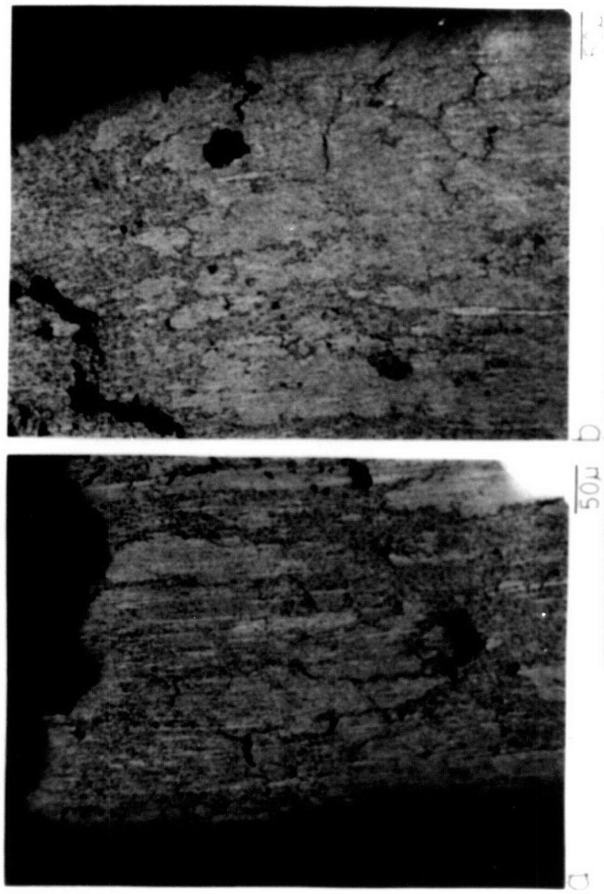

FIGURE 43. PHOTOMICROGRAPHS (LONGITUDINAL) OF STRESS RUPTURE FRACTURE OF N-3 ZAP AT 15.2 CM. (6 INCH)/HOUR AT 1300°C, TESTED AT 982°C: A. RIGHT SIDE OF SPECIMEN, B. LEFT SIDE OF SPECIMEN AND C. ABOUT 2 MM. BELOW FRACTURE SURFACE.

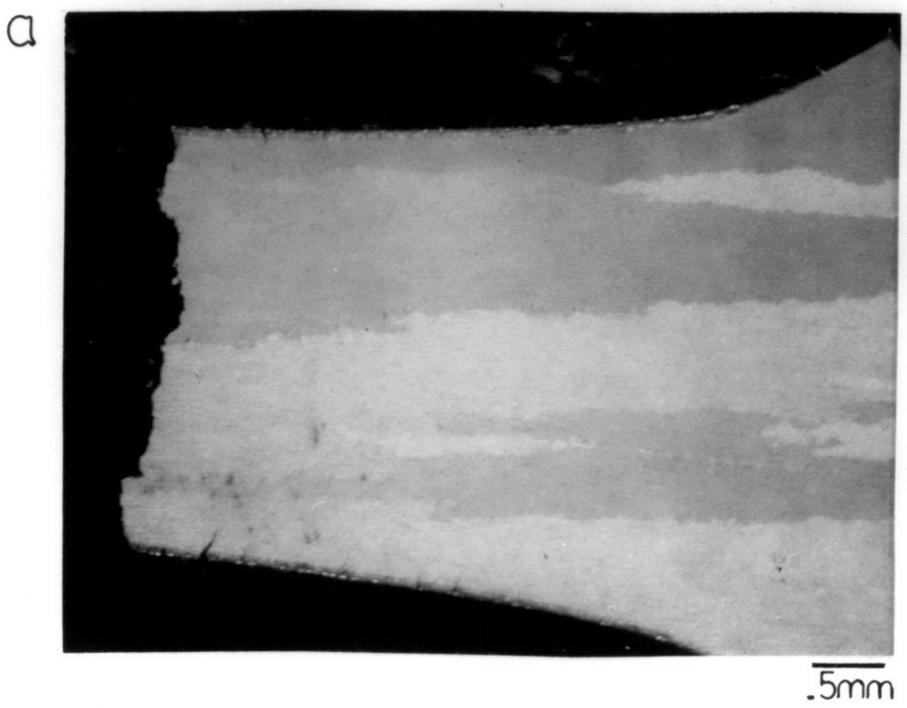

Figure 44. a. Photomacrograph of stress rupture fracture of N-5 ZAP at 7.6 cm. (3 inch)/hour at 1260°C, tested at 1093°C showing inter- and trans-granular cracking.

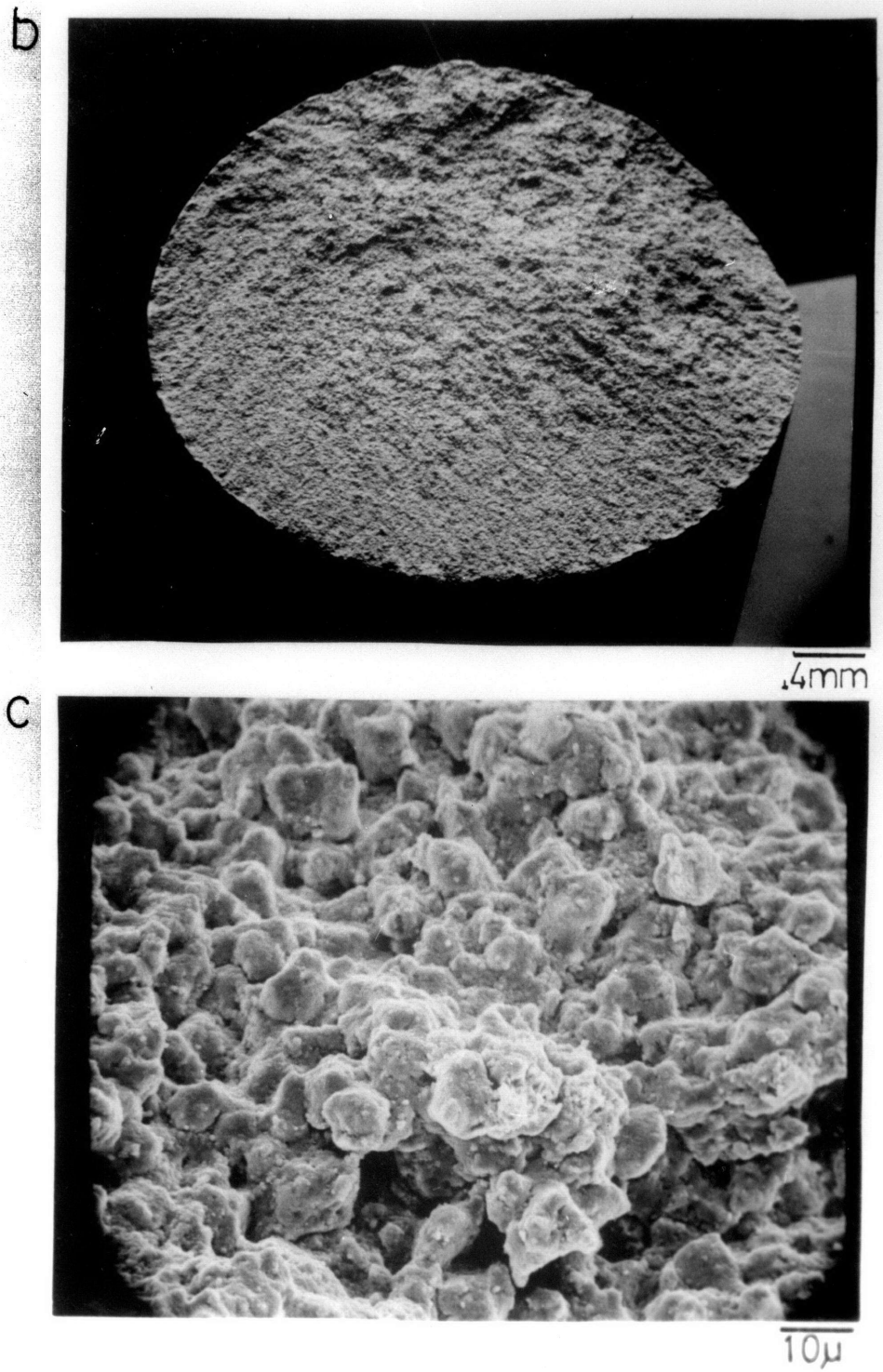

Figure 44. b. SEM micrograph of fracture surface.
c. Close up of fracture surface showing intergranular crack.

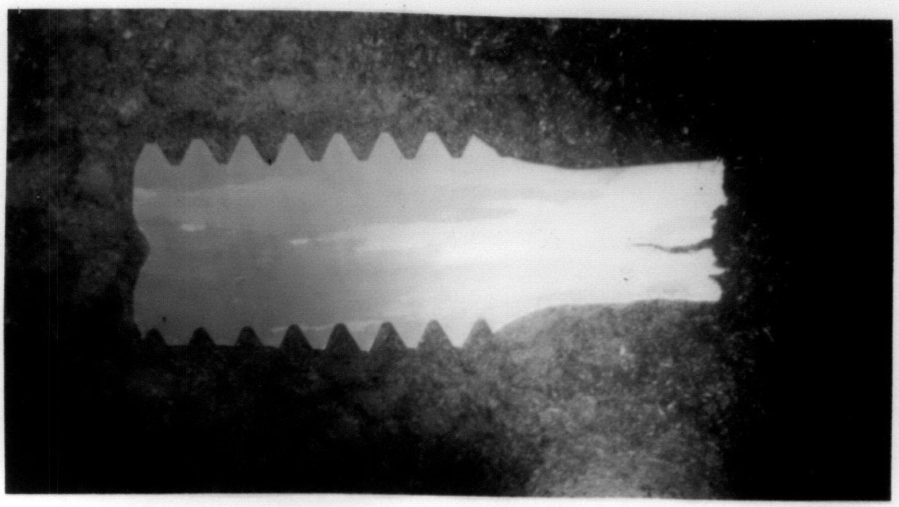

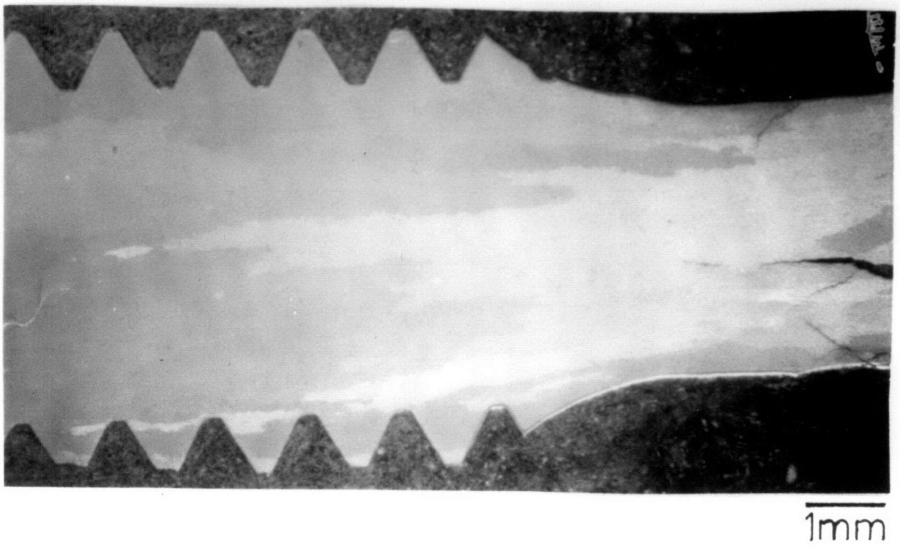

Figure 45. a. Photomicrograph of N-5, ZAP at 3.8 cm. (1.5 inch)/hour at 1260°C, stress rupture tested at 982°C, showing tearing.

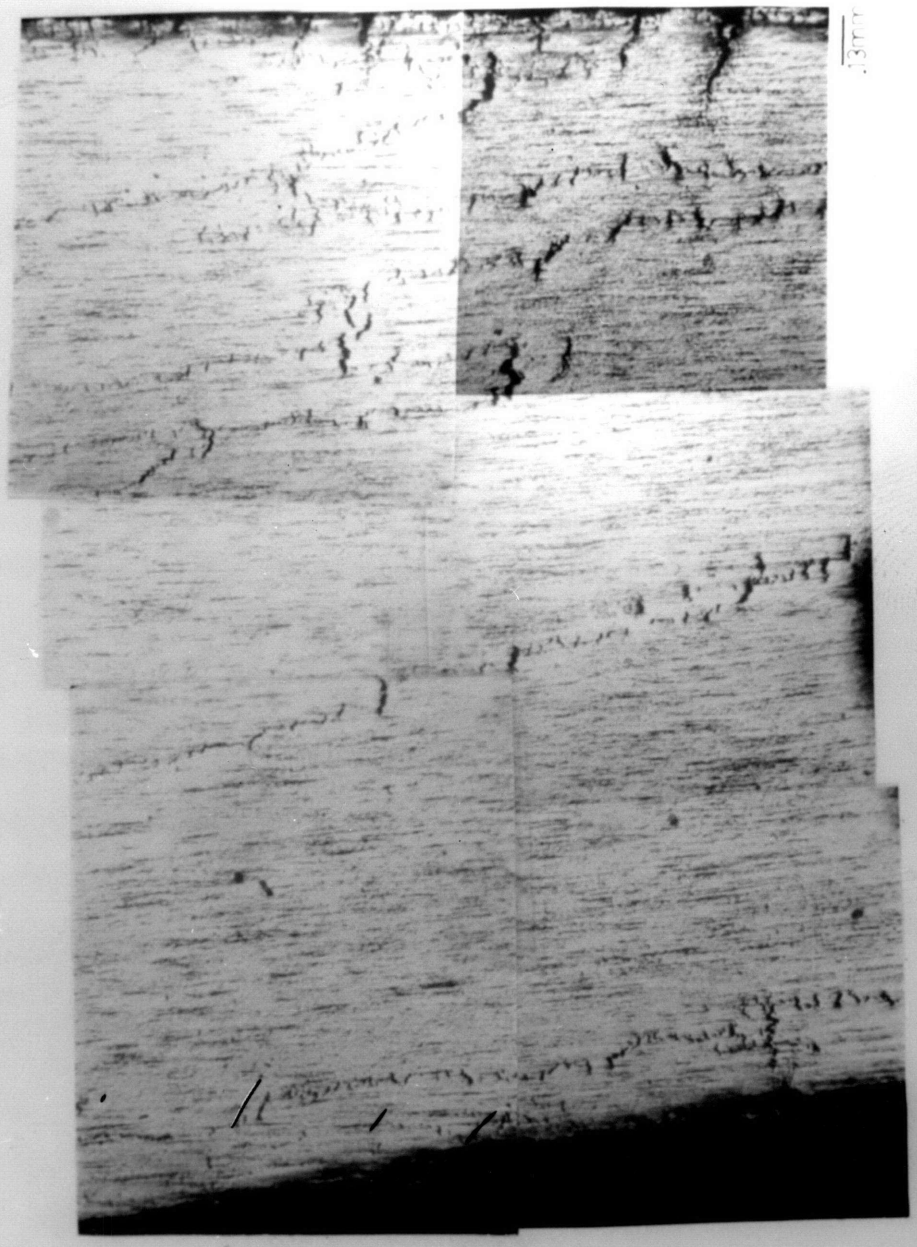

FIGURE 46. A. PHOTOMICROGRAPH OF N-5 ZAP AT 7.6 CM. (3 INCH)/HOUR AT 1260°C, STRESS RUPTURE TESTED AT 1093°C, SHOWING NATURE AND DISTRIBUTION OF CRACKS.

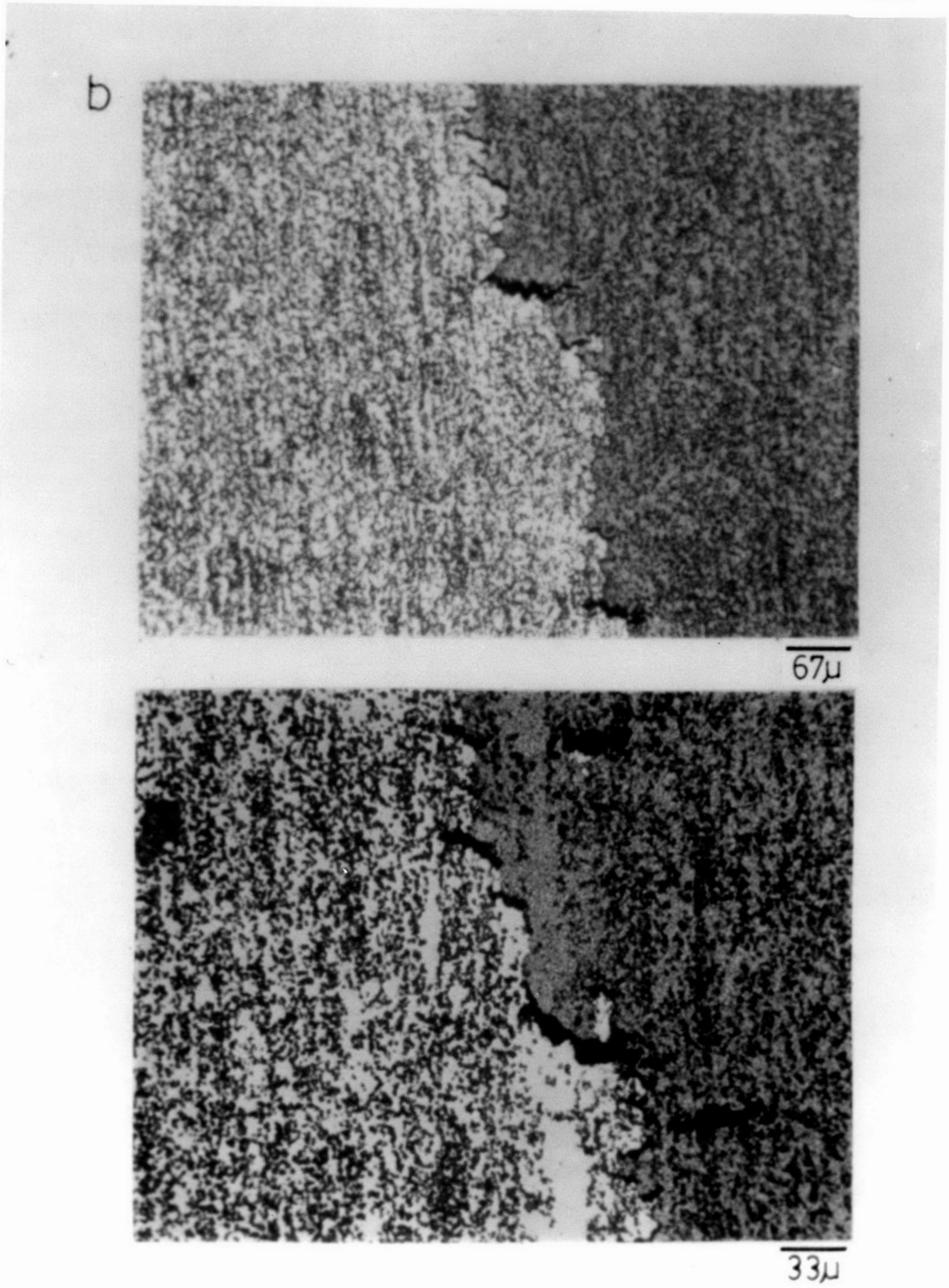

Figure 46. b. Close up of cracks at grain boundary in $\bar{N}$-5.

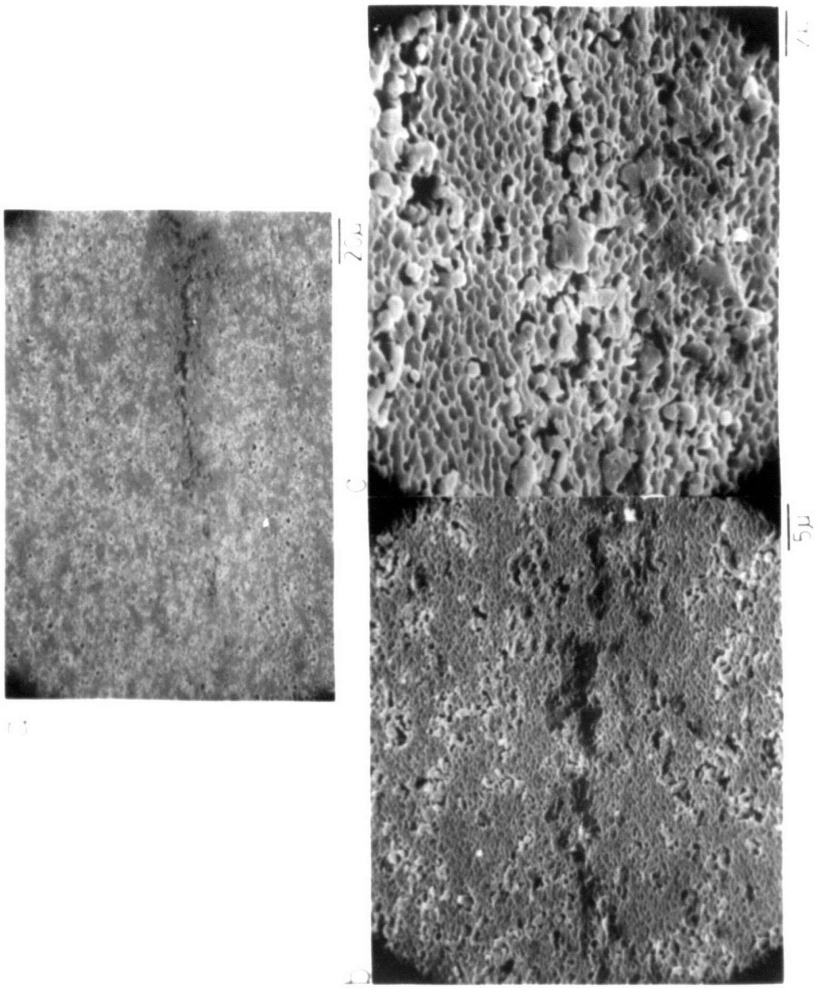

FIGURE 47. SEM MICROGRAPHS OF N-5, ZAP AT 3.8 CM. (1.5 INCH)/HOUR, STRESS RUPTURE TESTED AT 982°C: A. CRACK ABOUT 4 MM. BELOW FRACTURE SURFACE, B. CLOSE UP OF CRACK AND C. VOIDS ASSOCIATED WITH γ' PRECIPITATES.

FIGURE 48. TEM MICROGRAPHS OF N-5, ZAP AT 7.6 CM. (3 INCH)/HOUR AT 1260°C, STRESS RUPTURE TESTED AT 1093°C, SHOWING CRACKS IN A NUMBER OF γ′ PRECIPITATES.

in directionally recrystallized N-3; see Fig. 43a, b and c, where voids seem to initiate at the interface between equiaxed and columnar grains. Coalescence of these voids eventually led to fracture.

For alloy N-5, the fracture characteristics are very different. Firstly, cracking is not as severe as in N-1, N-2 or N-3. Secondly, cracking was both transgranular and intergranular as is demonstrated in Fig. 44a, b and c. (Fig. 45 shows fracture of N-5, ZAPed at 1.5.) Fig. 45 shows fracture of N-5, ZAPed at 1.5 inches/hour and stress rupture tested at 982°C. The fracture is similar to that of Fig. 44 except that tearing is also evident.

Fig. 46a and b attempts to demonstrate the nature and distribution of cracks across the specimen diameter. The cracks are concentrated mostly at grain boundaries., Fig. 46b, suggesting that they might have initiated there rather than at the surface. Fig. 47a, b and c shows SEM micrograph of cracks about 100μm below fracture surface. The evidence here is very suggestive that void initiation was somehow associated with the γ' precipitates present. Furthermore, Fig. 48 is a TEM micrograph detailing what appears to be cracks in the γ' precipitates, strongly indicating that this event led to void formation.

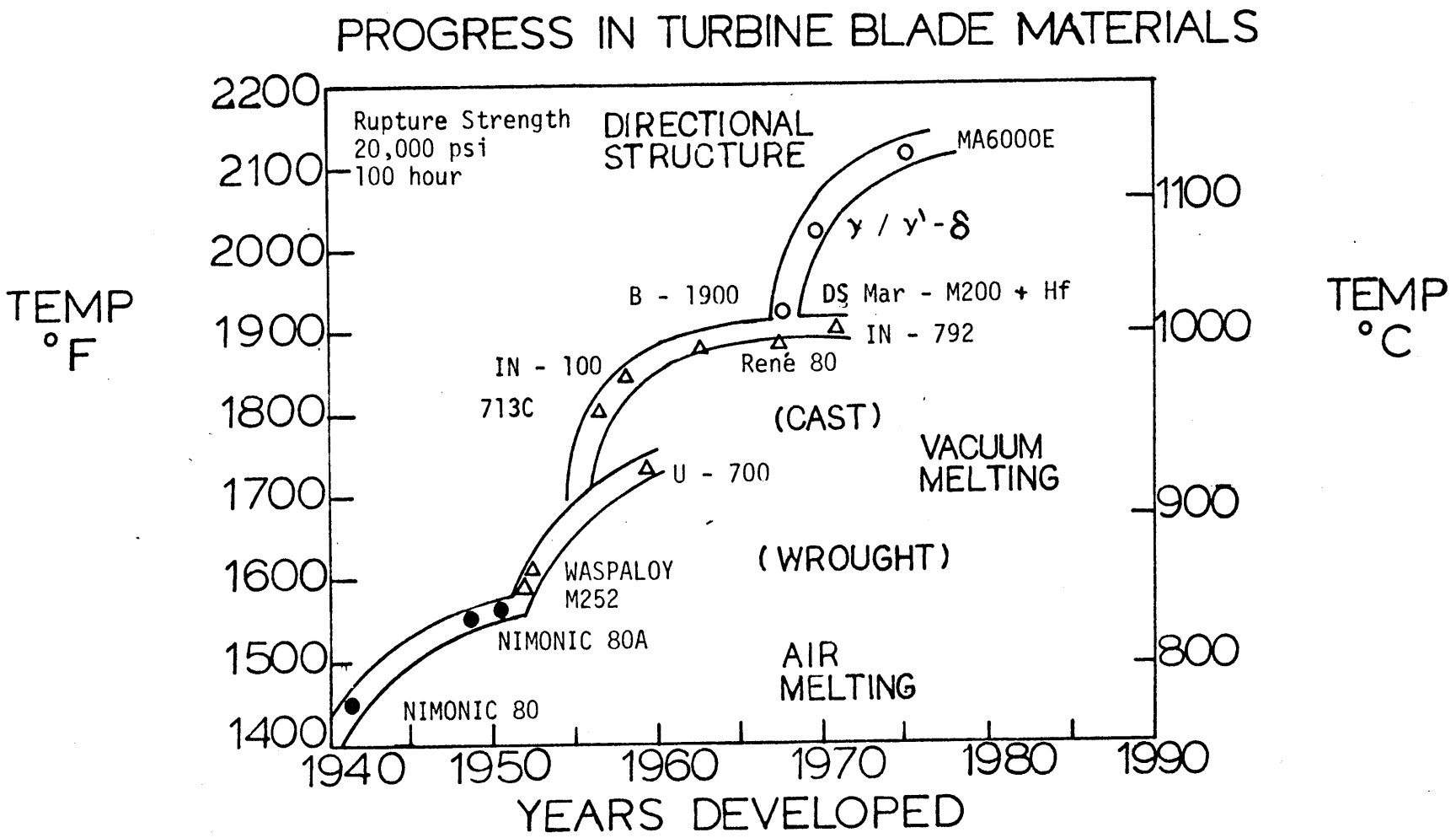

Figure 49. Progress in the temperature capability of superalloys over the last 40 years.

CHAPTER V

DISCUSSION

1. Processing

Effective and economic processing of alloys for very high temperature service for long periods of time is all important. Fig. 49 illustrates the progress in the temperature capability of superalloys over the last forty years. For many years, superalloys and process inventions enjoyed a symbiotic relationship. Many processes: vacuum induction melting, vacuum arc and electroslag remelting; investment casting, superplastic forming, directional solidification, were leaders in superalloy development. Recent progress in powder atomization, mechanical alloying, HIPing, superplastic forming/diffusion bonding and laser treatment have heralded a lively renewal of knowledge. One of these success stories, mechanical alloying (15), was used to produce Ni, Co, Fe and Al based oxide stabilized alloys. It is like so many others (5,28 to 40) unusually expensive, because the production of master alloy powders, and various elemental constituent powders for optimum blending and alloying is slow and expensive, as is the ball milling or attriting procedure.

The method of processing used for this project involved the following steps:

1. Melting or remelting of the fully alloyed master alloy.
2. Atomization, using methods which made possible high yields of fine powders (-44μ, for example); however, powders up to 70μ or 90μ were used provided the solidification rates were adequate to produce the desired refined structures. The atomized powders were fully alloyed except for the refractory fine oxide which was incorporated during ball milling. The advantages for rapidly solidified products over ingot or precision casting products have been well documented (97). Chemical segregation in fast cooled superalloy powders is controlled to a submicron level, massive phases are eliminated and most important, the solid solubility of alloying elements can be extended without deleterious phase reaction. Such fine fully alloyed powders are relatively cheaply produced.
3. Conversion of the fine powders to flake, see Table II.
4. Ball milling to incorporate the 200°A to 400°A refractory oxide particles (Table III).

The efficacy of the method is demonstrated based on the parameters outlined in Tables V and VI and in

structures of Figs. 6 to 9. Alloys N-1 and N-2 had inadequate oxide distributions because of an insufficient oxide addition and/or non-optimum distribution or dispersion. The best oxide distributions were identified with N-3 and N-5. The former had 5 v/o Y_2O_3 added while the latter had 2 v/o Y_2O_3 resulting in inter-particle spacings of 1050°A and 1210°A, respectively. Y_2O_3, Al_2O_3 and Y-Al-O_3 contributed as dispersoids to the 2.65% of oxides extracted from N-5. For N-3, 2.96% was extracted. Alloys N-1 and N-4 had about the same oxide content, i.e. 0.9% and 0.85%, respectively, even though N-1 had 0.5 w/o Al and N-4, 5.5 w/o Al. Perhaps the reason for the behavior can be deduced from the fact that the reactivity of Al as well as Ti is reduced when in the alloyed precipitated condition.

The technique of alloying is commonly used in pyrometallurgy for the addition of volatile elements. The thermodynamic activities (partial pressures) of the reactive elements are reduced by alloying them with one of the major consitituents of the alloy. An example is the addition of nickel-zirconium to a molten nickel-base alloy. The alloying technique was also used in powder metallurgy for the production of alloys containing reactive components (98). In the Ni-Al system, it has been shown that the activity coefficient of Al is 1.8×10^{-4} on the nickel rich

side of the intermetallic compound at 982°C. The activity of aluminum in this compound is reduced nearly ten-thousand fold beyond a simple Raoults law dilution (99). This evidence eclipsed whatever doubts there were of oxidizing completely the reactive elements Cr, Al, Ti and Zr that were present in alloys N-1, N-2, N-3, N-4 and N-5.

Significant oxidation of Cr, Al, and Ti did not occur. Analysis by x-ray, SEM, STEM and TEM conformed this. Deliberate surface oxidation of aluminum in N-1 and N-4 did not produce enough oxide in these alloys. One would have expected a higher oxide content in N-4 because of its high aluminum content, but this never materialized.

As shown in Fig. 4a and b, ball milling was continued until such time that there was consistency in the morphology of composite particles. The size of individual particles was not important, but it was the absence of flake-shaped particles that was. Additional oxidation of alloying elements was dependent on oxygen contamination of the argon gas in the drum or mill. It is surmised that once this oxygen was used up, further oxidation did not take place.

What was most reassuring here was the evidence in Fig. 14. The alloy was saturated with γ' precipitates,

determined to be 59 w/o. IN-100 has been documented to have 64 w/o γ' (86). The heat treatment given to this alloy (N-5) after the ZAP treatment was as stated previously, 1232°C (2250°F)/0.5 hour/AC + 954°C (1750°F)/ 2 hour/AC + 843°C (1550°F)/24 hour/AC. There were two types of γ' precipitates. Aging at 954°C resulted in 1000 to 4000°A precipitates and aging at 843°C precipitated the finer 200°A precipitates. This disparity in size was expected for two reasons. First, relief of the supersaturation at 843°C occurred in part by growth of the larger γ' particles already present. Second, Weins (105) has shown that the coarsening of a particle was strongly dependent on the size of the particles which surrounded it. Therefore, the large particles will coarsen when surrounded by small particles, and similarly, coarsening of the small particles will be retarded due to the presence of the large particles.

Growth of γ' has been predicted to obey $t^{1/3}$ coarsening kinetics in complex high volume fraction γ' Ni-base alloys by Kriege et al (112). Working with Udimet 700, the rate of coarsening was given by

$$(\bar{r}^3-\bar{r}_o^3)^{1/3} = At^{1/3}\left(\frac{Ce}{T}\right)^{1/3} \exp\left(\frac{-Q}{3RT}\right) \qquad (5)$$

where: $\bar{r}$ is the average particle radius at time t

$\bar{r}_o$ is the average particle radius at the time t=0

A: temperature dependent rate constant

Ce: concentration of solute (γ' forming elements) in equilibrium with a particle of infinite radius

Q: activation energy which is dependent primarily upon the diffusion rates of aluminum and titanium

It was suggested that the rates of γ' coarsening and the activation energy for diffusion found for Udimet 700 hold well for most other γ' containing nickel-base superalloys. It is not known what effect the presence of oxides would have on the kinetics, except that they should conceivably slow it down. The high volume fraction of γ' in alloy N-5 contributed to the alloys eventual failure in stress rupture testing. This observation is addressed later in this discussion.

2. Structural evaluation

The grain size of the alloys in their as-extruded condition were consistent with observations made by others (81,83). The highly deformed structures consisted of submicron sized equiaxed grains containing numerous annealing twins and a dislocation subgrain structure. It is believed that the very fine equiaxed grains were formed during the high temperature soaking given the highly cold worked flaked alloys before extrusion. Extrusion provided most of the deformation needed for developing the structures shown in Figs. 6 through 10. The presence of oxides in acceptable volume and distribution is of paramount importance since they helped in retaining the stored energy

in the substructure. They also effectively pinned grain boundaries, preventing grain growth during extrusion. It is this stored energy that provides the driving force for grain growth during subsequent ZAP treatments. The wide range of oxide particle sizes is illustrated quantitatively in Fig. 11a, b and c and in Table VI. This heterogenity contrasts with the relatively narrow size distribution that can be obtained for carbides and precipitates, for example, γ' in conventional alloys. It should be noted that the larger dispersoid particles present in alloy N-1 were absent in alloys N-2 and N-3. These large particles were broken up in the latter alloys during ball milling. This action certainly contributed to a better distribution of smaller particles and an improved interparticle spacing.

Alloy N-1 demonstrated that in the event of unacceptable oxide distribution, the as-extruded grain size is larger than desired, with a modicum of dislocation subgrain structure. N-1 did recrystallize after extrusion. A fine sub-structure is preponderant in alloys N-2, N-3 and N-5.

Contrary to the belief of others (81,83,92), the postulate that recrystallization occurs during and is complete after extrusion, and that the grain size increases progressively with extrusion temperature,

was not supported in this work. The presence of high concentrations of dislocations and a well developed substructure in alloys N-2, N-3 and N-5 is too convincing to justify supporting the proposed recrystallization claim. The larger grain size of N-1, i.e. 2.1 resulted from the lack of sufficient oxides necessary for grain boundary pinning during extrusion. Alloys N-4 and N-5 had similar compositions; Y_2O_3 was added to the latter, while the former depended on surface oxidized Al_2O_3. The fact that N-5 had a smaller grain size (0.4μ) than N-4 (0.6μ) is indicative of substantially more pinning of dislocations and grain boundaries in N-5.

3. Thermomechanical processing

Grant et al (5) obtained increases in the room temperature yield and tensile strength as well as improvements in high temperature yield, tensile and stress rupture properties by thermomechanical treatments. They attributed this to the formation of particle stabilized dislocation networks resulting in high levels of stored energy. Adachi and Grant (60) proposed that a large amount of stored energy of cold work in stable arrays is desirable for good high temperature properties. Chin and Grant (34) have experimentally measured a high value of stored energy (0.41 cal./gm.) to persist up to very high temperatures in a Cu-1.1 v/o Al_2O_3 alloy. Rasmussen and Grant (35) suggest

that it is not only the amount of stored energy, but also its distribution that must be considered in the stabilization of OD alloys.

Alloys N-1 and N-2 were thermomechanically treated. There were increases in room temperature yield and tensile strengths, and high temperature stress rupture strength over that of the alloys in their as-extruded conditions. Extraordinary high temperature strength values were not obtained. An insufficient oxide volume content resulted in very poor oxide distribution, hence stabilization of the structure resulting from TMT was not effected. Regular and irregular cell structures were developed varying in size from 208°A to 1700°A. These were located between low angle grain boundaries, 2μ to 3μ in width, as shown in Fig. 18. The inability of the alloy to retain this substructure was responsible for their poor high temperature performance.

The deformation substructure developed in alloys N-3 and N-5 from processing is a measure of the stored energy. TMT of these alloys was attempted but was impossible.

4. Mechanical property determination

a. Room temperature tensile tests

In the as-extruded condition all the alloys had high room temperature tensile strengths due to the extremely fine grain size of the extruded product and the residual strain energy derived from the

processing variables of attriting and ball milling.

Both categories of alloys studied responded to the Petch grain size relationship. For the ODS solid-solution alloys, N-1, N-2 and N-3, the lowest yield strength, 127 ksi, was for N-1 with a grain size of 2.1μ; N-3 with the high strength value of 239 ksi, had a grain size of 0.38μ. For the ODS precipitation hardened alloys, N-4 and N-5, the former, with a grain size of 0.62μ, had a yield strength of 223 ksi, while the latter, with a grain size of 0.4μ, had the highest strength of 326 ksi. The strength differences between the two categories are obvious and can be attributed to the presence of the γ' precipitates in the latter category.

The effect of TMT and annealing on room temperature mechanical properties is shown in Table VII. TMT of the ductile N-1, not only increased the yield strength, but the yield/tensile ratio, sacrificing ductility.

Grain coarsening in alloys N-3 and N-5 occurred in the temperature range 1093°C to 1316°C. Annealing at these temperatures caused a drop in the yield/tensile ratio and increased the work hardening response. This decrease in strength is dependent on the degree of recovery, grain growth and any particle growth which might have occurred. Clearly,

any strength increase derived through particle dislocation interplay was lost due to recovery, recrystallization and grain growth processes. IN 853 (81,83), a low volume fraction (15 v/o) γ'-oxide dispersed stabilized Ni-base superalloy displayed similar characteristics. Some properties for this alloy are given in Table VII for comparison.

b. Elevated temperature stability

One hour anneals for all the alloys at progressively higher temperatures demonstrated the stability that oxide particles impart to the highly strained structures. Alloys such as N-3 and N-5 remained stable to 1093°C because of suitable dispersions of Y_2O_3, Al_2O_3 and $Y\text{-}Al\text{-}O_3$, with small interparticle spacings. N-1 and N-2, with larger interparticle spacings did not maintain stability out to high temperatures. Lack of stability was determined to depend on large IPS, which was conducive to recovery, recrystallization, grain growth and particle coarsening. Particles were either γ' precipitates in the case of N-4 and N-5, and/or the hard oxide particles.

Some correlation between the stability of ODS alloys as indicated by room temperature hardness versus annealing temperature data (Appendix I) and stress for 100 hour rupture life values (Appendix II) is evident. Enhancing the stability of the structure by having a uniform particle distribution is reflected

from hardness versus annealing temperature data, and is confirmed by improved rupture strengths at elevated temperatures. This observation was also made by Grewal (90). It is significant in view of the simplicity of annealing studies, and should serve well for anticipating the trends in the stress rupture behavior of ODS Ni-base alloys.

c. Recrystallization and elevated temperature stress rupture strength

Grain boundaries are a source of weakness for high temperature properties of the complex ODS Ni-base superalloys. As a result, increases in GAR cause corresponding increases in high temperature rupture properties. The ZAP process produced larger and more elongated grains in the alloys (N-3 and N-5) investigated than those achieved by standard heat treatments, and thereby enhanced stress rupture properties. ZAP processing of N-3 resulted in similar 982°C/100 hour rupture stress to annealed N-3 but was superior at higher temperatures and for longer times. Both conditions increased the 982°C/100 hour rupture stress by more than a factor of three over that obtained for N-3 as-extruded. ZAP treatment of N-5 gave 982°C/100 hour rupture stress some four times that of the as-extruded and over twice that obtained by standard recrystallization heat treatments. Rupture ductilities

after ZAP treatments were generally lower than that for the as-extruded condition, and similar to that for standard heat treatments.

The maximum rate of specimen motion at which the columnar structure was achieved was found to depend on alloy composition and structure, on materials processing history, and on ZAP parameters. Under proper conditions, new grains were formed initially in the hot zone and grew in an opposite direction to the motion of the specimen. The first grains to form were relatively equiaxed but the steep temperature gradient suppressed nucleation of new grains and encouraged growth competition among existing grains. Those grains with the highest boundary mobility grew at the expense of those with less mobile boundaries. As the specimen traversed the gradient, the grain size increased to a maximum size which depended not only on the structure of the starting material, but also on several ZAP parameters. These included steepness of the temperature gradient, the rate of movement of the specimen and orientation with respect to the working direction.

Recrystallization temperature was the most important variable of the starting material. The recrystallization response was different between solid solution and precipitation strengthened ODS

alloys. The former (γ' free) exhibits a recrystallization response that is entirely dependent upon the material's prior thermomechanical history. In contrast, the high γ' alloy shows a delayed response. This behavior is attributed to the higher level of stored energy present and the presence of γ' precipitates which must first be solutionized before there can be any response. A fine uniform distribution of oxides proved essential to storage of energy. Maximum ZAP rate is thought to be controlled by the mobility of the interface between recrystallized and as-worked material. For N-3 the interface temperature was >1300°C and mobility was 7.6 cm. (3.0 inch)/hour to 15.2 cm. (6.0 inch)/hour, while for N-5, the interface temperature was >1260°C and mobility was 3.8 cm. (1.5 inch)/hour to 7.6 cm. (3.0 inch)/hour.

Evaluation of ZAP treated material showed that the dispersoid size was not affected by the treatment. Dislocations were virtually absent and strong (100) recrystallization textures were developed.

The mechanism by which a large, elongated, textured grain structure is produced from a randomly oriented as-worked structure is uncertain, but two factors are postulated to be governing; it has been reported previously (101) that:

1. boundary mobility is a function of the orientation of the boundary with respect to crystallographic orientation of the growing grain and
2. grain boundary mobility was shown to be strongly dependent upon the directional effects supplied by the distribution of the dispersoid particles.

The combination of these two effects yields not only irregular shaped grains but also a recrystallization texture (Figs. 21 and 22). Hence only those nuclei that are oriented so that the crystallographic "fast growth direction" coincides with the direction which has the lowest density of grain boundary pinning agents will have highly mobile boundaries. This conclusion is reasonable in view of the fact that the dispersoids are heterogeneously distributed. The (100) was the fast growth direction for both N-3 and N-5.

A stress for 100 hour rupture life at 1093°C of 22 ksi was obtained for alloy N-5. Fig. 37 demonstrates that this alloy has comparable strength properties to some of the best reported alloys, viz. MA6000E. One important finding of this work is the fact that stress rupture fracture may have emanated with the cracking of γ' precipitates. Alloy N-5 had about 60% γ', while MA6000E is reported to have 39% γ' (19) with 1093°C/100 hour rupture stress of 24 ksi. The difference in strength could be attributed

to the high γ' content of N-5. This γ' was sitting in a matrix made stronger by the presence of fine oxide particles. On applying the stress during stress rupture testing, the weaker γ' particles yielded in preference to the stronger matrix. All of the cracks were discerned in the larger γ' precipitates. Hence, some modification of the heat treatment given, intended to eliminate the formation of the larger γ' particles, would have been appropriate.

With a stress for 100 hour rupture life at 1093°C of 22 ksi, alloy N-5 has exhibited high temperature strength second only to MA6000E. Its strength excels some of the best superalloys available today viz., DS MAR-M 200, DS eutectics ($\gamma/\gamma'-\delta$) and single crystal alloys (PWA 1409). Appendix IV and Fig. 37 compare the high temperature rupture strength of many different types of nickel base alloys. The cost effective and very simple method of processing used for N-5 make it an interesting candidate over alloy MA6000E and many other alloys for industrial applications.

CHAPTER VI

Conclusions

1. Oxide dispersion stabilized Ni-base alloys were processed by relatively simple steps which should be cost effective, were developed and characterized.

2. It was established that fully prealloyed powders manufactured from remelt cast ingots via atomization (rapid solidification) can be used if:

   i. rapidly solidified powders are first comminuted to a sufficiently thin flake thickness preferably one to two microns.

   ii. fine refractory oxides are incorporated into a previously flaked, alloyed product either by ball milling or by high energy attriting.

3. Complex alloys with high percentages of chromium, or superalloys with highly reactive elements such as aluminum and titanium can be attritor processed in a slurry, then ball milled (or treated in a high energy attritor) in an inert atmosphere without significant Cr_2O_3 formation and without oxidizing to unacceptable levels the aluminum and titanium which are important for precipitation strengthening purposes.

4. Oxide dispersion stabilized alloys do not recrystallize during or after extrusion. The submicron

sized grains are formed before extrusion. Extrusion then contributes to a highly worked, highly strained matrix, with a high dislocation density. Cell formation is evident and indicates the tremendous levels of energy stored in the deformation substructure.

5. The importance of a satisfactory distribution of fine oxides to the development of the deformation substructure and to the storage and eventual release of energy as a driving force for grain growth was established.

6. Thermomechanical treatments (TMTs), for example, swaging with intermediate anneals, as a mechanism for stabilization of oxide dispersed alloys is restricted to simple alloy systems. The more complex alloys cannot as readily be TMTed. Their deformation substructures developed during processing (attriting, ball milling and extruding) have achieved their optimum energy level and further working is restricted.

7. Recrystallization response is different between solid solution and precipitation strengthened ODS alloys. The former showed a more immediate response. The delayed response exhibited by the latter is due to:

i. the higher level of stored energy present.

ii. the presence of γ' precipitates which must first be solutionized before there can be any response.

8. For solid solution and precipitation strengthened ODS alloys, annealing above 1316°C (2400°F) and 1243°C (2270°F) respectively causes abrupt increases in grain size to coarse elongated structures (typically 10 mm. x 2 mm. and 8 mm. x 2 mm., respectively).

9. Columnar grain structures with high GAR were successfully produced. A ZAP rate of 3 inch/hour was established as being satisfactory for both types of alloys. A maximum and minimum rate of specimen travel through the hot zone was observed, above which and below which columnar grains no longer formed. The microstructures developed by the ZAP process were found to be dependent upon:

i. the presence and uniform distribution of the fine refractory oxide particles.

ii. the metal working history of the specimen, i.e. the total energy stored.

iii. the severity of the temperature gradient and,

iv. the rate of specimen movement through the gradient.

Also, the width of columnar grains of an ODS precipitation strengthened alloy was always greater than that of a solid solution ODS alloy.

10. As-extruded bar is very strong at room temperature with low ductility. Alloys given standard annealing treatments to develop coarse elongated grain structures

or ZAP processed to produced columnar high GAR grain structures have lower room temperature tensile strengths, but the stress rupture strengths were increased dramatically.

11. The severity of cracking during stress rupture was shown to decrease from N-1 to N-5 due primarily to a better balance of strengthening modes in grains and at grain boundaries. Generally, cracking was intergranular, with transgranular cracking being restricted to alloy N-5. Intergranular cracks were observed more readily at grain boundary segments inclined to the stress axis. This is as expected. It is possible that for such a high γ' (59%) alloy, crack initiation could be associated with the cracking observed in γ' precipitates.

12. Alloy N-5 displayed the best high temperature behavior with stresses for 100 hour lives at 982°C and 1093°C of 28 ksi (193 MPa) and 22 ksi (152 MPa), respectively.

CHAPTER VII

Suggestions for Further Work

1. To process an ODS superalloy using a high energy attritor in preference to a ball mill. This could conceivably reduce processing time by half.

2. To process an oxide dispersion stabilized IN-100 by:

   i. varying the volume fraction of oxide added from 0.5 to 1.5 v/o,

   ii. changing the heat treatment after ZAP processing, i.e., in addition to 1232°C/0.5 hour/AC + 954°C/2 hour/AC + 843°C/24 hour/AC, use 1232°C/0.5 hour/AC + 843°C/24 hour/AC. The latter treatment will eliminate the coarse (0.4μ) γ' precipitates formed in the former.

These combined actions should create a more ductile matrix, allowing for accomodation of deformation within the grains and across grain boundaries and improved high temperature properties.

3. To process an ODS superalloy with a leaner volume fraction of γ', i.e., 30% to 45%, while at the same time varying the oxide content from 0.5 v/o to 2.0 v/o.

4. Studies on ODS alloys, viz. MA6000E (20), IN753 (107), IN853 (108) and TD-Ni (109) have revealed them to have endurance ratios (10^7 fatigue strength/UTS)

twice those of conventional superalloys. Also, the fatigue resistance of MA6000E was significantly better than that of MAR-M200 in conventionally cast or directionally solidified form (20). Further work should be done to determine both low and high cycle fatigue behavior of alloys developed by the simple and cheap process utilized in this work. The modes of crack propagation and fracture should be investigated. The importance of this type of work is significant since aligned microstructures were shown (110) to be potentially deficient in their inability to resist shear at blade root (gas turbine hardware) attachments when stressed in a direction coinciding with that of the aligned grain boundaries.

5. That a study of alloys processed by the method of this work in which the effect of differing extrusion ratios and temperatures on structures and properties is determined. This will certainly optimize conditions for the best high temperature strength characteristics.

REFERENCES

1. Decker, R. F. and Sims, C. T., "The Metallurgy of Ni-Base Alloys", The Superalloys, (Wiley, New York, 1972, Ed. by C. T. Sims and W. C. Hagel), p. 23.

2. Mayfield, J., "Single Crystal Technology Use Starting", Aviation Week & Space Technology, Oct. 1, 1979.

3. Wilcox, B. A. and Clauer, A. H. "Dispersion Strengthening", The Superalloys, (Wiley, New York, 1972, Ed. by C. T. Sims and W. C. Hagel), p. 197.

4. Rasmussen, J. G. and Grant, N. J., "ThO_2 Dispersion Strengthened Nickel and Nickel-Molybdenum Alloys Produced by Selective Reduction", Powder Met., 8, 15, 92, (1965).

5. Grewal, M. S., Sastri, S. A. and Grant, N. J., "Structure-Property Relationship in Thermo-mechanically Treated Beryllia Dispersed Nickel Alloys", Met. Trans., 6A, 1393, (1975).

6. Wolf, S. M. and Grant, N. J., "Structure-Property Relationships in Oxide-Dispersed Iron-Berrylia Alloys", J. of Powder Met. Int'l, 9, 2, (1977).

7. Ansell, G. S., "The Mechanism of Dispersion Strengthening", Oxide Dispersion Strengthening, (Gordon and Breach, New York, 1968), p. 61.

8. Jeffries, A., "Metallography of Tungsten", Trans. AIME, 60, 588, (1919).

9. Irmann, R., Metallurgia, 46, 125, (1952).

10. Preston, O. and Grant, N. J., "Dispersion Strengthening of Copper by Internal Oxidation", Trans. AIME, 221, 164, (1961).

11. Anders, F. J., Alexander, G. B. and Wartel, W. S., "A Dispersion Strengthened Nickel Alloy", Metal Prog., 82, 6, 88, (1962).

12. Bonis, L. J. and Grant, N. J., "The Structure and Properties of Dispersion Strengthened Internally Oxidized Alloys", Trans. AIME, 224, 308, (1962).

13. Gatti, A., "Iron-Alumina Materials", Trans. AIME, 215, 753, (1959).

14. Zwilsky, K. M., Nelson, R. C. and Grant, N. J., "Dispersion Strengthening of Iron", Precipitation from Iron-Base Alloys, Speich, G. R. and Clark, J. B., Eds. Gordon, Breach Science Pub., 327, (1965).

15. Benjamin, J. S., "Dispersion Strengthened Superalloys by Mechanical Alloying", Met. Trans., 1, 2943, (1970).

16. Gessinger, G. H., "Mechanical Alloying of IN-738", Met. Trans., 7A, 1203, (1976).

17. Kramer, K. H., "Dispersion Strengthened Superalloys", Powder Metallurgy International, 9, 105, (1977).

18. Curwick, L. R., "Oxide Dispersion Strengthened High Volume Fraction Gamma Prime Ni-Cr-Al Alloys Made by Mechanical Alloying", NADC-76204-30, December, 1977.

19. Merrick, H. F., Curwick, L. R. and Kim, Y. G., "Development of Oxide Dispersion Strengthened Turbine Blade Alloy by Mechanical Alloying", NASA CR-135150, January, 1977.

20. Merrick, H. F. and Kim, Y. G., "Characterization of an Oxide Dispersion Strengthened Superalloy, MAGOOOE, for Turbine Blade Application", NASA CR-159493, May, 1979.

21. Gregory, E. and Grant, N. J., "High Temperature Strength of Wrought Aluminum Powder Products", Trans. AIME, 205, (1954).

22. Lenel, F. V., Backensto, A. B., and Rose, M. V., "Properties of Aluminum Powders and Extrusions Produced from Them", Trans. AIME, 209, (1957).

23. Bloch, E. A., "Dispersion Strengthened Aluminum Alloys", Met. Reviews, 6, 193, (1961).

24. Busk, R. S. and Leontis, T. E., "The Extrusion of Powdered Magnesium Alloys", Trans. Met. Soc. AIME, 188, 297, (1950).

25. Eastwood, B. J. and Robins, D. A., "Some Properties of Tine Prepared from Tin Powder by Extrusion", Powder Met., 7, 99, (1964).

26. Pops, H. and Libsch, J. F., "Zn-ZnO Alloys for Dispersion Hardening", Trans. AIME, 218, 1131, (1960).

27. Zwilsky, K. M. and Grant, N. J., "Dispersion Strengthening of Cu Using a Variety of Dispersoids", Ultrafine Particles, ed., W. E. Kuhn, pp. 479-487, New York, (1963).

28. Bonis, L. J. and Grant, N. J., "Influence of Processing Variables on the Properties of Ni-Al_2O_3 Alloys", Trans. AIME, 218, 877, (1960).

29. Cremens, W. S. and Grant, N. J., "Preparation and High Temperature Properties of Ni-Al_2O_3 Alloys", Proc. ASTM, 58, 714, (1958).

30. Gregory, E. and Goetzel, C. G., "Some High Temperature Properties of Nickel-Alloy Powder Extrusions Containing Non-Metallic Dispersions", Trans. Met. Soc. AIME, 212, 868, (1958).

31. Bufferd, A. A., "Dispersion Strengthened Iron", Sc.D. Thesis, MIT, (1965).

32. Gatti, A., "Iron-Alumina Materials", Trans. AIME, 215, 753, (1959).

33. Singh, B. N., Cotterill, P. and Waldron, M. B., "The Effect of Dispersoid Properties on Dispersion Strengthening of Carbonyl Iron", Powder Met., 12, 157, (1969).

34. Chin, L. J. and Grant, N. J. "Release of Stored Energy in Oxide Dispersion Strengthened Copper", Powder Met., 10, 20, 344, (1967).

35. Rasmussen, J. G. and Grant, N. J., "ThO_2 Dispersion Strengthened Nickel and Nickel-Molybdenum Alloys Produced by Selective Reduction", Powder Met., 8, 15, 92, (1965).

36. Murphy, R. and Grant, N. J., "Properties of Ni-ThO_2 Alloys Prepared by Thermal Decomposition of Thorium Nitrate", Powder Met., 10, 1, (1962).

37. Bovarnick, B. and Flood, H. W., "Dispersion Strengthening Principles of Improved Iron Powder", Progress in Powder Met., 20, 64, (1964).

38. Anders, F. J., Alexander, G. B. and Wartel, W. S., "A Dispersion Strengthened Nickel Alloy", Metal Prog., 82, 6, 88, (1962).

39. Schilling, W. F., "Dispersion Strengthened Alloys Produced by Surface Oxidation Technique", Sc.D. Thesis, MIT, (1969).

40. Swisher, J. H. and Turkdogan, E. T., "Solubility, Permeability and Diffusivity of Oxygen in Solid Iron", Trans. AIME, 239, 426, (1967).

41. Hildeman, G. J., "The Effect of Structure on Properties of Oxide Dispersion Strengthened Iron-Beryllia Alloys", Sc.D. Thesis, MIT, (1978).

42. Hunkeler, F. J., "Oxide Dispersion Strengthened Iron-Beryllia Alloys", Sc.D. Thesis, MIT, (1968).

43. Lee, S. H., "A Dispersion Strengthened Nickel Base Alloy Produced by Internal Oxidation", Sc.D. Thesis, MIT, Cambridge, (1976).

44. Komatsu, R. H. and Grant, N. J., "Thermal Stability of Cu-SiO_2 and Cu-Al_2O_3 Alloys", Trans. AIME, 224, 705, (1962).

45. Seebohm, R. H. and Martin, J. W., "The Effect of Internal Oxidation on Some Properties of Copper Alloys Sintered Compact", Metallurgia, 61, 163, (1960).

46. Edelson, B. I. and Baldwin, Jr., W. M., "The Effect of Second Phases on the Mechanical Properties of Alloys", ASM Trans. Quart., 55, 230, (1962).

47. Clauer, A. H. and Wilcox, B. A., "Steady-State Creep of Dispersion-Strengthened Nickel", Met. Sci. J., 1, 86, (1967).

48. Clauer, A. H. and Wilcox, B. A., "The Role of Grain Size and Shape in Strengthening of Dispersion Hardened Nickel Alloys", Acta. Met., 20, 743, (1972).

49. Petrovic, J. J. and Ebert, L. J., "Elevated Temperature Deformation of TD-Nickel", Met. Trans., 4, 1301, (1973).

50. Benjamin, J. S. and Bomford, M. J., "The Effect of Yttrium Oxide Volume Fraction and Particle Size on Elevated Temperature Strength of a Dispersion Strengthened Superalloy", Met. Trans., 5, 615, (1974).

51. Fraser, R. W. and Evans, D. J. I., "Strengthening Mechanisms in Dispersion-Strengthened Nickel", Oxide Dispersion Strengthening, eds. Ansel, G. S. et al, Gordon Breach Science Pubs., 375, (1968).

52. Wilcox, B. A. and Clauer, A. H., "Creep of Thoriated Nickel Above and Below $0.5T_m$", Trans. AIME, 236, 570, (1966).

53. Wilcox, B. A. and Clauer, A. H., "Dispersion Strengthening", The Superalloys, eds. Sims, C. T. and Clark, J. B., J. Wiley and Sons, 1972.

54. Aust, K. T., "The Art and Science of Growing Crystals", Chapter 23, eds. Gilman, J. J., J. Wiley and Sons, 1973.

55. Allen, R. E., "Directionally Recrystallized TD-Ni-Cr", Proceedings of Seven Springs Conference, MCIC-72-10, September, 1972.

56. Fischmeister, H. and Straube, H., "Part II: Powder Metallurgy Processing", Forging and Powder Consolidation of Superalloys, pub. by Applied Science Publishers Ltd., England, 790, 1978.

57. Schilling, W. F., "Dispersion Strengthened Fe-Cr-Al-Y Alloys by Flake Powder Processing", Superalloys Metallurgy and Manufacture, Proc. of 3rd Int'l Sym. eds. Kear, B. H., Muzyka, D. R., Tien, J. K. and Wlodek, S. T., Claitor's Pub. Div., 1976.

58. Yim, W. M. and Grant, N. J., "The Effect of Prior Strain and Polygonization on the Creep-Rupture Properties of Nickel", Trans. Met. Soc. AIME, 227, 868, (1963).

59. Lagneborg, R., "Recovery Creep in Materials Hardened by a Second Phase", J. Mat. Sci., 3, 596, (1968).

60. Adachi, M. and Grant, N. J., "The Effect of Stored Energy and Recyrstallization on the Creep Rupture Properties of Internally Oxidized Copper Alumina and Copper-Silica Alloys", Trans. AIME, 218, 881,(1960).

61. Clegg, M. A. and Lund, J. A., "Substructure Strengthening in Dispersion Strengthened Nickel Alloys", Met. Trans., 2, 2495, (1971).

62. Sherby, O. D., Klundt, R. H. and Miller, A. K., "Flow Stress, Subgrain Stability at Elevated Temperature", Met. Trans., 8A, 843, (1977).

63. Doble, G. S. and Quigg, R. S., "Effect of Deformation on Strength and Stability of TD Nickel", Trans. AIME, 233, 410, (1965).

64. Whittenberger, J. D., "Observation on the Relationship of Structure to the Mechanical Properties of Thin TD-Ni-Cr Sheet", Met. Trans., 7A, 611, (1976).

65. Orowan, E., SYMPOSIUM ON INTERNAL STRESSES, Inst. of Metals, London, 451, (1947).

66. Ansell, G. J., "The Mechanism of Dispersion Strengthening--A Review", OXIDE DISPERSION STRENGTHENING, p. 61, Gordon and Breach, New York, (1968).

67. Ashby, M. F., "The Theory of Critical Shear Stress and Work Hardening of Dispersion Hardened Crystals", OXIDE DISPERSION STRENGTHENING, p. 143, Gordon and Breach, New York, (1968).

68. Place, T. A. and Lund, J. A., "Low-Temperature Mechanical Properties of Thoria Dispersed Strengthened Iron", Met. Trans., 3, 1613, (1972).

69. Jones, R. H., "Predicting the Stress-Strain Behavior of Polycrystalline-Iron Containing Hard Spherical Particles", Met. Trans., 4, 2799, (1973).

70. Doble, G. S., Leonard, L. and Ebert, L. J., "The Effect of Deformation on Dispersion Hardened Alloys", Final Report on NASA Grant NGR36-033-094, (1967).

71. Ansell, G. S. and Weertman, J., "Creep of a Dispersion-Hardened Aluminum Alloy", Trans. AIME, 215, 838, (1959).

72. Wilcox, B. A. and Clauer, A. H., "High Temperature Creep of Ni-ThO_2 Alloys", OXIDE DISPERSION STRENGTHENING, Ansel, G. S. et al, eds., Gordon and Breach Publishers, p. 323, (1968).

73. McLean, D. and Hale, H. F., "Structural Processes in Creep", p. 19, Iron and Steel Institute, London, (1961).

74. Sherby, O. D., "Factors Affecting the High Temperature Strength of Polycrystalline Solids", Acta Metall., 10, 135, (1962).

75. Lund, R. W. and Nix, W. D., "On High Creep Activation Energies for Dispersion Strengthened Metals", Met. Trans., 6A, 1329, (1975).

76. Malu, M. and Tien, J. K., "The Elastic Modulus Correction Term in Creep Activation Energies: Applied to Oxide Dispersion Strengthened Superalloy", 9, 1117, (1975).

77. Lin, J. and Sherby, O. D., NASA Contr. Rep. NASA-CR-135432, (1978).

78. Von Zeerleder: Z. Metallik., no. 8, p. 228, (1950).

79. Zwilsky, K. M. and Grant, N. J., "Dispersion Strengthening in Copper-Alumina System", Trans. AIME, 221, 371, (1961).

80. Zwilsky, K. M. and Grant, N. J., "Copper-Silica and Copper-Alumina Alloys of High Temperature Interest", Trans. AIME, 209, 1197, (1957).

81. Cairns, R. L., "Affect of Annealing on Structure and Properties of a Dispersion Strengthened Superalloy, IN-853", Met. Trans., 5, 1677, (1974).

82. Chin, L. L. J. and Grant, N. J., "Release of Stored Energy in Oxide Dispersion-Strengthened Copper", Pow. Met. 10, 20, 344, (1967).

83. Cairns, R. L., Curwick, L. R., and Benjamin, J. S., "Grain Growth in Dispersion Strengthened Superalloys by Moving Zone Heat Treatment", Met. Trans., 6A, 179, (1975).

84. Rose, H. E. and Sullivan, R. M. E., "Ball, Tube and Rod Mills", Chem. Publ. Co., 117, (1958).

85. Gaudin, A. M., "Principles of Mineral Dressing", McGraw Hill Book Co., New York, p. 106, (1939).

86. Kriege, O. H. and Sullivan, C. P., "The Separation of Gamma Prime from Udimet 700", ASM Trans. Quarterly, 61, 278, (1968).

87. Golubtsova, R. B., "Separation of Intermediate Ni_3Al from a Ni-Cr-Al Alloy", Izo. Akad Nauk SSSR Metally., 174, (1966).

88. Matti Kurkela Technical expertise and private help.

89. Hutchinson, W. B. and Wilcox, B. A., "The Influence of a Thoria Dispersion on Preferred Orientation in Nickel Alloys", Met. Sci. J., 7, 6, (1973).

90. Grewal, M. S., "Dispersion Strengthened Ni-base Alloys Produced by Internal and Surface Oxidation", Sc.D. Thesis, MIT, Cambridge, (1972).

91. McHargue, C. J., Jetter, L. K. and Ogle, J. C., "Preferred Orientation in Extruded Aluminum Rod", Trans. Met. Soc. AIME, 215, 831, (1959).

92. Sellars, C. M. and Petkovic-Luton, R. A., "Creep of Dispersion-Strengthened Alloys", Materials Science & Engineering, 46, 74, (1980).

93. Cullity, B. D., "Elements of X-ray Diffraction", Addison-Wesley Publishing Co., Inc., Reading, MA., p. 215, (1967).

94. Howson, T. E., Mervyn, D. A. and Tien, J. K., "Creep and Stress Rupture of a Mechanically Alloyed Oxide Dispersion and Precipitation Strenthened Nickel-Base Superalloy", Met. Trans., 11A, 1609, (1980).

95. The International Nickel Company, Inc., "High Temperature, High Strength Nickel Base Alloys", 3rd. ed., New York, (1977).

96. Kenton, D. J. and Grant, N. J., "Titanium Carbide Dispersion Strengthened Nickel Base Alloys", FINE PARTICLES-SECOND INTERNATIONAL CONFERENCE, W. E. Kuhn, Ed., The Electrochemical Soc. Inc., Princeton, NJ, p. 308, (1974).

97. Robinson, R. K., "Development of P/M Cobalt-Base Alloys Using Rapidly Quenched, Pre-Alloyed Powders", Sc.D. Thesis, MIT, Cambridge, (1972).

98. Joly, P. A. and Mehrabian, R., "Complex alloy Powders Produced by Different Atomization Techniques: Relationship between Heat Flow and Structure", J. Of Mat'l. Sci., 9, 1446, (1974).

99. Dubost, B. J., "The Microstructural Response of P/M In-100", M.S. Thesis, MIT, Cambridge, (1974).

100. Merrick, H. F., "Precipitation Within γ' Particles in Nickel-Base Superalloys", Met. Trans., 4, 885, (1973).

101. Oblak, J. M., Doherty, J. E. and Kear, B. H., "Precipitation of γ in γ' of Nickel-Base Superalloys", Met. Trans., 5, 1252, (1974).

102. Grant, N. J., "A Review of Various Atomization Processes", RAPID SOLIDIFICATION PROCESSING (Proceedings) Ed. R. Mehrabian, B. H. Kear, M. Cohen, Claitor's Publ. Div., Baton Rouge, LA., (1977).

103. Howe, G. H., "Sintered Alnico", Powder Metallurgy, J. Wulff, ed., ASM, p. 530, (1942).

104. Steiner, A. and Komarek, K. L., "Thermodynamic Activities of Solid Nickel-Aluminum Alloys", Trans. TMS-AIME, 230, 786, (1964).

105. Weins, J. J., "The Effect of Environment on Coarsening", Ph.D. Thesis, MIT, Cambridge, (1970).

106. Brown, J. R., "Development of Preferred Orientations in Silicon Iron", J. Of App. Phy., 29, 359, (1958).

107. Weber, J. H. and Bomford, M. J., "Comparison of Fatigue Deformation and Fracture in a Dispersion-Strengthened and a Conventional Nickel-Base Superalloy", Met. Trans., 7A, 435, (1976).

108. Weber, J. H. and Bomford, M. J., "High-Cycle Fatigue Properties of a Dispersion Strengthened Nickel-Base Superalloy", FATIGUE AT ELEVATED TEMPERATURES, ASTM STP 520, pp. 427-437, (1973).

109. Ham, R. K. and Wayman, M. L., "The Fatigue and Tensile Fracture of TD-Nickel", Trans. AIME, 239, 721, (1967).

110. Bartlett, E. S., "Shear Strength of MA6000E", SUPERALLOYS, Metals and Ceramics Information Center, Selected Developments in Metals and Ceramics, CAB, 109, 5, (1982).

111. VerSnyder, F. L. and Shank, M. E., "The Development of Columnar Grain and Single Crystal High Temperature Materials Through Directional Solidification", Mater. Sci. Eng., 6, 213-247, (1970).

112. Van Der Molen, E. H., Oblak, J. M. and Kriege, O. H., "Control of γ' Particle Size and Volume Fraction in the High Temperature Superalloy Udimet 700", Met. Trans., 2, 1627, (1971).

APPENDIX I

A. Specimen Preparation for Optical Metallography

Specimens (bulk and powders) were mounted in bakelite and ground through 600 grit silicon carbide polishing paper. Polishing was done on felt wheels with 0.3 and 0.06 micron alumina in distilled water. Kalling's Reagent was used as the etchant.

B. Specimen Preparation for Electron Microscopy

1. Transmission Electron Microscopy

3.05 to 3.1 millimeter diameter bar specimens were machined from bulk specimens. (Thin slices were machined from bulk specimens.) Thin slices of 0.015 inch thickness were then cut from the bar specimens with a high concentration diamond wafering blade that was oil cooled. The disc specimens were then polished to a final thickness of 0.004 inch using 240 through 600 grit silicon carbide paper.

Final polishing was accomplished on the Fishione dual jet electrolytic polisher. Two types of polishing solutions were used. For alloys N-1, N-2 and N-3, the solution was 90% methanol-10% perchloric acid and was maintained at -52°C by a dry ice and acetone cooling system. A current density of 25 milliampers was sufficient to thin a specimen in 10 minutes. For alloys N-4 and N-5, the electrolyte was 90% glacial acetic acid-10% perchloric acid at ambient

temperature. A current density that varied between 35 and 40 milliampers was sufficient to thin a specimen in 5 minutes. After completion of the jet polishing process, the specimens were cleaned by dipping them in baths of methanol, distilled water, ethanol, distilled water with a final rinse of ethanol.

2. Scanning Electron Microscopy

Both powders and fracture surfaces were mounted directly onto a specimen stage treated with a commercial conductive silver paint. After drying, the specimens were transferred to a vacuum chamber and gold coated.

APPENDIX II

Room Temperature Hardness (Rockwell "C") Versus Annealing Temperature (°C)

Alloy and Condition	RT	427	649	982	1093	1204	1316
N-1; As-Extruded	33.2	32.7	33.0	30.5	29.8	25.8	25.0
N-1; As-Extr. + 13% R.A.	42.6	42.5	42.0	34.0	26.0	-	-
N-2; As-Extruded	48.5	48.5	48.0	47.5	47.4	44.0	37.3
N-3; As-Extruded	52.3	52.5	52.4	51.6	50.5	49.6	39.4
N-4; As-Extruded	52.8	52.6	51.2	51.2	50.5	46.2	-
N-5; As-Extruded	58.5	58.7	59.5	58.0	57.5	55.0	42.0

APPENDIX III

Stress Rupture Data

815°C

Alloy and Condition	Stress psi (MPa)	Rupture time (hrs.)	Elong (%)	R.A. (%)
N-1; As Extr. + 20% R.A.	12,000 (83)	1.0	-	8.0
WIA 982°C	8,000 (55)	60.0	9.0	10.0
N-1; As Extr. + 20% R.A.	18,000 (124)	5.1	4.0	4.0
WIA 750%C + 1 hr. 1100°C	11,000 (76)	65.0	8.0	15.0
+10% R.A.				
N-2; As Extr. + 80%	25,000 (172)	0.5	-	5.0
R.A. WIA 1260°C	15,000 (103)	25.0	5.0	6.5

982°C

N-1; As Extr.	6,000 (41)	0.3	-	17.0
	3,000 (21)	3.0	-	18.5
N-1; As Extr. + 30% R.A.	4,000 (28)	0.8	-	8.0
	3,000 (21)	5.0	-	10.0
N-1; As Extr. + 20% R.A.	4,000 (28)	0.6	-	2.2
WIA 750°C	3,000 (21)	4.0	-	2.0
N-1; As Extr. + 20% R.A.	4,000 (28)	1.1	-	4.5
WIA 815°C	2,500 (17)	21.0	4.9	4.8
N-1: As Extr. + 30% R.A.	4,000 (28)	1.0	-	4.9
WIA 815°C	2,500 (17)	25.0	4.4	5.6
N-1; As Extr. + 60% R.A.	4,500 (31)	1.9	-	5.4
WIA 815°C	3,000 (21)	28.3	6.0	6.7
N-1; As Extr. + 20% R.A.	5,000 (34)	2.1	-	8.5
WIA 982°C	3,500 (24)	19.5	5.5	8.5
N-1; As Extr. + 40% R.A.	6,000 (41)	1.1	-	8.5

982°C (Cont'd)

WIA 982°C	4,000 (28)	60.0	12.5	12.0
N-2; As Extr.	6,000 (41)	0.5	45.0	40.0
	3,000 (21)	7.0	65.0	50.0
N-2; As Extr. + 40% R.A.	6,000 (41)	2.5	4.0	4.0
WIA 1260°C	4,000 (28)	60.0	5.5	6.3
N-2; As Extr. + 80% R.A.	6,000 (41)	0.5	-	2.0
WIA 1260°C	3,700 (26)	25.0	3.5	3.0
N-3; As Extr.	6,000 (41)	1.0	-	15.0
	4,000 (28)	10.0	22.0	18.0
N-3; As Extr. + 0.5 hr/	15,000 (103)	0.2	3.2	5.6
1316°C/AC	8,500 (59)	140.0	4.5	7.5
N-3; As Extr. + ZAP 6"/	10,000 (69)	9.0	3.0	4.5
hr at 1300°C	8,500 (59)	25.0	3.5	3.0
N-3; As Extr. + ZAP	12,000 (83)	9.5	2.2	3.2
3"/hr at 1300°C	9,500 (66)	85.0	5.5	8.0
N-4; As Extr. + ZAP	10,000 (69)	0.3	2.4	5.0
0.75"/hr at 1260°C	6,000 (41)	6.0	1.6	3.0
N-4; As Extr. + ZAP	10,000 (69)	0.2	0.2	2.5
3"/hr at 1260°C	6,000 (41)	12.0	4.5	4.1
N-5; As Extr.	10,000 (69)	0.6	5.4	15.2
	8,000 (55)	15.0	6.0	19.4
N-5; As Extr. + 1243°C/	15,000 (103)	23.1	4.2	5.5
0.5 hr/AC + 954°C/2hr/				
AC + 843°C/24 hr/AC	12,000 (83)	125.0	10.4	11.5
N-5; As Extr. + ZAP	35,000 (241)	0.35	1.5	3.0
3"/hr at 1260°C	25,000 (172)	114.4	9.4	12.4

	982°C (Cont'd)			
N-5; As Extr. + ZAP	35,000 (241)	0.7	2.4	3.5
1.5"/hr at 1260°C	24,000 (166)	110.7	9.0	11.5
	1093°C			
N-5; As Extr. + ZAP	27,000 (186)	1.5	2.1	3.5
3"/hr at 1260°C	23,000 (159)	43.5	4.5	6.5
	21,500 (148)	72.5	3.5	6.2

APPENDIX III

Stress for 100 Hour Rupture Life

815°C

Alloy and Condition	Stress psi (MPa)
N-1; As Extr. + 20% R.A. WIA 982°C	7800 (54)
N-1; As Extr. + 20% R.A. WIA 750°C +1 hr/1100°C/AC + 10% R.A.	10,500 (72)
N-2; As Extr. + 80% R.A. WIA 1260°C	13,000 (90)

982°C

N-1; As Extr. + 30% R.A.	2000 (14)
N-1; As Extr. + 20% R.A. WIA 750°C	2000 (14)
N-1; As Extr. + 20% R.A. WIA 815°C	2000 (14)
N-1; As Extr. + 30% R.A. WIA 815°C	2100 (14.5)
N-1; As Extr. + 60% R.A. WIA 815°C	2700 (18.6)
N-1; As Extr. + 20% R.A. WIA 982°C	2700 (18.6)
N-1; As Extr. + 40% R.A. WIA 982°C	3000 (21)
N-2; As Extr.	2000 (14)
N-2; As Extr. + 40% R.A. WIA 1260°C	4500 (31)
N-2; As Extr. + 80% R.A. WIA 1260°C	3500 (24)
N-3; As Extr.	2800 (19)
N-3; As Extr. + 0.5hr/1316°C/AC	10,000 (69)
N-3; As Extr. + ZAP 3"/hr at 1300°C	9700 (67)
N-3; As Extr. + ZAP 6"/hr at 1300°C	8000 (55)
N-4; As Extr. + ZAP 0.75"/hr at 1260°C	3600 (25)
N-4; As Extr. + ZAP 3"/hr at 1260°C	4600 (32)

982°C (Cont'd)

N-5; As Extr.	7500 (52)
N-5; As Extr. + 1243°C/2hr/FC/1150°C/AC + 954°C/2hr/AC + 843°C/24hr/AC	12,000 (83)
N-5; As Extr. + ZAP 1.5"/hr at 1260°C	23,500 (162)
N-5; As Extr. + ZAP 3'/hr at 1260°C	27,500 (190)

1093°C

N-5; As Extr. + ZAP 3"/hr at 1260°C	22,000 (152)

APPENDIX IV

Comparison of Stress for 100 Hour Rupture Life for Several Superalloys

Alloy	Ref.	100 Hour Rupture Strength, ksi (MPa) 982°C (1800°F)	1038°C (1900°F)	1093°C (2000°F)
MAR-M 200(DS)	95	29(200)	20(138)	-
MAR-M 200 (Cast)	95	26(179)	16(110)	9(62)
IN100(Cast)	95	25(172)	18(124)	-
MAR-M 509 (Co-base)	95	15(103)	12(83)	8(55)
PWA 1409(Mono crystal)	111	30(207)	-	-